LASER-ASSISTED TRANSFECTION, OPTOGENETIC STIMULATION AND ITS DETECTION IN MAMMALIAN CELLS

by

KAMAL RAJ DHAKAL

Presented to the Faculty of the Graduate School of

The University of Texas at Arlington in Partial Fulfillment

of the Requirements

for the Degree of

DOCTOR OF PHILOSOPHY

THE UNIVERSITY OF TEXAS AT ARLINGTON

May 2015

To my parents who were the first teachers in my life.

Acknowledgements

I would like to remember and thankfully acknowledge everyone involved, whose guidance and support has been influential in successful completion of my doctorate degree.

Foremost, I would like to express my sincere gratitude to my research and thesis advisor, Dr. Samarendra Kumar Mohanty, for his continuous support for the completion of PhD and research. I am highly inspired by his motivation, enthusiasm and encouragement. Though I did not have any prior knowledge and expertise in research field, he entrusted and involved me in different projects which eventually led me the successful completion of my doctoral degree/research. I thank him for accepting me as his student and nurturing my growth both as researcher and as a good human being.

I would like to thank my dissertation committee Dr. Ali R.Koymen, Dr. Suresh C. Sharma, Dr. Qiming Zhang and Dr. Young-tae Kim for reviewing this document and being a part of my dissertation committee. Without their insightful comments, valuable inputs, and relevant questions, this dissertation wouldn’t have come to fruition. Special thanks to our collaborator Dr. Young-Tae Kim for providing me cells, reagents, and valuable advice.

I would like to express sincere thanks to my graduate advisor Dr. Qiming Zhang. I was fortunate to take many of his theory classes. He not only instilled to me sound academic background but was very helpful and supportive throughout my graduate program.

I like to thank Dr. Ling Gu , Fransisco and Chris Cote for teaching me cell culture, patch-clamp, and molecular biology, respectively. I would especially like to thank Dr. Subrata Batabyal for his friendliness and helpfulness and Dr. Bryan Black, my colleague, for his continuous help, support and friendship. I thank to all my friends and members of research group especially Sarmishta Satpathy for proofreading this document.

At last but not least, I would like to thank all my family members especially to parents; Chandrakala Dhakal and Laxmi Prasad Dhakal for their love and imbibing in the right morals and spiritualism and my wife Bishnu Regmi for her companionship. Finally, I would like to thank my cute kids Ishan Dhakal and Aayan Dhakal being one more reason of my happiness and success.

Above all, I would like to thank Almighty for his compassion and for giving me the chance to be a witness to this mysterious existence and its manifestation.

April 7, 2015

Abstract

LASER –ASSISTED TRANSFECTION, OPTOGENETIC STIMULATION AND ITS DETECTION IN MAMALIAN CELLS

Kamal Raj Dhakal, PhD

The University of Texas at Arlington, 2015

Supervising Professor: Samarendra Kumar Mohanty

Stimulation of cells, especially neurons is of significant interest both for basic understanding of neuronal circuitry as well as clinical intervention. Existing electrode-based methods of stimulation is invasive and non-specific to single cells or cell type. Recently, optical stimulation of targeted neurons expressing light-sensitive proteins (opsins) has surfaced as an emerging and a powerful technique (Optogenetics) in neuroscience. Various transfection methods such as viral-based, lipofection, electroporation have been developed to express the opsin. However, these methods are not suitable for transfection of a single cell. In order to achieve single cell transfection, we have used femtosecond pulsed laser microbeam to make a transient hole in the cell membrane in order to deliver exogenous molecules such as plasmids:Channelrhodopsin-2 (ChR2), and red-activatable Channelrhodopsin (ReaChR) or cell impermeable dye

(Rhodamine Phalloidin). This method allowed live cell imaging following injection of actin-staining dye Rhodamine Phalloidin. Plasmids encoding for light sensitive proteins ReaChR, ChR2 and white opsin were also transfected into the cells by laser-assisted optoporation.

Using optogenetics tools as a minimally invasive technique for cells and tissues is limited to the study of superficial regions, since a significant amount of the visible light is lost due to absorption and scattering. We have used fiber optic two-photon optogenetic stimulation (FO-TPOS) in order to enhance the in-depth stimulation. Photothermal contributions which occur due to absorption of NIR light during optogenetic stimulation, has been modeled and discussed. Near-infrared TPOS will allow localized stimulation so as to enable probing and manipulation of neural circuitry with high spatial resolution.

Several electrode-based methods have been developed in order to detect and measure the electrical activity of cells and tissues during stimulation such as patch-clamp and multi-electrode arrays(MEAs) recording. These methods are invasive, potentially non-sterile and require cumbersome instruments which often generate noise and artifacts. We have used calcium imaging to detect the activation of cells as a result of optogenetic stimulation.

Table of Contents

List of Illustrations

Chapter 1

Introduction

1.1 Overview

One common problem faced in the field of neuroscience is the inability to stimulate chemically identical cells in the vast heterogeneous group of neuronal cells and tissues. The problem becomes more complicated when we need to activate a single cell or even a sub-cellular regions such as the dendritic spines within the cell. Neuronal-electrode interfacing technology allows us to study brain functions and neuronal circuitry. This technology has been widely used for treatment of several brain disorders such as seizure and Parkinson's diseases. However, this method suffers from numerous drawbacks such as the inability of spatially localized stimulation, interference from electrical noises, the possibility of damaging the neural circuitry while inserting the electrodes and it is highly invasive. Unfortunately, these drawbacks have huge scientific and clinical impact. A long time ago, Nobel laureate Francis Crick in his article "Unrealized prerequisites for assembling a general theory of the mind," observed that the ability to manipulate individual units of the brain would require "a method by which all neurons of just one type could be inactivated, leaving the others more or less unaltered" [1]. His vision could not be realized in practice until recently, when optogenetics, a new method in

neuroscience emerged. In a broad sense, optogenetics is a technology which can stimulate or inhibit cellular activities upon irradiation minimal light intensity where light sensitive proteins are expressed [2]. While high resolution neuronal imaging has enabled the mapping of the physical connectome [3] of the brain, there is now a growing need for an efficient high-resolution method to functionally map the multitude of neural connections in the brain. Brain mapping is the most ambitious project of this decade. The Obama administration has announced a big project called “The BRAIN Initiative”, (Brain Research through Advancing Innovative Neuro-technologies) which is also known as the Brain Activity Map Project. The goal of the project is to map the activity of every neurons in the human brain. This research would map the activity of the neurons in mice and other mammals and eventually in humans. The cost of the project is $300 million per year for ten years (Wikipedia/brain initiative). A similar big project ($1.6 billion) has also been announced by EU (European Union) called “The human brain project”. The development of technology that helps us readout the activity of single entity of the brain will be required for the success of these projects. There are various techniques which help to map the structure of the brain, such as MRI and fluorescent (transparent) brain imaging [4]. However, understanding the functional relationships among neurons located in different regions of brain is challenging. This has been

achieved to certain extent by electrical stimulation methods but these methods lack the required cellular specificity.

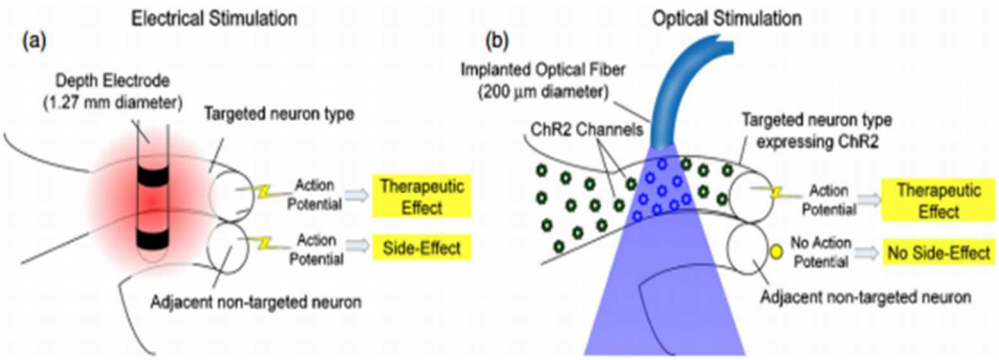

Figure 1.1: Comparison between electrical and optogenetic stimulation. (a) Electrical stimulation is non-specific and non-localized stimulation which activates all the cells near the electrode. (b) Optogenetic stimulation is localized stimulation which stimulates only the opsin (ChR2 in this example) expressing cells where light intensity exceeds the threshold (*Aravanis et.al* J. Neural Eng., 4, S143, 2007).

Attempts have been made to manipulate cellular electrical activities (by electrical stimulation) within specified volume. This may have allowed high temporal precision, but still lacks cellular specificity as well as possesses clinical side effects as shown in Figure 1.1. Pharmacological and genetic manipulations can target specific cells within certain expression profiles, but they lack temporal precision on the timescale of neural coding and signaling (i.e. milliseconds) [5]. In fact, until recently, no existing method could achieve both the temporal precision and cellular specificity required

for selective neuronal activation within vast neural network of billions of cells. Optogenetics, on the other hand, is able to excite or inhibit with millisecond temporal precision and grant single cell specificity without causing the deleterious effects as described above in Figure 1.1.

1.2 Optogenetics

The technique of using light to activate microbial opsin in biological interventions is a new development. Laser light has been used to inhibit targeted proteins by deactivating them sometimes that a geneticist would call “loss of function” [6]. Again, lasers can be used to stimulate neurons or cells directly (such as genetically targeted opsin-expressing cells) what a geneticist would call “gain of function [7]. These microbial opsins are widely found in nature which behave as ion channel and increases in conductivity occurs after interactions with the light.

The read out for activation of neurons (by light or other means) is primarily by electrical means though optical read out methods are emerging [8-11]. Theoretical understanding of neuronal communication (action potentials) was understood after developing a purely physical model, called H-H model, developed by Hodgkin and Huxley. Their model describes the generation and propagation of an electrical signal, called an action potential, by which neurons communicate [12]. This model treats axon as a charged capacitor and ion channels as resistors forming an electrical circuit.

Whenever there is conductance of ions across the ion channels, electrical signals are produced [13], commonly known as action potentials.

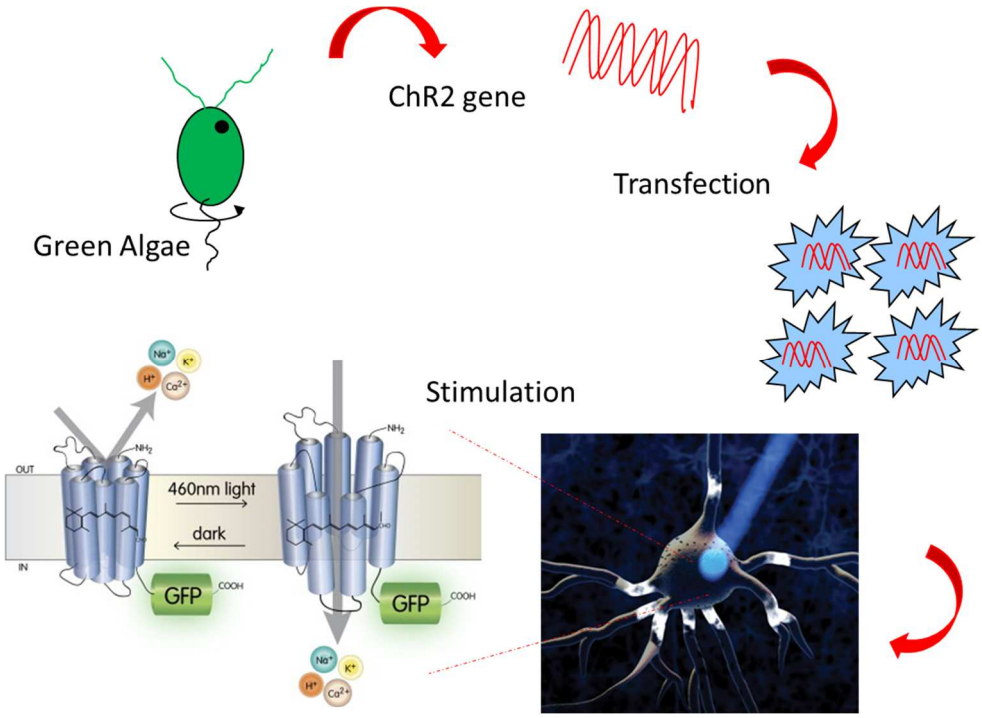

Figure 1.2: Optogenetics: Steps involved in optogenetics. (ChR2 is extracted from single cell green algae (chlamydomonas reinhardtii) and transfected in to cells *(in vivo* as well as *in vitro*). Upon irradiance with blue light, ChR2 opens and closes exchanging the ions with the extracellular environment (bottom left-Flannery *et.al*, Neuron, 2006.03.027 and bottom right-McGovern Institute for Brain Research at MIT).

The use of optogenetics, which combines genetics and optics to modulate and control the activity of specific neurons or cells, is now widely adopted as a tool in neuroscience research. Recently, visible light-assisted activation of selected neuronal groups have been made possible with high

temporal precision by introducing a light-activated molecular channel; Channelrhodopsin-2 (ChR2) [14-16] or one of its variants. As shown in Figure 1.2, genes encoding for Channelrhodpsin-2, are derived from algae, and can be transfected and expressed in targeted cells. Upon irradiation with blue light, the chromophore 'all-trans retinal' absorbs the light energy and changes its conformation from a 'cis' to 'trans' structure which leads to opening of opsin channels. This method has several advantages over electrical stimulation [17-19], such as cellular specificity and minimal invasiveness. Therefore optogenetics is growing as a valuable tool in neuroscience research.

1.3 Challenges in optogenetics

1.3.1 Targeted delivery of light-sensitive gene-encoding plasmids

One of the underlying challenges in optogenetic stimulation is the selective expression of light sensitive proteins in spatially localized regions. The commonly used techniques for transfection are viral-delivery, electroporation, and gene gun. None of these methods are suitable for spatially targeted delivery. In understanding the neural signal processing and functional study, the role of even small subpopulation of cells or single cells is very important in the group of large population or heterogeneous group of cells [20]. Further, for dissecting the neuronal circuitry by means of optogenetic stimulation, we are required to deliver multiple genes into

single cells or different gens into adjacent neighboring cells in heterogeneous tissues.

In this study, we have found laser-assisted plasmid delivery method is one of the best alternative to achieve localized delivery of opsin-encoding plasmids in optogenetics and results are discussed in Chapter 2.

1.3.2 Spatially localized optogenetic stimulation

As the use of light-activatable ChR2 for *in vivo* models is increasing, there exists some limitations of its utility. Although optogenetics methods require very low intensity of light (0.5-10 mW/mm^2) [15], at the activation wavelength for ChR2 (460 nm), significant absorption and scattering of light occurs. This leads to a very limited (shallow) penetration depth for the stimulation beam [21]. Thus, in order to stimulate cells in the ventral areas of the brain, one has to choose between one of two undesirable alternatives: the first is to maintain the minimally invasive qualities of the approach which requires that the average blue light beam power be significantly increased. Unfortunately, this approach often leads to significant deleterious effects on the cells' viability in the vicinity of the target, and thus severely limits the translational potential of this technology. The second alternative approach is to use an optical fiber [22-24] or micro-light emitting diodes (μLEDs) [25]- which can deliver activation light to neurons which are in close proximity. This approach severely compromises the minimally invasive quality of

optogenetics because optical fibers (similar to electrodes used in electrical stimulation techniques) or μLED(s) need to penetrate through more superficial brain tissue in order to reach ventral brain regions. In this way, the superficial brain tissue and cells along the path of the fiber/ μLED probe get damaged; and such damage can lead to difficulty in interpreting the outcome of deep-brain stimulation and circuit analysis. Therefore, several attempts have been made to shift the activation peak of ChR2 from the blue to the red wavelength region [26-28], where biological tissue absorption and scattering is reduced. While there has been some success at the cost of altered light-activation kinetics, it seems near-infrared opsins would be ideal for in-depth cell-specific optogenetic stimulation of excitable cells in an organism. However, the success in developing a near-infrared opsin would still not permit applicability of the method for localized activation of specific regions in deep (ventral) brain areas, since the single-photon (red or infrared) stimulating beam will also stimulate neurons outside of the spatially-targeted region. Thus, two-photon optogenetic stimulation is more desirable over the single photon optogenetic stimulation when localized and in-depth stimulation is required. Details of the two-photon optogenetics will be discussed in Chapter 3.

1.3.3 Detection of optogenetic stimulation.

The conventional methods for detection of optogenetic stimulation is electrical recording (patch-clamp, single electrode recording, and multi-electrode recording) which requires physically touching the cell. This can be very invasive, intrusive and leads to the cell damage. Due to lack of other standard techniques, gold standard method of electrophysiology recording is still patch-clamp. Further, electrophysiological detection from every single opsin-expressing cell during optogenetic stimulation would require electrodes implanted (poked) in every cell. In addition, patch-clamp recording from the depth of tissue is difficult to acheive.

Recently, significant interest has been shown to develop optical methods that are non-invasive, sterile and allow detection from large number of cells simultaneously. With the advent of voltage sensitive dyes, it was demonstrated that membrane potential information could be detected optically with increased spatial information. Quantitative phase microscopy techniques can be also applied to observe the changes happening during optogenetic stimulation in large field of view. Calcium imaging technique has been used in our study to detect optogenetic stimulation and results are presented in Chapter 4.

1.4 Application of optogenetics

Application of optogenetics has been rapidly increasing as many researchers are being attracted towards this field as use of opsins and its mutants is allowing sensitization of specific neuronal networks *in vitro* as well as *in vivo.* Advancements in optics technologies such as development of spatially-modulated laser beams, millisecond shutter, scanning devices and novel focusing optics are necessary for realizing full-potential of this technology. In recent years, researchers in this field have carried out interesting experiments controlling the activity and behavior of animals by inserting one end of a fiber in brain of freely behaving mice and coupling the other end to the appropriate light source. Those experiments were able to modulate learning [29], wakening [30] , somatosensation [31], vision [32], breathing [33] and movement [34]. In 2009, it was demonstrated that ChR2 can be used safely to stimulate neuron without effecting the immune system or causing the death of neurons in non-human primate brain [35].

Chapter 2

Laser-assisted delivery

2.1 Mechanism of laser ablation

Laser ablation is the process of removing material by evaporation, sublimation, or plasma formation when intense laser light is incident upon the sample. When a light usually a pulsed laser of sufficient intensity is incident on the biological tissue, highly localized and confined plasma is formed at the focal volume of the laser pulse which causes the ablation of biological sample. When a focused laser microbeam is incident upon a biological sample, the sample material absorbs the irradiation either through single photon absorption or multiphoton (nonlinear) absorption, depending on the irradiation frequency, the intensity (laser power in unit area) and the pulse duration [36, 37]. Though both single photon and multiphoton irradiation can lead to photo-thermal ablation, single photon absorption causes extensive damage to the sample due to deposition of laser energy. The main contributing factor for multiphoton absorption efficiency is the peak power which is defined as (pulse energy)/(pulse duration) [36, 37]. Therefore, microsecond or nanosecond pulse lasers are not efficient for multiphoton absorption. Though there has been a recent discovery of attosecond pulse (10^{-18} s) [38], the attosecond laser is not commercially available yet. Commercially available femtosecond (10-100 fs) laser beam

is sufficient for laser ablation (nonlinear process). However, using high pulse energy can lead to heating, shockwave production, and cavitation bubble formation, all of which can lead to spatially extended damage[39, 40]. Therefore, in nonlinear absorption shorter pulse width is preferred as it is this multiphoton absorption process that initiates the localized chemical decomposition of the sample [74].

The excitation of electrons from the ground state to a quasi-ionized excited state (conduction band) takes place via a nonlinear process when multiple photons excite the ground state electrons virtually at the same time (simultaneously) [41]. These excited electrons are the initial ‘seed electrons’ for plasma mediated ablation process. Once the first seed electron has jumped to the conduction band, it absorbs another photon within the pulse duration of the laser, reaching higher energy states within the conduction band [41]. This process continues until the kinetic energy of the electron is sufficient to ionize a new seed electron from the valence band. Once this happens, these two electrons now repeat the process; reaching the threshold energy necessary to impact-ionize more electrons. Energy is gained through impact ionization and new seed electrons are promoted to the conduction band until a critical number of these ionized electrons (plasma) is reached. After the critical plasma density, breakdown of the material (sample) starts which is called plasma breakdown.

2.2 Optical poration of biological sample

Optical poration of biological sample is an purely optical method of creating a transient hole in a cell membrane or organelle by briefly (on the scale of milliseconds) exposing it to a focused pulsed laser microbeam of sufficient intensity [42]. In the case of *in vitro* studies, this method allows for single cells to be targeted, and may be interfaced with microfluidic devices [43] or additional, fast-scanning optics for relatively high-throughput studies[44, 45]. Furthermore, since optoporation is a non-contact method, and it can take place within a completely enclosed system, it is absolutely sterile.

The primary mechanism by which a cellular membrane is optoporated varies depending on pulse width and laser intensity. Many hypotheses have been proposed, such as plasma formation, dielectric break down, cavity formation, local heating, shock wave formation [46, 47], and photo-acoustic effects [48, 49]. In case of a femtosecond pulsing laser, we have assumed that direct plasma breakdown is the primary cause of the observed optoporation effect. The size of the hole which is formed during laser irradiance is dependent upon the pulse-energy, pulse-width, and wavelength of the laser beam being used. Since the diffraction-limited spot size is directly proportional to the wavelength of light, ultra-violet (UV) wavelengths may seem to be better-suited over other wavelengths in near-

infrared (NIR) regimes for optoporation. However, UV light carries a high risk of damage to the cells since it is highly absorbed by cellular components. Therefore, the use of UV light may not be suitable [50, 51]. CW argon lasers operating at 488 nm, or Nd: YAG lasers which operate at 532 nm, have also been employed for optoporation. However, many cell organelles have high absorption coefficient at these wavelengths, so the possibility of detrimental effects in the visible range cannot be ruled out. It is well known that the absorption of light by intracellular components is low in the NIR (700-1000 nm) range. This range of wavelengths is, in fact, often referred to as the 'therapeutic window' for their ability to probe biological samples with low deleterious effects [52]. We have chosen wavelengths in the range of 800-850 nm.

2.3 Insertion of impermeable molecules in live cells

It is necessary in many biological and medical studies to introduce impermeable molecules such as fluorescent markers or dyes into cells to facilitate visualization of filamentous actin, tubulin, or to observe functional alteration [53] of cellular processes. Though cells can be fixed and fluorescently stained with cytoskeletal dyes, there has always been significant interest in the visualization of cytoskeletal dynamics within living cells. Several physical methods have been developed to accomplish this aim. Among them, one widely used method is viral transfection of actin-GFP

plasmids. However, viral transfection methods cause expression in large populations of cells. Other mechanical methods have also been developed for localized injection of exogenous factors and visualization of cytoskeletal dynamics, with the two most widely employed methods being electroporation [54] and microinjection [55]. These methods are either highly invasive, increase the possibility of contamination, or lack spatial and temporal specificity. For example, microinjection frequently causes unintended cell damage, whereas electroporation has been reported to achieve relatively low efficiencies [56]. Chemical methods, such as lipofection and DEAE-dextran, have also been employed for the introduction of exogenous factors [57, 58]. These methods may also lead to adverse effects [59], and are currently only relevant in large populations of cells. With the advent of laser technology, light has been increasingly utilized for safe and sterile biological applications, such as micro-surgery [60] and single cell manipulation [43, 61-63].

In this study, we have used ultrafast laser pulses to create a single transient hole in the cellular membrane in order to inject nanomolar concentrations of Rhodamine Phalloidin (RP), cell-impermeable dye for staining filamentous actin dye molecule, into single viable mammalian cells (both HEK 293 and primary rat cortical neurons). Dynamics and kinetics of the dye diffusion in the cell have been discussed and numerical simulations

of diffusion time constants are found to be corroborating the experimental results.

2.4 Laser-assisted delivery of plasmid into mammalian cells

Recently, there has been considerable interest in optically transfecting cells using ultrafast pulsed light [39, 64-72] because of its selective targeting capability, higher efficiency and viability (>90% reported *in vitro* [71]) as compared to other methods. Further, femtosecond (fs) near–infrared laser based transfection has been shown to be safe, providing high efficiency and survival (93%) of optoporated embryo during development [73], as well as for *in vivo* gene delivery [74]. Our lab has already demonstrated [75] the use of ultrafast NIR laser microbeam for optical delivery of opsin (ChR2)-YFP-plasmids to spatially-localized regions of retina. Since non-linear interaction between ultrafast laser beam and cell occurs only within a micron of the focus, only ganglion cell layer (which is proximal to laser beam) and even a single retinal ganglion cell (RGC) could be made light-sensitive. However, to achieve higher sensitivity of cells towards ambient broad-band (white) light, it will be advantageous to deliver multiple opsin with spectrally-separated activation peak into targeted cells. Delivery of large fusion constructs of multiple spectrally-separated opsins (e.g. ChR2, C1V1, ReaChR) [76-78] is challenging for the currently-achievable safe viral methods. Separate delivery of different opsins by

multiple viral vectors can lead to immune reaction and may cause unwanted transfection of non-targeted tissue. Though several non-viral approaches such as electroporation and lipofection exist, these methods suffer from low transfection efficiency, loss of cell viability and non-targeted transfection similar to viral methods. Ultrafast near-infrared laser-mediated optoporation [65, 72] can address these issues and has promise to deliver large multi-opsin constructs with targeted transfection with single cell resolution and high efficiency. With the advent of technology and laser-microscope interface software, optoporation has become more user friendly and achieved the single cell delivery with very high speed 100 cells/ minute [20].

Here, we have shown comparative study of lipofection vs laser-transfection of single as well as multiple opsins. The fs laser transfection method is found to be capable of delivering large sized (>10 kb) multi-opsin construct. Membrane to intracellular expression ratio was found to be higher in case of laser transfection as compared to lipofection owing to the less-perturbed cellular morphology. Higher photocurrent was observed in case of HEK 293 cells transfected with multi–opsin fusion construct as compared to ChR2 sensitized HEK 293 cells under white light stimulation. Application of spatially-targeted laser transfection of multiple-opsins in degenerated retina will allow stimulation of the retinal ganglion cells (RGCs) by

broadband white light, leading to vision restoration in certain diseases such as retinitis pigmentosa and age-related macular degeneration.

2.5 Materials and Methods

2.5.1 Cell culture

All experimental procedures were conducted according to UT Arlington Institutional Animal Care and Use Committee approved protocol. The cortical neurons were isolated from embryonic 18 day rat embryos. The cortical tissues were dissected, cleaned (meningeal layer), enzymatically dissociated (0.125% trypsin in L-15 medium) for 20 minutes at 37 ^{0}C. The dissociated cortical neurons (100,000/device) were seeded on Poly-D-lysine (PDL, 0.01%, Sigma) pre-coated cover glass with Polydimethylsiloxane (PDMS) barrier well (Sylgard 184, Dow corning), and the serum-free culture medium (Neurobasal medium supplemented B-27 with BDNF and NT-3, 10 ng/ml) was changed every 3 days. The cell cultures were maintained at 37°C in a 5% CO_2, humidified atmosphere prior to experiments. The experiments were performed in an environment with controlled temperature, humidity, and CO_2 levels.

HEK 293 cells were routinely cultured in Dulbecco's modified eagle's medium (DMEM, Sigma Aldrich), supplemented with 10% fetal bovine serum (FBS, Sigma Aldrich) and 1% Penicillin/streptomycin antibiotics. For laser-assisted insertion of Rhodamine Phalloidin (RP) (Cytoskeleton Inc.),

cells were trypsinized and plated on poly-D-lysine coated glass-bottom 35 mm Petri dishes (MatTek Corporation). In case of gene transfection , visualizing of the reporter (YFP or Citrine) fluorescence under suitable illumination was performed to identify the transgene expressing cells. For optogenetic stimulation, cells were loaded with all-trans retinal (ATR, 1 μM final concentration) for at least 6 hours before conducting the experiments.

2.5.2 Dye selection and incubation

Propidium iodide dye is widely used for demonstrating optical injection (optoporation), as it is an impermeable molecule which stains the nucleus [79, 80]. Here, we have selected Rhodamine Phalloidin (RP), a dye marker which is routinely used in visualizing filamentous actin (in fixed cells), and is impermeable as well as toxic at high concentrations. One of our main challenges was to determine an optimal concentration of RP which would allow for filamentous actin imaging, as well as ensure the cell's survival following optoporation. Determination and implementation of these parameters will allow the dynamical study of filamentous actin polymerization and cytoskeletal reorganization in viable cells. In order to inject the appropriate amount of RP, the cell medium (DMEM) was gently removed and replaced with RP+dye+DMEM solution and allowed to incubate at 37°C for 15 minutes prior to optoporation. Calcein is commonly used in cell viability assays due to its retention in living cells. In order to

determine the viability of cells following optoporation, Calcien-AM (4 μM) was introduced to the cell medium and allowed to incubate for 10 minutes prior to imaging.

2.5.3 Optical Setup

A schematic diagram of the experimental setup is shown in Figure 2.1(a). A tunable (690 - 1040 nm) Ti: Sapphire laser (Newport Spectra-Physics, Inc.) beam (repetition rate: 80 MHz, pulse width: ~100 fs) was directed toward the sample by a dichroic mirror (DM1) through an inverted optical microscope (Nikon). A 100x (NA = 1.4) objective was used to focus the laser beam to a diffraction limited spot at the top surface of the cell as shown in Figure 2.1 (a). Special steps were taken to ensure that the laser focal plane matches with the imaging focal plane of the top cell membrane. A second dichroic mirror (DM2) was used to reflect the fluorescence excitation light from the mercury lamp along the same path as the fs laser beam. In the same filter cube as DM2, the excitation (Ex) and emission (Em) filters were used to transmit and collect the appropriate bands of visible light to and from the sample, as well as block any remaining backscattered laser light. All images were acquired by cooled EMCCD (Cascade 1K, Photometrics Inc.) and were processed with ImageJ (NIH) software. The number of fs laser pulses irradiating each sample was controlled by an external mechanical shutter (S, Uniblitz Inc.). The sample-site laser beam

power was controlled by the fs laser software (Mai Tai), with fine adjustments made by altering the orientation of the polarizer (P).

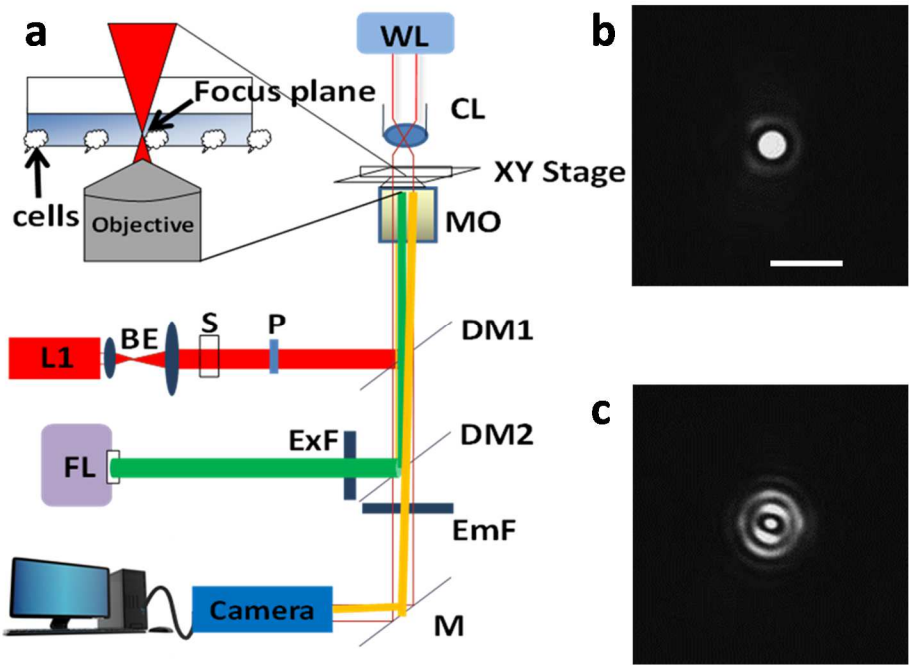

Figure 2.1: (a) Experimental setup for femtosecond laser-assisted optoporation. L: Ti: Sapphire laser; BE: beam expander; S: shutter; P: polarizer; Fl.: fluorescence excitation source; Ex: excitation filter; Em: emission filter; MO: microscope objective; CL: condenser lens; DM1 and DM2: dichroic mirrors; M: mirror; WL: halogen lamp. (b-c) Symmetric laser spot focused above and at the sample's surface plane (scale bar: 10 μm).

The sample-site beam power (after the objective) was calculated by multiplying the transmission factor of the microscope objective [81] with the power measured at the back aperture of the objective. Fluorescence and bright field images were taken before and after optoporation experiments.

Time lapse fluorescence images were taken immediately following optoporation in order to monitor the rise in fluorescence intensity with time

2.5.4 Plasmid isolation and amplification.

LB agar plate: 14 gm of LB agar (Sigma Aldrich) was weighed and poured into measuring cylinder. DI water was added to make the final volume equal to 400 ml (35 gm/liter). The mixture was swirled to make sure all powder is dissolved in water, then the solution was poured in to 1L conical flask and capped with aluminum foil, and labeled with autoclave tape. The LB-agar solution was then autoclaved for 30 minutes and left over in room temperature to cool down to the temperature 55°C. 200 µl of ampicillin (100 mg/ml) was added to the conical flask to make the final concentration 50 µg/ml. When solution starts to polymerize, 20 ml of LB agar solution was poured in each 10 cm polystyrene dishes at center. Lazy (L) spreaders were used to spread the solution uniformly in the dish without bubble formation. The dish was closed with lid and kept for 30-60 minutes (until it solidifies) in room temperature. Once, the LB agar is completely polymerized, the plate was marked with Amp^+ (Ampicillin coated), wrapped with parafilm and kept at 4°C in inverted position.

LB broth solution: LB broth solution was prepared by dissolving 20 g of power from of LB broth (Sigma Aldrich) in 1 liter of DI water. The solution was then autoclaved. Antibiotic (ampicillin) was added to make the final

concentration 50 µg/ml and LB broth solution was stored in 4°C for future use.

S.O.C media: S.O.C media consists of 2% tryptone, 0.5% yeast extract, 10 mM NaCl, 2.5 mM KCl, 10 mM $MgCl_2$, 10 mM $MgSO_4$, and 20 mM glucose and was purchased from Life Technology.

Plasmid Transformation: One vial of JM 109 Chemically Competent E. coli for each transformation was thawed in ice bucket and 1 to 5 µl of the DNA (ReaChR or ChR2, 10 ng to 100 ng) was added into a vial of JM 109 cells and then was mixed gently. The cell mixture was incubated on ice for 30 minutes. Heat-shock was given to the cells for 60 seconds at 42°C without shaking. Vials were removed from the 42°C water bath and placed on ice for 2 minutes. 250 µl of S.O.C media was added to each vial. The vials were capped tightly and shaked horizontally at 37°C for 1 hour at 220 rpm in a shaking incubator. 75-100 µl of the transformation mix was spread by a lazy spreader uniformly on a pre-warmed LB agar plate (Amp^+). Additional plates were plated, if desired. Plates were incubated at 37°C overnight. Visible colonies appeared in the duration of the overnight incubation. Single colony of transformed bacteria was inoculated and grown overnight in 2 ml of pre-warmed LB broth media in a shaking incubator at 220 rpm. In order to get higher concentration of plasmids, four different individual colonies were chosen.

Isolation of plasmid: Commercially available PureYield™ Plasmid Miniprep kit (Promega) was used to isolate the plasmids. PureYield™ Plasmid Miniprep quick protocol is described as bellow.

Lysate: 600 µl of bacterial culture was added to a 1.5 ml micro-centrifuge tube. 100 µl of Cell Lysis Buffer (Blue) was added and mix by inverting the tube 6 times. 350 µl of cold (4–8°C) Neutralization solution was then mixed into the micro-centrifuge tube and mixed thoroughly by inverting couple of times and was centrifuged at maximum speed (14000 rpm) in a micro-centrifuge for 3 minutes. Supernatant (~900 µl) was transferred to a PureYield™ mini-column without disturbing the cell debris pellet, the mini-column was placed into a collection tube and then centrifuged at maximum speed in a micro-centrifuge for 30 seconds. Finally flow through liquid was discarded and the mini-column was placed into the same collection tube.

Wash: 200 µl of Endotoxin Removal Wash (ERB) was added to the mini-column and centrifuged at 1400 rpm in a micro-centrifuge for 30 seconds. 400 µl of Column Wash Solution (CWS) was added to the mini-column and centrifuged at maximum speed in a centrifuge for 30 seconds.

Elute: Above mentioned mini-column was transferred to a clean 1.5 ml micro-centrifuge tube (with cap removed) and then 30 µl of Elution Buffer or nuclease-free water was added directly to the mini-column matrix, incubated for 1 minute at room temperature, and centrifuged for 15 seconds

to elute the plasmid DNA. The centrifuge tube was caped, and eluted plasmid was stored at 20°C.

DNA gel electrophoresis: 1g of agarose was weighed and was mixed with 100 ml of 1x TAE buffer (Tris-acetate buffer). The solution was kept in the microwave for 1-3 min until the agarose is completely dissolved and there is a nice rolling boil. The agarose solution was allowed to cool down for 5 min. Ethidium bromide (EtBr) was added at this point to a final concentration of approximately 0.2-0.5 µg/mL. The agarose gel was poured into a gel tray with the well comb in place. It was kept in room temperature until the gel solidified. Once it is solidified, the agarose gel was kept into the gel box (electrophoresis unit). The gel box was filled with 1xTAE (or TBE) until the gel was covered. In the first lane of the gel, DNA ladder was carefully loaded. In the additional wells, the samples were loaded. Then the gel was run at 80-150 Volt until the dye line is approximately 75-80% of the way down the gel. Then after switching off the power supply, the gel was carefully removed and was kept under UV light for imaging (Gel Logic 212 PRO). The name of plasmids, restriction enzymes and fragments size are tabulated in Table 1.

2.5.5 Opsin expression and optogenetic stimulation

Expression of the opsins was observed after 36 hours of transfection (lipofection, optoporation) using epifluorescence microscopy. A one-tailed

t-test was used to determine the statistically significant difference in the fluorescence expression. The broad-band white light from a halogen lamp coupled to a multimode optical fiber was used for optogenetic stimulation. Light power at the sample plane was measured using a power meter (PM 100D, Thorlabs). An electro-mechanical shutter was used to control the exposure (pulse) duration. The shutter was synchronized with the electrophysiology recording system (Axon Instruments, Molecular Devices).

2.5.6 Opto-electrophysiology setup

The patch-clamp recording set up consists of a fluorescence microscope and an amplifier system (Axon Multiclamp 700B, Molecular Devices). Parameters of the pipette puller were optimized in order to obtain desired borosilicate micropipettes of resistance from 3 MΩ for whole-cell patch-clamp. The micropipette was filled with a solution containing (in mM) 130 K-Gluoconate, 7 KCl, 2 NaCl, 1 MgCl2, 0.4 EGTA, 10 HEPES, 2 ATP-Mg, 0.3 GTP-Tris and 20 sucrose. The electrode was mounted on a XYZ motorized micromanipulator. The standard extracellular solution containing (in mM): 150 NaCl, 10 Glucose, 5 KCl, 2 $CaCl_2$, 1 $MgCl_2$ was buffered with 10 mM HEPES (pH 7.3) was used. The output from the amplifier was digitized using Digidata (Molecular devices). For electrophysiological recording, the hardware was interfaced with patch-clamp software (pClamp10, Molecular Devices). For activation of opsin expressing cells,

the stimulation beam was delivered by the optical fiber. For generating and controlling pulses of light, the electromechanical shutter in the light path was interfaced with a PC. TTL pulses of desired frequency were generated using Digidata card in order to generate required pulses for activation. The whole system was electrically isolated by means of a Faraday cage that was placed around the setup. pClamp 10 (Molecular Devices) software was used for patch-clamp data analysis.

2.6 Results

2.6.1 Optimization of laser parameters

First, optimization of laser parameters was done in the experimental set up as shown in Figure 2.1. In order to optoporate efficiently, the focused laser beam should be symmetric and share a focal plane with the cell's top membrane. This can be verified by symmetry of the spot as well as circular rings around the spot which is shown in Figure 2.1 (b-c). Optimization of the laser parameters was undertaken by varying the laser power and exposure time (macro-pulse duration, 20–50 ms), while keeping the wavelength constant (800 nm). At higher average laser powers (at or above 90 mW) and macro-pulse durations (above 20 ms), HEK cells were observed to die (quick rise in RP-fluorescence and significant change in morphology) as seen in Figure 2.2. It is known that the Phalloidin family of dyes are toxic to

living cells, and can cause or contribute to cell death in some extent [82] at high concentrations.

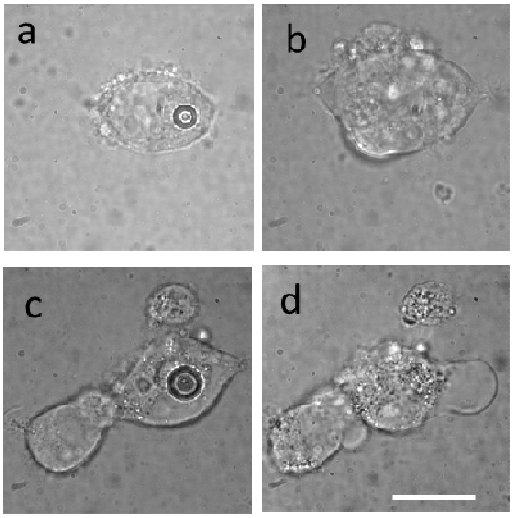

Figure 2.2: Optimization of laser power and exposure time. Higher average laser power above 90 mW with 20 ms exposure time (top row) and exposure time longer than 20 ms at 90 mW (bottom row) leads to observable deleterious effects or cell death. Images a and c represent before optopration and images b and d are after optoporation (Scale bar: 10 μm).

Therefore, imaging is typically performed on fixed cells to visualize the cytoskeletal filamentous actin network. In this study, we have found a window of optimized RP dye concentration by monitoring the cell viability (by morphology and calcein exclusion assay) and RP-fluorescence following optoporation. Calcein AM is a cell-permeant dye that can be used to determine cell viability in most eukaryotic cells. In live cells the non-

fluorescent calcein AM is converted to a green-fluorescent calcein after acetoxymethyl ester hydrolysis by intracellular esterases.

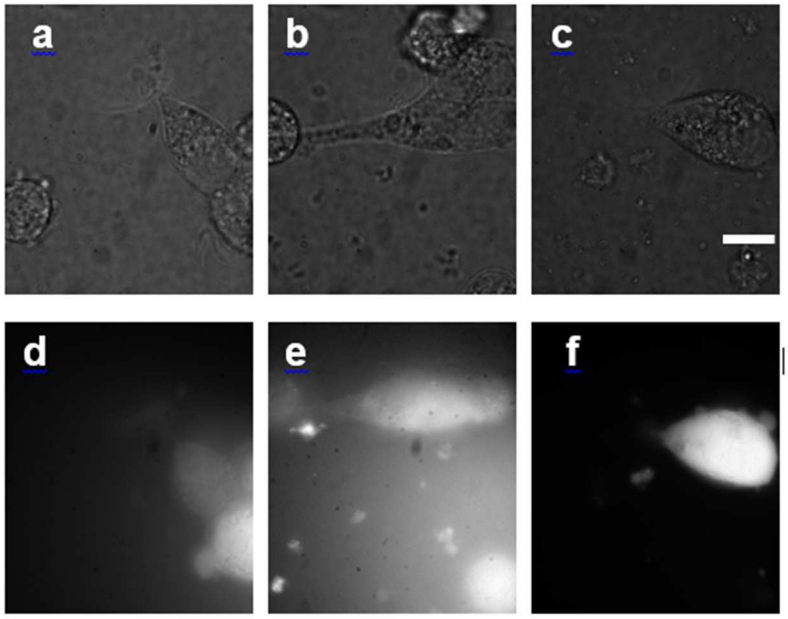

Figure 2.3: Viability test of optoporated cells. Bright field (a-c) and fluorescent (d-f) images of HEK cells treated with Calcein-AM following optoporation at optimized laser parameters to test cell viability (Scale bar: 10 μm).

Calcein AM imaging was performed in those optoporated cells to check their viability. Figure 2.3(d-f) show the bright field and Calcein-AM stained images of the HEK cells following optoporation which implies that the cells are alive after optopration since Calcein-AM is not excluded from live cells.

2.6.2 Optimization of dye concentration for optoporation and live cell actin imaging

Laser transfection parameters were kept constant while the RP concentration was varied from 40 nM to 200 nM. At concentrations of 42 nM or lower, we did not observe any increase in intra-cellular fluorescence intensity. At higher RP concentration (168 nM), optoporated cells showed a sharp increase in fluorescence immediately following optoporation. This may be not attributed to live cell RP dye binding to actin since notable changes in cell morphology was observed, as RP is permeable to the dead cell. If the cell is dead, RP will enter inside the cell through the membrane and abrupt and sharp increase in fluorescence is expected.

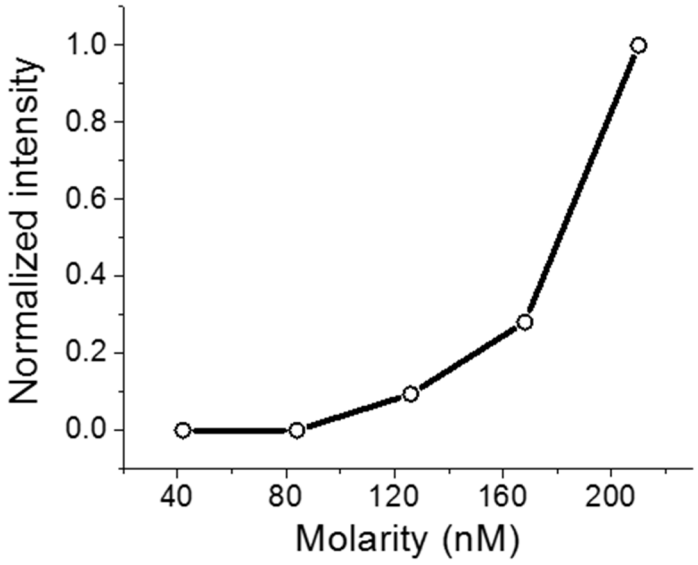

Figure 2.4: Optimization of dye concentration for optoporation and live cell imaging.

Morphology of the cell was also observed while evaluating the effect of RP concentration. Above RP concentration 160 nM or higher, intensity increased sharply as shown in Figure 2.4. Further, morphology changed drastically as shown in Figure 2.5 (e-h), indicating cell death. Since the cell viability was retained following optoporation and injection of 126 nM, this concentration was assumed as optimized concentration for further experiments. Optimized parameters (laser power, exposure time, and RP concentration) were used for optoporation into HEK 293 cells and rat cortical neurons. First, RP was optically injected into HEK 293 cells. There was a clear, observable increase in the cell's fluorescence as shown in Figure 2.5 (a–d) over a time period of approximately 10 minutes. The fluorescence signal increased slowly and ultimately approached a saturation level (independent of quenching) as predicted by Fick's law of diffusion (discussed in the following sections). As can be clearly seen in Figure 2.5 (c), the most intense fluorescence is observed along the periphery of the cell's, where the filamentous actin network is mostly dense.

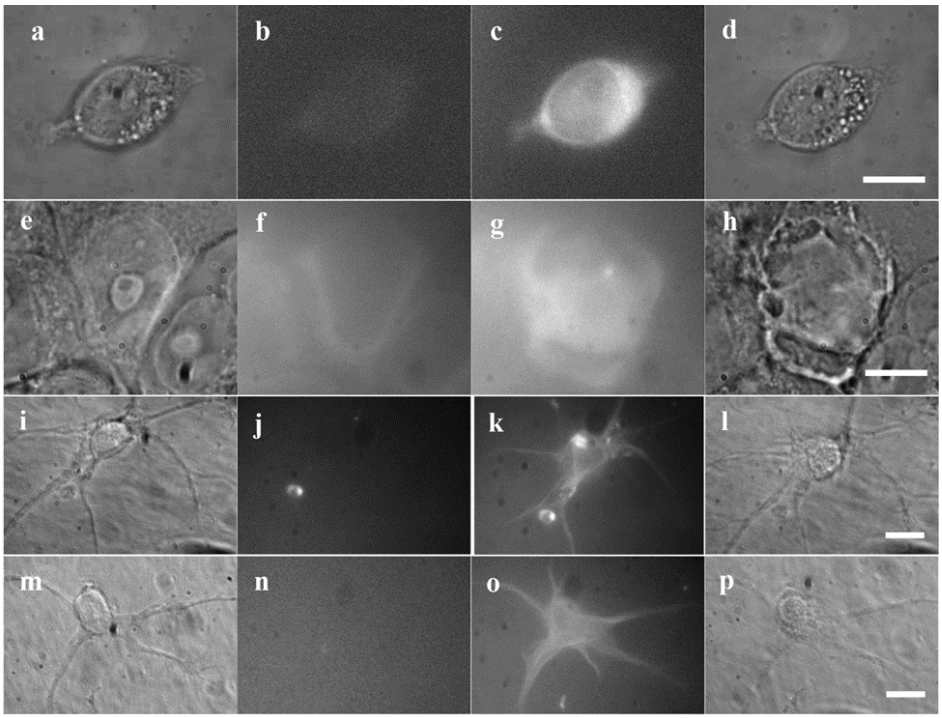

Figure 2.5: Effects of Rhodamine Phalloidin's concentration on cell viability. (a-d) HEK cells, 126 nM RP concentration. (e-h) HEK cells, 168 nM RP concentration. (i-l, m-p) Rat cortical neuron, 120 nM RP concentration. First two columns represent bright field and fluorescence images before optoporation and last two columns represent fluorescence and bright field images following the optoporation (Scale bars: 10 μm).

Next, we demonstrate the introduction of RP by optoporation into viable primary embryonic rat cortical neurons (RCNs). Figure 2.5 (i-p) show the significant increase in fluorescence in the cell soma as well as neurites of the RCN. Hence, with optimized laser parameters and dye concentration, cell-impermeable RP-dye could be successfully injected to the individually targeted cells, without comparing their viability.

2.6.3 Femtosecond laser-assisted spatially-targeted dye injection

The targeted delivery into cells (e.g. cancers, neurons) of individual cell type or spatially-targeted cells is critical to studies of drug delivery, function, and therapeutics. This is more important even in neuroscience, for example, the brain contains a large network of neurons, astrocytes, etc., the organization and dynamics of which characterize and control bodily functions. These cells form physio-chemical connections with one another and form an elaborate circuitry. In order to study the connections and communication within these cells, it may often prove necessary to inject dyes, opsin-encoding genes [63, 83], or plasmids [84]. This can be achieved by femtosecond laser–based cellular optoporation.

By injecting biological markers (plasmids, dyes) into a single neuron (or small subpopulation of cells) among a larger network of neurons, researchers will be able to distinguish individual cellular processes and functions in the networks. Figure 2.6 shows spatially-targeted delivery of RP in rat cortical neurons. Figure 2.6(a-c) represent bright-field images and Figure 2.6 (d-f) show fluorescence images before the optoporation. Figure 2.6 (e-i) represents fluorescence images and Figure 2.6 (j-k) represent bright field images after optoporation. Optoporation sites have been shown by red arrows in Figure 2.6 (a-c). Figure 2.6(g) shows clearly an optoporated cell whose components were fluorescent in an intermingled cellular

network, illustrating the potential of optoporation for studying single-cell structures within larger cellular networks.

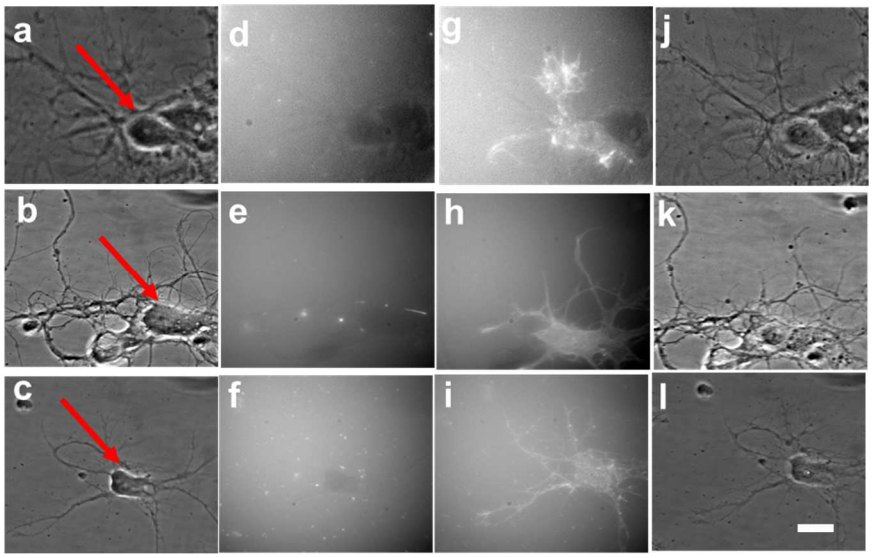

Figure 2.6: Targeted delivery of RP dye. First column (a-c) represents bright-field images and second column (d-f) is fluorescence images before the optoporation. Third column (e-i) represents fluorescence images, and fourth column (j-k) represents bright field images after the optoporation. Arrows indicate the poration sites (Scale bar: 10 μm).

Figure 2.6 (g-i) show that only the targeted neuron and its processes can be labelled among the complex network of other cells. This spatially-targeted delivery of dye is very important to find out the neural circuitry in nervous system.

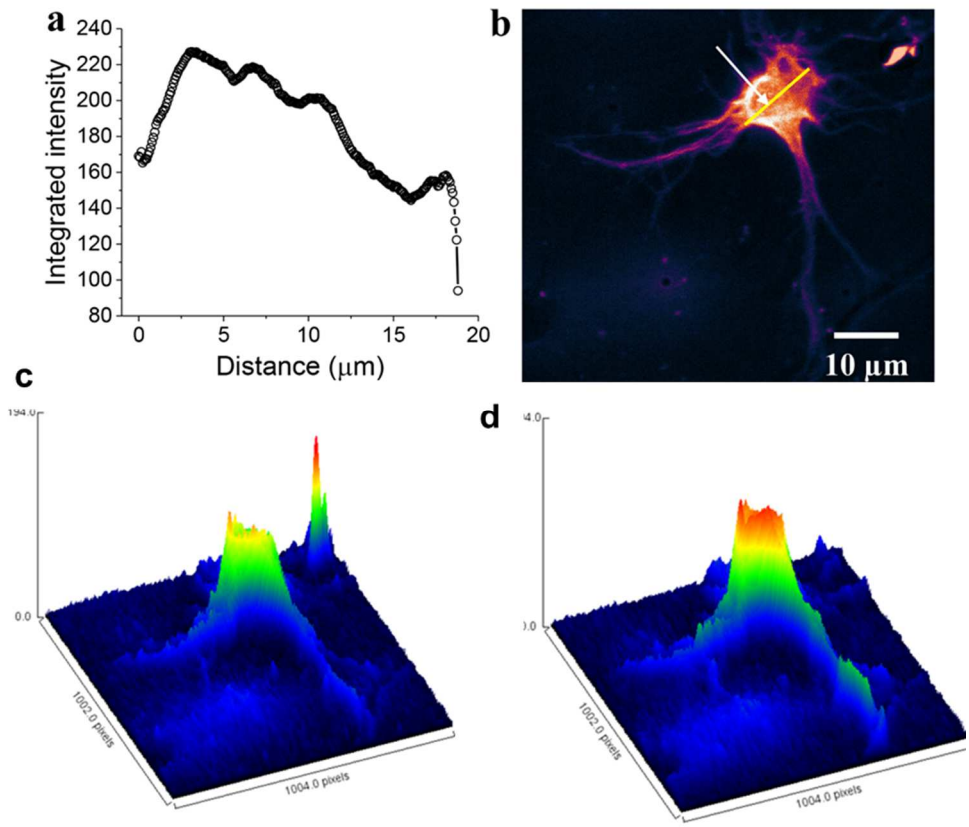

Figure 2.7: Non-uniform distribution of dye in the cell body. (a) Fluorescence intensity along the line, (b) is maximum near the poration site and decreases away from the poration site, (c) surface plot of intensity immediately following the optopration, and (d) after 10 minutes of optoporation.

In order to further quantify the change in distribution of fluorescence intensity after optoporation, fluorescent intensities across the cell (line) were plotted .The fluorescence intensity is at its maximum in the membrane near the optoporation site (center of cell soma) and decreases away from the poration site as shown in Figure 2.7(a-b). Figure 2.7 (c-d) show the time-

lapse surface intensity profile immediately after the optoporation and after 10 minutes of optoporation.

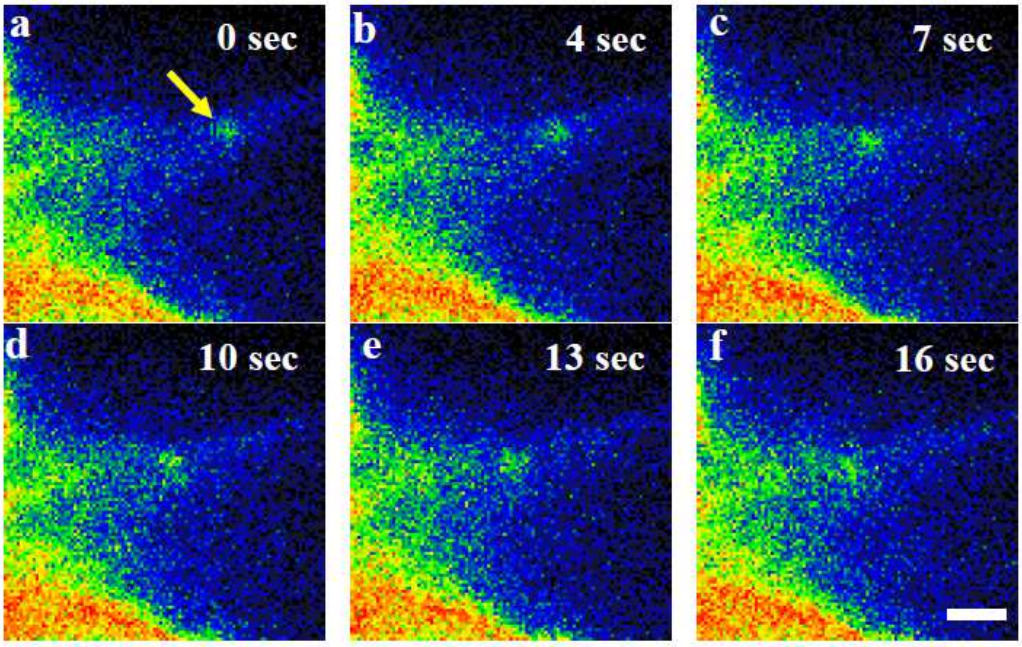

Figure 2.8: Transport of intracellular organelle following optical poration and rhodamine phalloidin staining (a-f). Time -lapse images immediately following the optoporation (Scale bar: 2 μm).

Following optical injection of RP, it was possible to detect the dynamics of intracellular organelle or vesicle as shown in Figure 2.8, which could have been a mitochondrion since mitochondrion are known to be non-selectively stained by Rhodamine Phalloidin [85]. This illustrates the potential of this method for studying other intracellular transport besides actin network reorganization and other dynamic processes in cells using molecular markers (e.g. antibody).

2.6.4 Numerical simulation of laser ablation based poration of cells

Many laser parameters, such as laser intensity, pulse width, repetition rate, and the focal volume (interaction volume) play important roles in laser-assisted optoporation [42]. Optoporation is only possible when the peak laser intensity reaches a threshold-value, producing sufficient free electron density at the focal volume. We are considering that the mechanism of poration via biological membrane ablation using a femtosecond laser is primarily due to low density plasma formation at the focal volume [37]. The low density plasma is formed by multiphoton ionization process, often referred to as cascade or avalanche ionization. The energy of a single photon with wavelength of 800 nm is 1.56 eV. In order to cross the band gap, which can be considered as 6.5 eV (that of water) for cell culture medium, we need at least five photons to cause electron transitions to the excitation band. The critical free electron density (plasma) at the laser's focus, above which laser ablation starts, is defined by

$$Q_{cr} = \frac{\omega^2 \varepsilon_0 m_c}{e^2} \qquad 2\text{-}1$$

where Q_{cr} is the critical plasma density, ω is plasma frequency, ε_0 is the dielectric constant in vacuum, and m_c is the mass of the electron. At 800 nm wavelength, this corresponds to a Q_{cr} =1.8x10^{21} cm^{-3}. Previous

investigations [86, 87] have correlated this to a necessary power density of 1.3 - 2.6x10^{13} W/cm^2. It is on this basis that we have chosen an experimental power density of 2.24 x 10^{13} W/cm^2 during optoporation, which lies within the theoretically predicted limit.

The axial cross-section of focal volume has been demonstrated to be an ellipsoid [88]. The short (*d*) and long (*l*) dimension of the ellipsoid focal volume are given by the following relations [89], assuming a large solid angle,

$$d = \frac{1.22\lambda}{NA} \qquad \text{2-2}$$

which results in a short (*d*) and long (*l*) axis values of 750 and 1800 nm, respectively.

$$\frac{l}{d} = \frac{1-\cos\alpha}{\sqrt{3-2\cos\alpha-\cos\alpha}} \qquad \text{2-3}$$

We have used the Gaussian distribution of laser irradiance at the focal volume with the above-mentioned major (*d*/2) and minor axes (*l*/2) to determine the ellipsoid distribution of irradiance.

$$I(r,z) = I(0,0)\exp\left(-2\left(\frac{r^2}{a^2}+\frac{z^2}{b^2}\right)\right) \qquad \text{2-4}$$

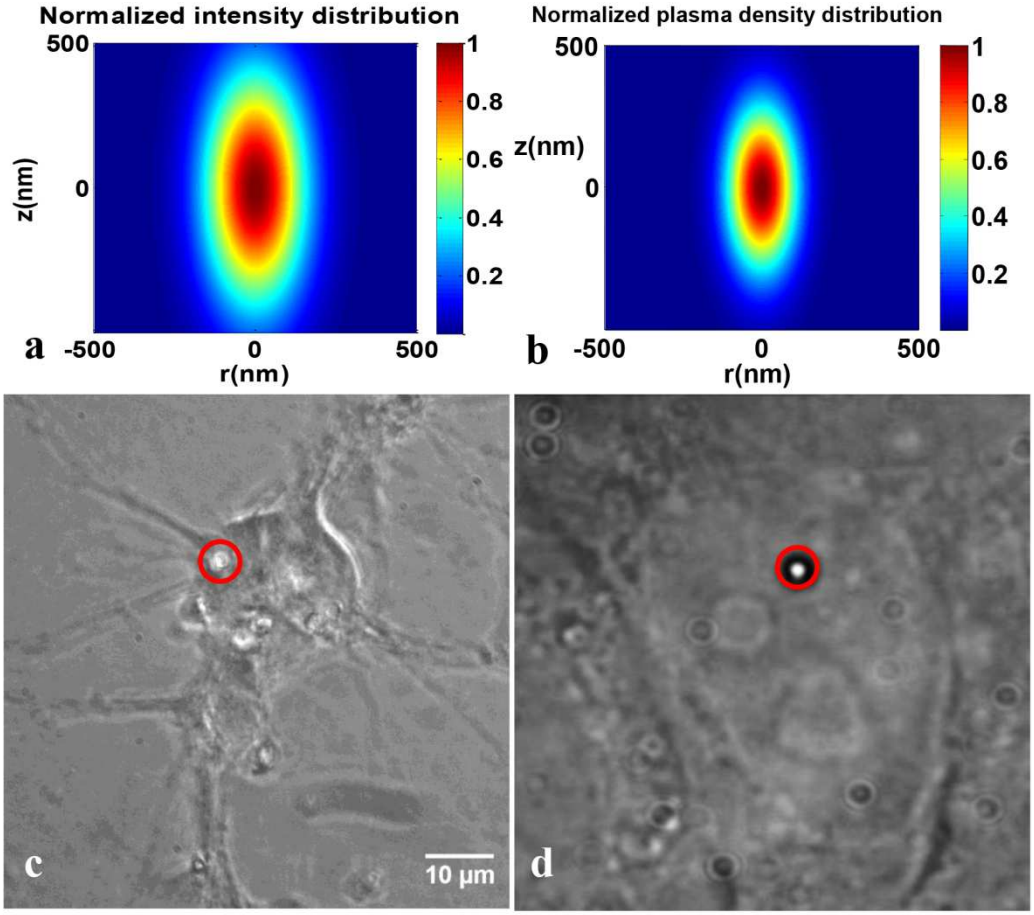

Figure 2.9: Theoretically calculated intensity (a) and plasma distribution (b) of the fs-pulsed focused laser beam at the focal plane. Transient holes observed during optoporation of cortical neuron(c), and HEK cells (d).

Where r and z are the coordinate in radial and axial distribution ($a=d/2$, and $b=l/2$).The free electron density produced during the laser irradiation is proportional to the intensity I^k [37], where k is the number of photons required to ionize the medium (k = 5, in our case).

$$Q(r,z) = \left[I(0,0) \exp\left(-2\left(\frac{r^2}{a^2} + \frac{z^2}{b^2} \right) \right) \right]^K \qquad 2\text{-}5$$

$$Q(r,z) = Q(0,0) \exp\left(-2K\left(\frac{r^2}{a^2} + \frac{z^2}{b^2} \right) \right) \qquad 2\text{-}6$$

where $Q(0,0) = I(0,0)^k$ represents the free electron density at the center of the focal plane. Plots of equations 2-5 and 2-6 are shown in Figure 2.9 (a -b). Experientially calculated pore size was 1.6 μm ±0.79 μm and theoretical calculation shows 0.7 μm. Plasma formed at the core region of the intensity distribution is expected to be smaller. Figure 2.9 (b - c) show the pore as observed at the instance of pulsed laser irradiation during bright-field imaging.

2.6.5 Dynamics of dye diffusion after optoporation

The dye diffusion time constant was experimentally determined by fitting the change in normalized fluorescence intensity with time (following optoporation) using Fick's law. Fick's first law of diffusion, $C - C_0 = D(dC/dt)$, a standard treatment for steady state diffusion, was used, where C is the concentration of fluorescent dye in optoporated cells at any instantaneous time, C_0 is the concentration of the dye in extracellular medium, and D is the diffusion coefficient. Thus, the increase in fluorescence intensity with time could be fitted to a single exponential function as follows:

$C/C_0 = 1-e^{-(t-t_0)/\tau}$, where C/C_0 is the normalized concentration of the fluorescent dye at time t, and t_0 is the initial time of dye influx with τ being the rise-time constant [52]. To calculate the diffusion coefficient and the diffusion time constant at different concentrations, we have used the flux equation. The flux through a unit area can be calculated as

$$J(x,t) = C(x,t) \cdot v(x,t) \qquad 2\text{-}7$$

where C is the concentration of dye molecules contained in the intracellular medium and *v* is the velocity of the dye.

The chemical potential is related to the concentration gradient by

$$\mu = \mu_0 + K_B T \cdot \ln\left(\frac{C}{C_0}\right) \qquad 2\text{-}8$$

where K_B is Boltzmann constant. The velocity of the particle in the viscous medium is calculated by

$$\vec{v} = \sigma \vec{F} \qquad 2\text{-}9$$

where $\sigma = 1/6\pi\eta r$*v*,

r being the molecule's radius of gyration and F; viscous drag force which is equals to the potential gradient. Differentiating eq. 2-8,

$$F = -\nabla\mu = -k_B T \cdot \nabla C \qquad 2\text{-}10$$

From above equations,

$$J = -\frac{k_B T}{6\pi r \cdot \eta} \cdot \nabla C \qquad 2\text{-}11$$

Comparing with Fick's law, we see that

$$J = -D\nabla C \qquad \text{2-12}$$

$$D = \frac{k_B T}{6\pi r \eta} \qquad \text{2-13}$$

with r = radius of gyration which is equivalent to $\sqrt{3/5}$ R,R:radius of dye molecule.

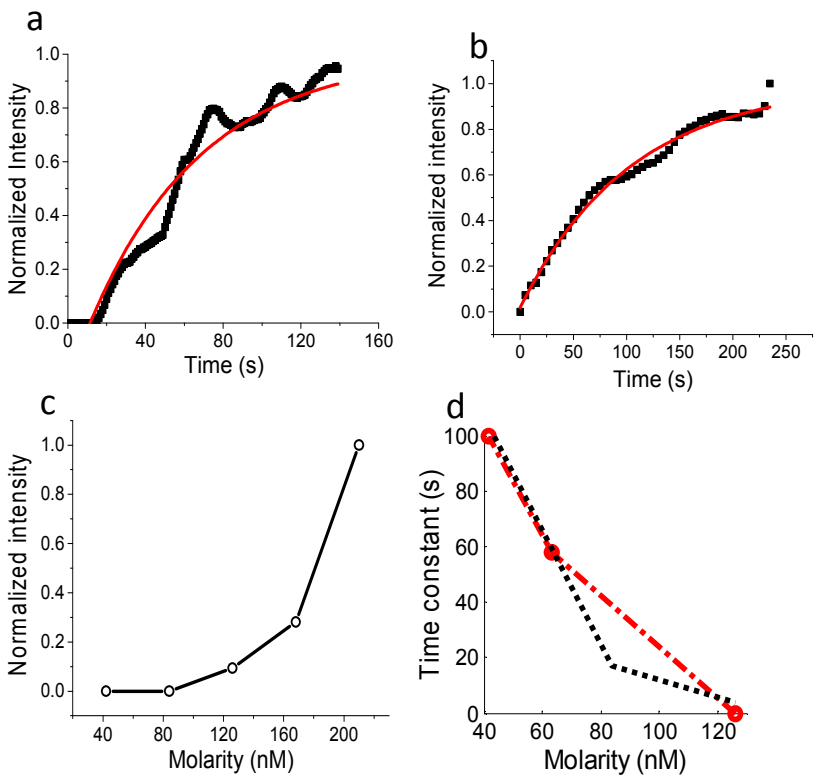

Figure 2.10: Dynamics of dye diffusion of optoporated cells. Increase in normalized fluorescence intensity of RP following optoporation in the case of (a) HEK cells (84 nM) and (b) rat cortical neuron (120 nM), and(c) HEK cells at 142 nM. (Fitted line is shown in red color), (d) Theoretical (red) and experimental (blue) variation of diffusion time constant as a function of molarity.

The solution of equation (2-12) in one dimension can be written as

$$C = C_0\left(1 - \exp\left(-\frac{t}{\tau}\right)\right) \qquad 2\text{-}14$$

$$\tau = \frac{t}{\ln\left(1 - \frac{C}{C_0}\right)} \qquad 2\text{-}15$$

Figure 2.10 (d) shows comparison of diffusion time constant between experimental values (blue line) and numerical simulations (red line) based on equation (2-14), where the time (t) has been fixed (40 sec). Using the previously measured [90] intracellular viscosity coefficient, the diffusion coefficient (D) was calculated by equation (2-13) and was found to be 2.13 $X10^{-8}$ cm^2/s, which matches with experimentally determined values of the diffusion coefficient of RP (1.38 $X10^{-8}$ cm^2/s).

2.6.6 Targeted laser assisted transfection of single opsin-plasmids

To achieve targeted transfection (optoporation) of cells with opsin encoding plasmids(ChR2 and ReaChR), we used the optimized laser parameters [72] for optoporation. Before optoporation, extracellular media was changed with new DMEM media containing plasmids (ReaChR or ChR2) with final concentration of 1 μg/ml and incubated for 30 minutes. Using this localized optoporation method, spatially-targeted cells can be selectively optoporated as shown Figure 2.11.

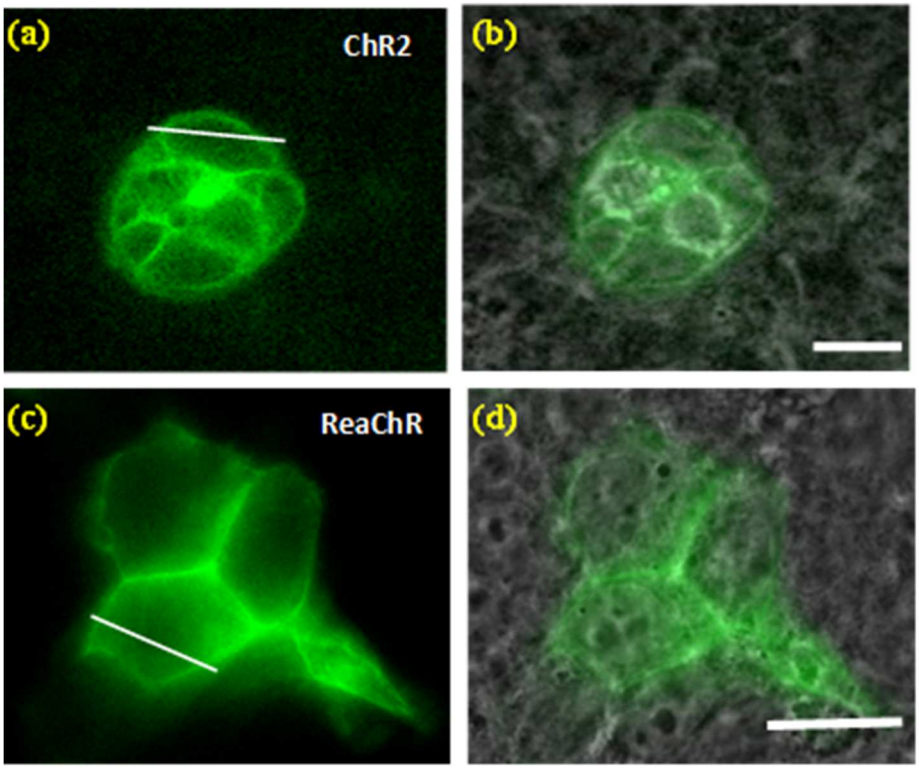

Figure 2.11: Targeted laser assisted transfection of single opsin-plasmids. (a) Representative fluorescence image of targeted ChR2-YFP optoporated HEK293 cell, overlaid on bright field image (b) showing highly-packed cells in mono layer. (c) Representative fluorescence image of targeted HEK293 cells optoporated with ReaChR-Citrine, overlaid on bright field image showing cells in monolayer (d). Scale bar: 15 μm.

Figure 2.11(a,c) show targeted femtosecond laser assisted transfection of single opsins (ReaChR and ChR2) in to HEK293 cells. The representative fluorescence image of targeted ChR2-YFP optoporated HEK cells (Figure 2.11a) and overlaid on bright field image (Figure 2.11b) has been shown. Similarly, Figure 2.11c and Figure 2.11d show fluorescence

images of the representative laser-targeted ReaChR-Citrine transfected HEK293 cells and overlaid with bright field image, respectively . Cellular morphology after laser transfection was found to be intact after 24-36 hours of post optoporation.

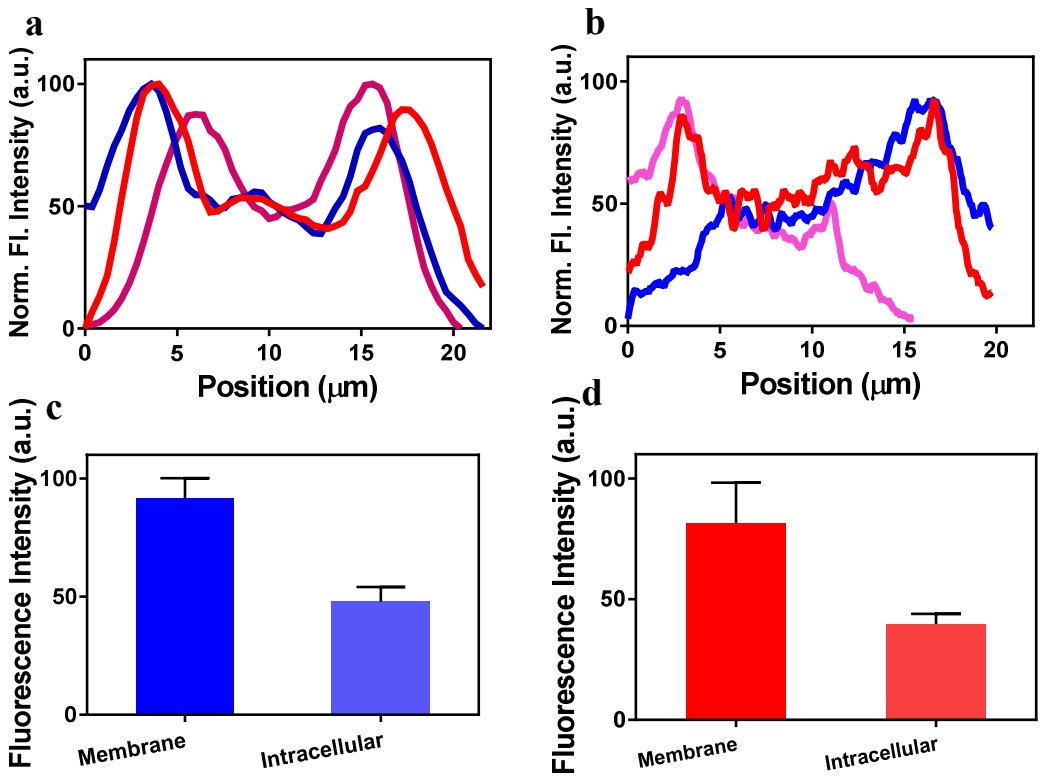

Figure 2.12: Representative fluorescence intensity (a,b) profiles of reporter proteins along lines drawn across cells as shown in Figure 2:11. Quantitative comparison (c,d) of expression on membrane and intracellular components in cells optoporated with ChR2 and ReaChR (N=5/each opsin, average ± S. D. *p<0.01 between membrane and intracellular components of opsin expressing cells).

Fluorescence intensity profiles of opsin-reporter proteins (YFP, Citrine) along the lines drawn across representative cells (Figure 2.11 a, c) have been shown Figure 2.12(a,b). The graphs show distinct peak at plasma membranes implying localized expression of ChR2 and ReaChR on plasma membrane. In Figure 2.12(c, d), the average value of reporter protein fluorescence intensity in membrane and intracellular region has been plotted for ChR2 and ReaChR (n=5).

2.6.7 Laser assisted transfection of large fused multi-opsin constructs: functional evaluation using broadband light

Figure 2.13 shows targeted laser assisted transfection of White-opsin (fusion of multiple opsins) into HEK293 cells and broad-band (white) light based optogenetic stimulation. Similar to ChR2 and ReaChR-optoporated cells, the White-opsin plasmids delivered by the femtosecond laser was found to be expressed on plasma membrane (Figure 2.13 a). Figure 2.13 b shows representative fluorescence intensity profiles of reporter proteins along lines drawn across cells (dotted white line in Figure 2.13 a). Quantitative comparison of expression on membrane and intracellular components in cells optoporated with White-opsin is shown in Figure 2.13c.

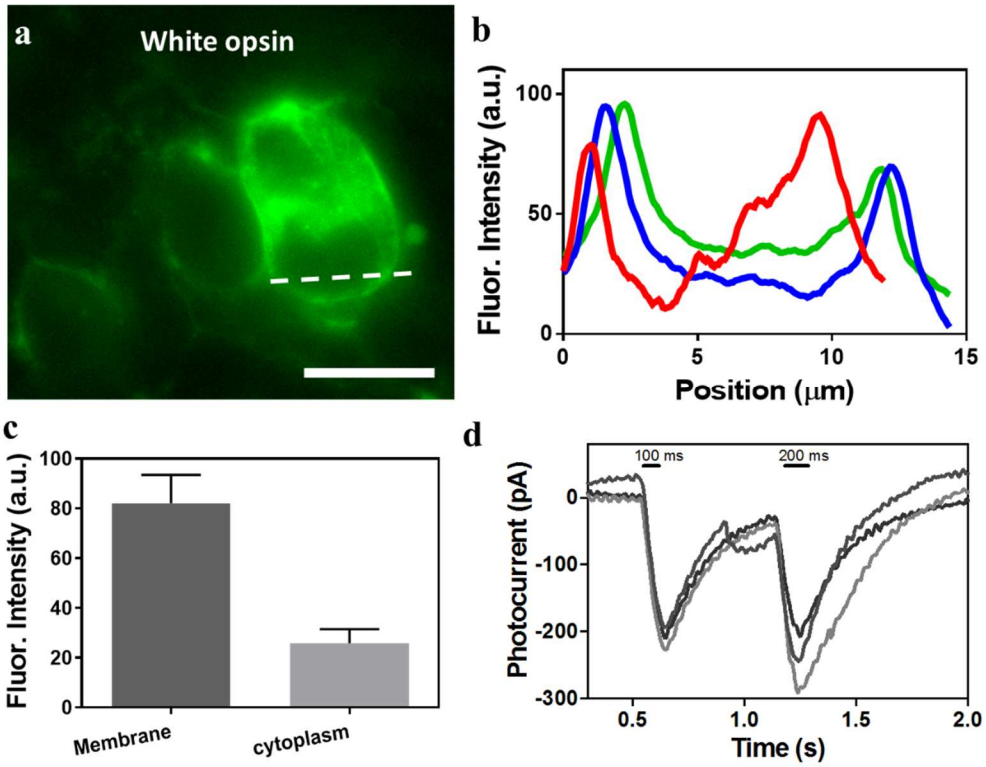

Figure 2.13: Laser delivery of large multi-opsin construct. (a) Fluorescence image of HEK cells after optoporation with White-opsin. Scale bar: 15 μm. (b) Representative fluorescence intensity profiles of reporter proteins along lines drawn across cells (dotted white line in a). (c) Quantitative comparison of expression on membrane and intracellular components in cells optoporated with White-opsin (N=5, average ± S. D. *p<0.01 between membrane and intracellular component of white-opsin expressing cells). (d) Representative inward photocurrent profiles in response to white-light optogenetic stimulation (0.06 mW/mm^2) at two different pulse widths (100 and 200 ms).

To evaluate the functional activation of White-opsin, broadband stimulation of White-opsin expressing cells was carried out using patch-

clamp electrophysiology. Representative inward photocurrent in response to white-light optogenetic stimulation (0.12 mW/mm^2) at two different pulse widths are shown in Figure 2.13 d, suggesting that low intensity broadband light can be used for generation of robust photocurrent in a spatially-targeted manner with high temporal resolution in case of White-opsin plasmids transfected cells.

2.6.8 Transfection of single and multiple opsin(s) using lipofectamine

Quantification of lipofectamine based transfection of different opsins is shown in Figure 2.14. In Figure 2.14 a,d & g, we show the representative fluorescence images of HEK293 cells transfected with ChR2-YFP, ReaChR-Citrine and White-opsin, respectively by lipofectamine.

In order to quantify protein expression in plasma membrane and intracellular components, intensity line profiles were plotted and have been shown in Figure 2.14 b, e and h for ChR2, ReaChR and White-opsin respectively (lines were drawn across representative cells). Quantitative comparison of expression on membrane and intracellular components in ChR2 is shown in Figure 2.14 c. Similarly, expression of ReaChR-Citrine (Figure 2.14 f) and White-opsin (Figure 2.14 i) has been shown.

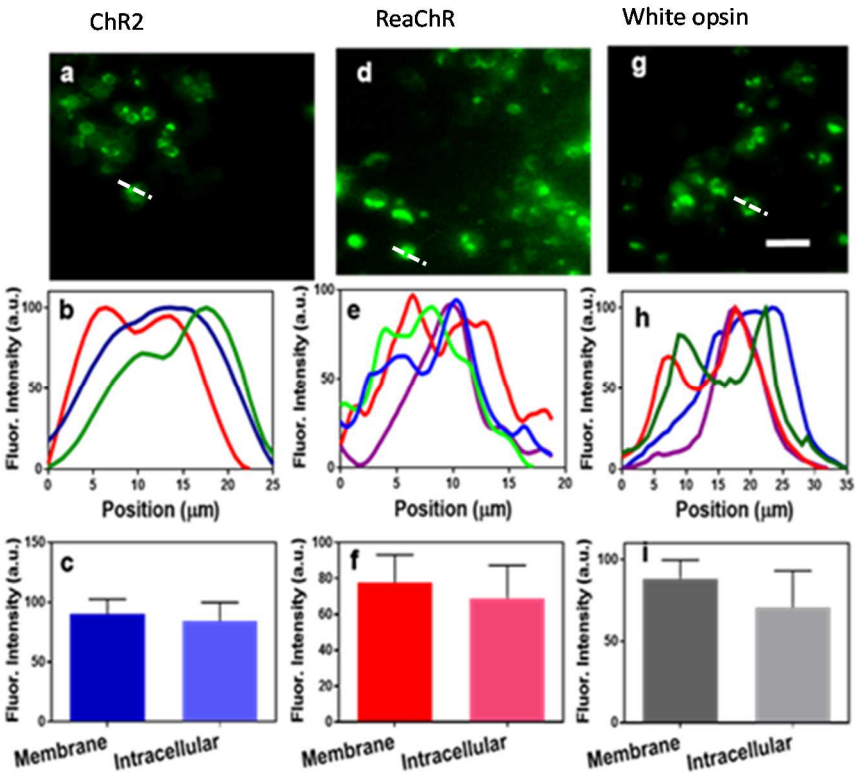

Figure 2.14: Quantification of lipofectamine based transfection of different opsin-plasmids. (a-c) ChR2; (d-f) ReaChR; (g-i) White-opsin, transfected HEK 293 cells. Scale bar: 20 μm. (b, e, h) Representative intensity profiles of opsin-reporter protein fluorescence along lines drawn (shown in dotted lines) across cells. Quantitative comparison of protein expression ChR2 (c), ReaChR (f) and White-opsin (i). N=6/opsin. Average ± S. D.

In cells lipofected by opsin-plasmids, higher intracellular fluorescence leading was observed and no distinct peaks (across membrane) as can be seen in Figure 2.14b, e&h. Therefore, no statistical significance difference between membrane and intracellular expression was observed in lipofected cells.

2.6.9 Quantitative comparison between optoporation and lipofection

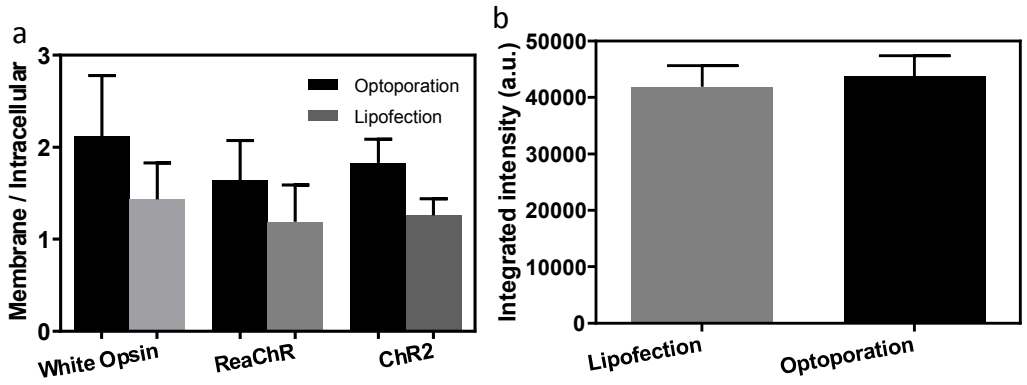

Figure 2.15: Quantitative comparison between opsin expression distribution, ratio of membrane to intracellular (a) by optoporation and lipofection and (b) fluorescence intensity of opsin in same ROI.

Figure 2.15 a summarizes the quantitative comparison between opsin expression distributions (ratio of membrane to intracellular) as a result of two non-viral gene delivery methods: optoporation and lipofection. Higher membrane to intracellular ratio of expression in optoporated cells as compared to lipofection (Figure 2.15 a) can be attributed to the spread morphology of opsin-expressing cells in case of optoporation as compared to those transfected by lipofection (which tend to become spherical). The amount of expressed protein is quantified by measuring the intensity of reporter fluorescence signal both in case of lipofection and optoporation selecting the equal area ROI both in lipofection and optoporation. This has been shown in Figure 2.15 b. Calculation of the total intensity from individual cells shows no significant differences between lipofection and optoporation.

2.6.10 Visualization of plasmid insertion after transfection

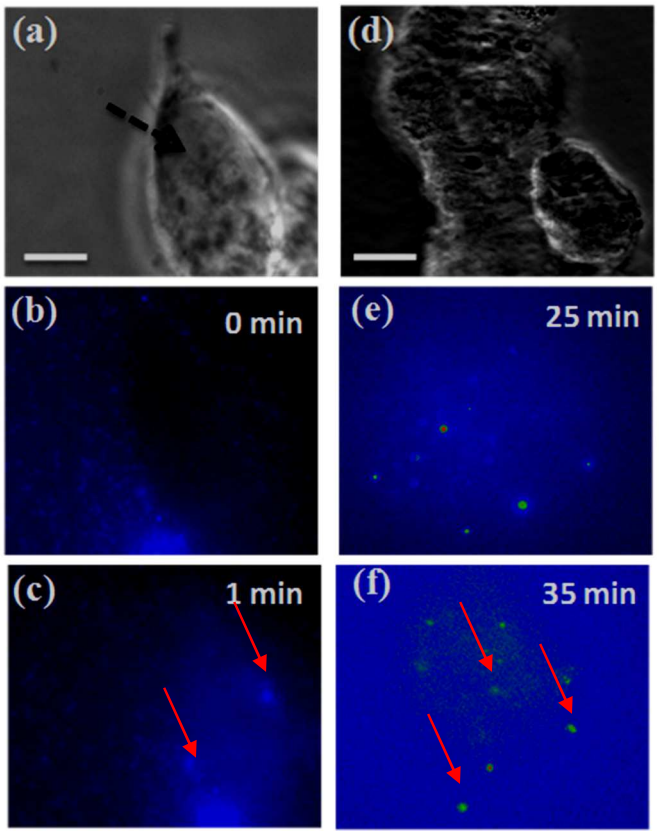

Figure 2.16: Visualization of white-opsin plasmids insertion into HEK cells. (a-c) Optoporation: (a) Bright field, (b) fluorescence of Propidium iodide stained White-opsin plasmids in extracellular medium, (c) Increase in intracellular fluorescence (and few distinct specks, marked by red arrow, attributed to PI-stained plasmids) after optoporation (at site black arrow-marked in a).(d-f) Lipofection: Bright field image of multiple HEK cells (d), and fluorescence images of PI-stained White-opsin plasmids after 25 min (e), and 35 min (f) of incubating the cells with lipofectamine-plasmid mixture (Scale bar: 5 μm).

Visualization of White-opsin plasmids insertion by optoporation or lipofection into HEK cells is shown in Figure 2.16. Increase in intracellular fluorescence (and few distinct specks marked by arrow attributed to propidium iodide-stained White-opsin plasmids) is observed after optoporation (Figure 2.16c). Similarly, the propidium iodide-stained white-opsin plasmids were observed in the cytoplasm of the lipofected cells (Figure 2.16 e, f).

2.7 Discussion and conclusion

The targeted optical injection of impermeable dye (Rhodamine Phalloidain) and plasmids (ChR2 and ReaChR) into HEK cells and rat cortical neurons is an important step in the advancing technologies used to visualize intracellular actin networks as well as detection of cellular and intra-cellular activities. It is notable that Rhodamine Phalloidin is one of the most trusted and widely used markers for f-actin networks *in vitro* due to its fluorescence efficiency and small relative size. On the other hand, use of light-sensitive (visible to NIR band) opsins to modulate the electrophysiological activities of cells and tissues has rapidly advanced the field of neuroscience. The existing non-intrusive methods of delivery of exogenous molecules, indicators, or plasmids lack localized and targeted delivery. Delivery of o impermeable molecules into the cytoplasm of targeted cells requires microinjection by mechanical needles or

microelectrodes, which often causes rupture of cells, and contamination. The virus-based transfection method is also prone to cause unexpected inflammatory responses, immunological reactions, and limits the size of plasmid that can be packaged for delivery, whereas optical delivery of the impermeable dye or other exogenous molecules (opsin-plasmids) into cells by femtosecond laser beam offers significant advantages over other methods of injection/transfection.

A substantial barrier to clinical translation of optogenetics method for vision restoration is delivery of opsin-encoding genes into spatially-targeted regions of degenerated-retina. For example, spatially-targeted delivery of opsin-encoding gene is required in peripheral retina or macula, which begins to lose light sensitivity due to loss of photoreceptors in case of RP and AMD respectively. Furthermore, patient-to-patient variability and time-dependent changes in spatial-distribution of retinal-degeneration demands site-specific expression of opsins. Unlike viral method, use of spatially-targeted optoporation will allow expression of the opsin(s) in areas of retinal degeneration, allowing effective vision restoration. With viral or other non-viral (e.g. electroporation, lipofection) method, the constructs will be delivered everywhere, causing un-controlled expression over the whole retina, perturbing the already-functioning retinal regions. Further, delivery of macro construct encoding multiple opsins with spectrally-separated

activation peaks over the whole visible spectrum will lead to higher photocurrent in response to ambient white light as demonstrated in Figure 2.13. This will enable generation of action potential in White-opsin sensitized neurons at much lower intensity spectral density (intensity/bandwidth) than conventional use of monochromatic light (e.g. Blue) and single narrow-band opsins (like ChR2). Though different viral vectors can separately deliver different plasmids encoding for the different spectral component-opsins, same stoichiometric expression of the different spectrally-sensitive components in each cell cannot be guaranteed. Therefore, we believe the application of spatially-targeted laser transfection of macro-constructs of White-opsins in degenerated retina will allow efficient stimulation of higher order retinal cells in areas of photoreceptor-degeneration by ambient white light, leading to visual restoration.

However, there is great challenge to optoporate myriads of cells simultaneously without compromising the cell viability. Multiplexing the laser beam using spatial light modulator (SLM) and estimating proper laser parameters before conducting experiments will help to overcome this problems. To conclude, ultrafast near IR laser microbeam was used for delivery of single and multi-opsin constructs to targeted cells. Effectiveness and functioning of the multiple-opsin sensitized cells is confirmed by patch-clamp electrophysiology. The near-infrared optoporation method will not

only eliminate the requirement of multiple viral delivery and possible immunogenic reactions, it will also be able to deliver wide-spectrally sensitive opsin encoding macro-constructs to spatially-targeted degenerated retina areas. Such spatial delivery of genes to peripheral retina/macula is ideal for sensitizing degenerated-retinal areas, thus paving the way for restoring lost-vision of RP/AMD patients. This will allow higher sensitivity of opsin sensitized higher-order neurons in targeted retinal areas (having photodegeneration) to ambient white light, and therefore, significantly lower activation-threshold in contrast to conventional approach of narrow-band opsin and/or intense, narrow-band light based active-stimulation.

In this study, femtosecond-based optoporation of biological cell for the delivery of plasmids or dyes has been demonstrated and discussed. This method can be also used for delivery of multiple genes in a single cell, or single gene in multiple cells by multiplexing the laser beam and provides an invasive and sterile alternative to traditional cell transfection techniques. Optoporation can be done in any existing multiphoton microscopy system (no need for additional experimental set up), and the same system can be used to transfect as well as provide localized stimulation (two-photon stimulation). Therefore it might play an important role in the ambitious neural activity mapping project [91]. Further, viral delivery method limits the size of

plasmid that can be packaged for delivery which may restrict its use to carry single opsin plasmid rather than multiple opsins (such as White-opsin). Optoporation of opsin-plasmid(s) into cells offers significant advantages over other methods of delivery (e.g. micro-injection, electroporation, lipofection, and viral transfection) owing to its capability of delivering large therapeutic molecules (e.g. >10 kb), spatial and temporal selectivity and absolute sterility.

Chapter 3

Two- photon optogenetic stimulation

3.1 Two-photon excitation

The concept of two-photon optogenetic stimulation is similar to the two-photon florescence excitation. Two-photon excitation is based on the idea that two-photons of approximately half the energy that is needed for single photon excitation can also excite atoms or molecules in one quantum event. Each photon carries approximately half the energy necessary to excite the molecule [92] .

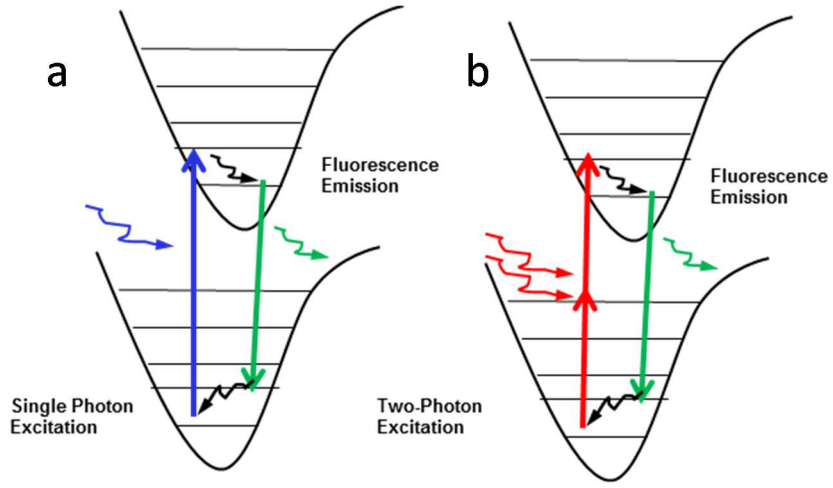

Figure 3.1: Jablonski diagram. Molecule gets excited to higher state by absorbing photon and gives fluorescence light during relaxation by (a) single-photon excitation and (b) two-photon excitation.

These two-photons should hit the excitable molecule virtually at the same time. Since the two-photon cross-section is extremely low, this

process requires high density of photons, only possible from focused pulsed laser sources. The two-photon excitation or transition of molecule is proportional to the square of the excitation intensity, a non-linear process [93].

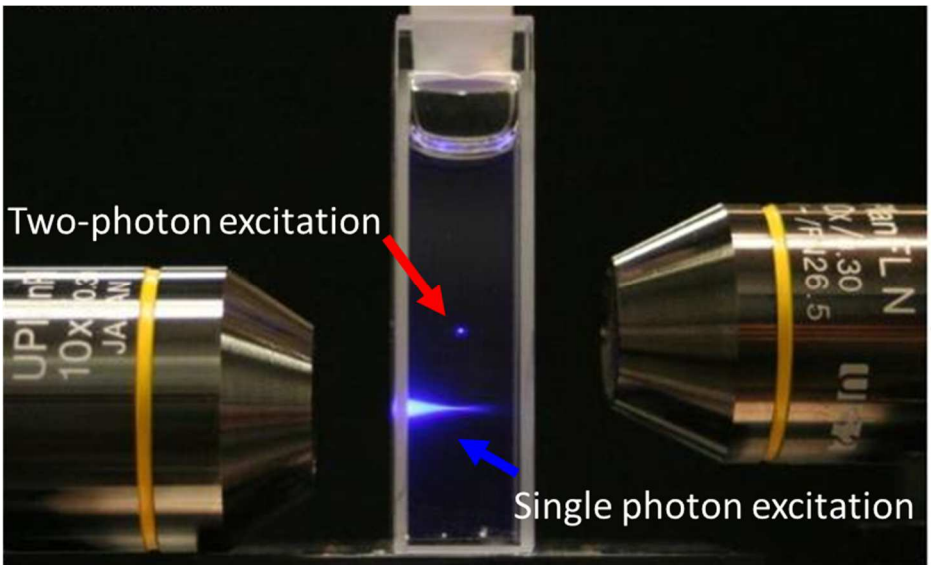

Figure 3.2: Visualization of two-photon and single photon excitation. The light from a tunable Ti: Sapphire laser (tuned to 760 nm, 200 fs pulse width, 76 MHz repetition rate) was equally split into two beams and SHG crystal was placed in one of the beam. Figure shows two-photon excitation of fluorine (shown in red arrow) and single photon excitation (shown in blue arrow), (http://chemistry.cos.ucf.edu/belfield/photophysics).

The discovery of two-photon microscopy is an important step in imaging of biological sample. Figure 3.2 shows the experimental comparison between two-photon (red arrow) and single photon (blue arrow) excitation of fluorine. As it can be seen, two-photon excitation is localized in

sub micrometer axial transverse dimension whereas single photon beam excites the sample along its path above and below the focal plane as well. Thus, two-photon excitation of the biological sample provides unique advantages over the single photon excitation. These advantages include less photo-damage of the sample, localized excitation with sub-micrometer resolution and in-depth excitation capabilities [94]. Theoretically multiphoton excitation was predicted by Maria Goeppert-Mayer in her doctoral dissertation on the theory of two-photon quantum transitions in atoms in 1931. However, it took long time to verify this theory in the lab due to lack of availability of the high intensity ultra-fast laser source at that time. After 32 years of theoretical prediction, in 1963, Franken et al published the first report on two-photon excitation (TPE) of CaF2:Eu2C fluorescence [95]. After this discovery, intensive research began in the field of two-photon excitation. Two-photon excitation is not only important in imaging of biological sample, but is equally important in understanding the electronic structure of the sample.

3.2 Two-photon optogenetic stimulation

Deep brain stimulation is a widely used method to treat patients suffering from muscle tremors, stiffness, impaired or slowed movement, and partial paralysis, which occurs in conditions like Parkinson's disease [96].

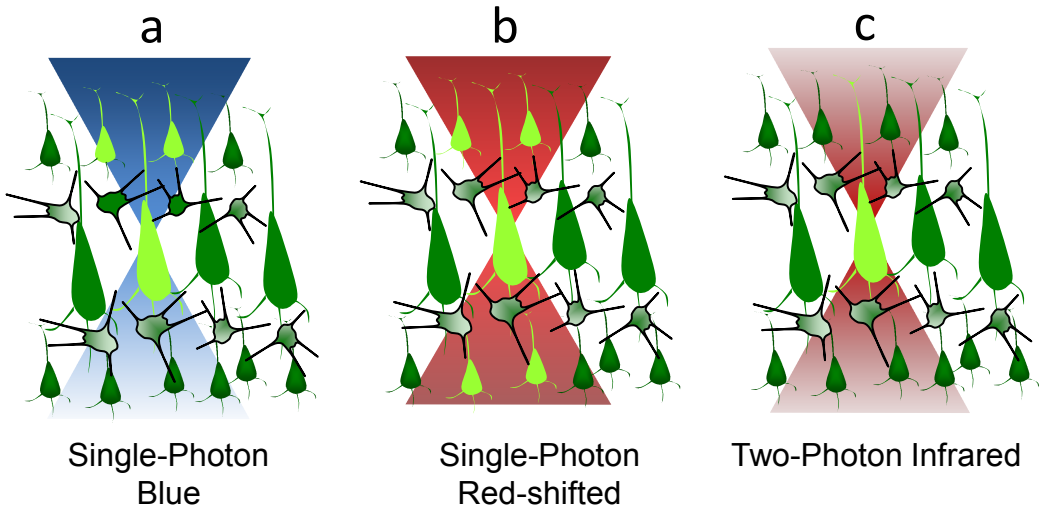

Figure 3.3: Schematic comparison: (a) single-photon blue excitation, (b) single-photon red-shifted excitation, and (c) two-photon optogenetic stimulation (TPOS).

Treatment provided through deep brain stimulation can block abnormal nerve signals [97] and reduce or eliminate neurological movement disorders. Conversely, deep brain stimulation can be employed to facilitate the firing of many neurons simultaneously, which can lead to the release of hormones like oxytocin [98]. Though electrical simulation has severe side effects such as widespread damage of cells and non-specific deep brain stimulation, doctors are still using this method owing to the lack of other methods to replace it.

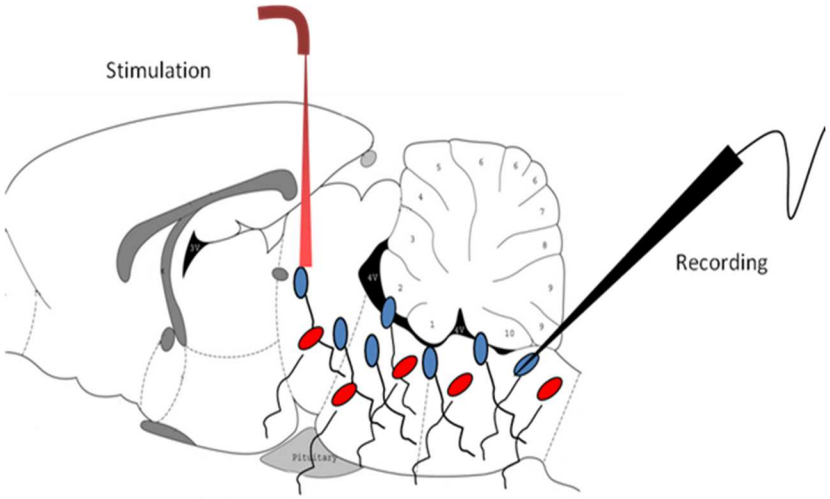

Figure 3.4: Schematic diagram showing method of probing functional relationship between neurons at different location in two-photon localized optogenetic stimulation. Red and blue represents different types of neuron.

Optical stimulation would be much more advantageous than electrical stimulation in several ways such as spatially and genetic selectivity . Though single photon optogenetic stimulation may replace the conventional stimulation methods, it is not suitable to stimulate the cells located at depth greater than 1 mm due to significant absorption and scattering of visible light. Moreover, we cannot get localized stimulation by using single photon optogenetic stimulation. The two-photon optogenetic activation using near infrared laser beam can provide both deep penetration and high spatial precision, achieved by virtue of the non-linear nature of ultrafast light interaction as shown in Figure 3.3. Thus, targeted stimulation

and functional connectivity in the brain can be mapped as shown in Figure 3.4.

3.3 Channelrhodopsin-2: light-gated membrane channel

Channelrhodopsin-2 (ChR2) is a light gated cation channel derived from the microbial *Chlamydomonas reinhardtii* algae [99]. ChR2 can be expressed in other biological cells including mammalian cells. Recent developments in neuroscience have shown that ChR2 can modulate activities of neurons as well as other cell type [100]. These types of opsins in conjunction with light depolarize (channelrhodopsin-2) or hyperpolarize (halorhodpsin) [101] the cells, thereby evoking or inhibiting action potentials in neurons. Though ChR2 has been widely used in biology as well as in neuroscience research, many questions still remain unanswered regarding the channel activation response and its complete photocycle. Several modified forms of the light sensitive opsin, each encoded with single gene, have been expressed in excitable cells to alter their conductance [102].

3.4 Photocycle of Channelrhodopsin-2

The details of the photocycle of ChR2 are still unknown. However, three or four states photocycles of ChR2 have been proposed to explain its photochemical cycle. To understand in a simple way, a two state photocycle of ChR2 would comprised of an open state (O) and closed state (C) [103]. The opening and closing of ChR2 is on the scale of milliseconds [99], which

is highly useful for studying neuronal modulation and complex circuitry. The opening of ChR2 molecules is primarily due to conformational change of all-trans retinal (ATR). Upon incidence of blue light, ATR changes from trans to cis conformation which leads to ChR2 molecule opening as shown in Figure 3.5 [104]. This change in conformational state depolarizes the cells by passing cations across the channel and cell membrane. In absence of light, the channel closes letting the cell to once again reach its resting membrane potential within millisecond time scale.

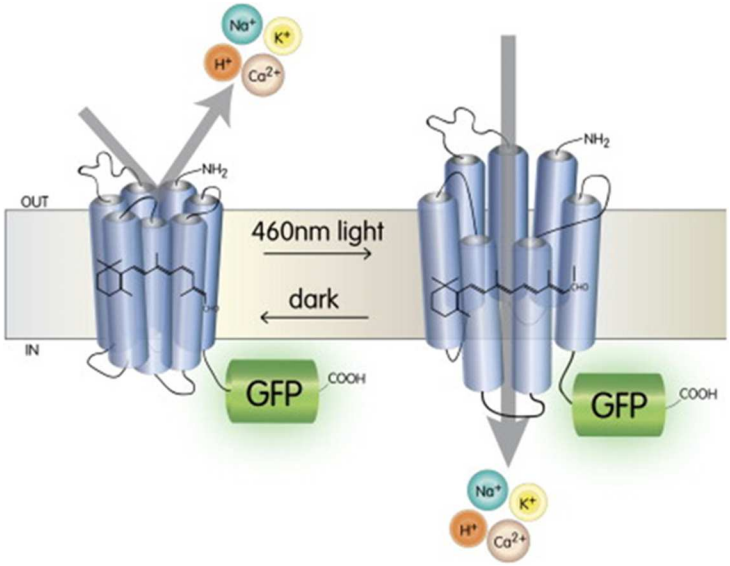

Figure 3.5: Photoisomerization of Channelrhodopsin-2 (*Flannery et.al*, Neuron, 2006.03.027).

Even in the case of single photon excitation, since photocycle of the ChR2 is not known completely, understanding dynamics of ChR2 upon two-photon excitation of ChR2 is complex. Further, All-trans-retinal molecule is

known to produce second harmonic generation (SHG) which can enhance ion channel opening by single photon excitation process [105]. Other possibilities such as resonance energy transfer from the neighboring molecule and photothermal excitation along with two-photon optogenetic stimulation cannot be completely ignored in a ultrafast laser based stimulation.

3.5 Simplified theory of two-photon optogenetic stimulation

A simplified model of saturation-limited ChR2 activation by two-photon excitation (TPE) was applied to understand the two-photon activation ChR2 sensitized HEK cells [106]. This model describes only the transient photocurrent arising from a population of illuminated ChR2 molecules and assumed that the population of molecules was initially homogenous and in the excitable ground state. A ChR2 molecule with a Two-photon absorption cross-section σ_2 and illuminated with intensity $I(t)$, should absorb light at a rate $(\sigma_2/2)I(t)^2$. For this single-photocycle model, the concentration $\rho_g(t)$ of molecules in the ground state is given as [106]

$$\rho_g(t) = \rho_{g0} e^{-\frac{\sigma_m}{m} I(t)^m t} \qquad 3\text{-}1$$

where m =1,2 for single photon and two-photon,

$$\rho_g(t) = \rho_{g0} e^{-\frac{\sigma_2}{2} I(t)^2 t} \qquad 3\text{-}2$$

where ρ_{g0} is the ground-state concentration at t=0. Considering the cell membrane to be in a plane, the ChR2-molecules are illuminated with a radially symmetric profile $I(r, t)^2$. The rate of recruitment to a particular excited state with a population $N(t)$ is given by [106],

$$\frac{dN(t)}{dt} = \eta \frac{\sigma_m}{m} \int_s I(r, t)^m \rho_g(r, t)\, dA \qquad 3\text{-}3$$

where m=1,2 for single-photon and two-excitation; η is the quantum efficiency; $\rho_g(r, t)$ having an explicit spatial dependence. $N^*(T)$, the number of current-conducting molecules at time $t = T$ after light onset, can be calculated by weighting the excitation rate with the channel's impulse-response function and integrating in time,

$$N^*(T) = \int_0^T \frac{dN(t)}{dt} [e^{-\frac{T-t}{\tau_2}} - e^{-\frac{T-t}{\tau_1}}] dt \qquad 3\text{-}4$$

where τ_1 denotes latency of molecules entering the current-conducting population after excitation and τ_2 denotes the characteristic decay time constant of these currents. Equation 3-4 gives the total number of ChR2 molecules excited under illumination. As ChR2 is a non-specific cation channel, total current from single ChR2 molecule depends on the permeability of sodium, potassium and calcium ions through the membrane [107].

Let G_{Na}, G_K and G_{Ca} be the conductance of respective ions during ChR2 opening as ChR2 is non selective cation channel and V_m is the membrane potential.

The Then, $I = V_m * G_{Na} + V_m * G_K + V_m * G_{Ca}$ instantaneous current is given by

$$I^*(T) = I * N^*(T)$$

Integrating equation 3-4 and neglecting the decay time to compare with experimentally measured peak,

$$N^*(T) = N_t \eta \{ \frac{\tau_1}{\tau_g - \tau_1} (e^{-\frac{T}{\tau_g}} - e^{-\frac{T}{\tau_1}}) \quad 3\text{-}5$$

where τ_g is the ground state life time, defined as $1/\sigma_1 I$ for single photon and $2/\sigma_2 I^2$ for two-photon excitation.

Here, $I^*(max) = \eta * I * N^*(T)$

Simplifying this equation,

$$I^*(Max) = I * \alpha * \eta * I_0^2 * (e^{-cI_o^2})$$

where I = Single channel ionic current

α = proportionality constant

C = constant

η = quantum efficiency

I_0 = Intensity.

An experiment was designed to study the variation of current with the increasing intensity. All other parameters were kept constant at given time and only intensity was varied. The nature of this equation is non-linear with quadratic-dependence on intensity. However, two photon activation of ChR2 is not similar to the two-state fluorescence excitation since the fluorescence excitation is electronic state transition whereas the ChR2 activation is led by conformational change of its chromophore (All-trans-retinal). Further, we hypothesize that the optogenetic stimulation may contain contribution from photothermal alteration in membrane and second harmonic generation (SHG) by the all-trans-retinal molecule, which activates the ChR2 via single-photon [108].

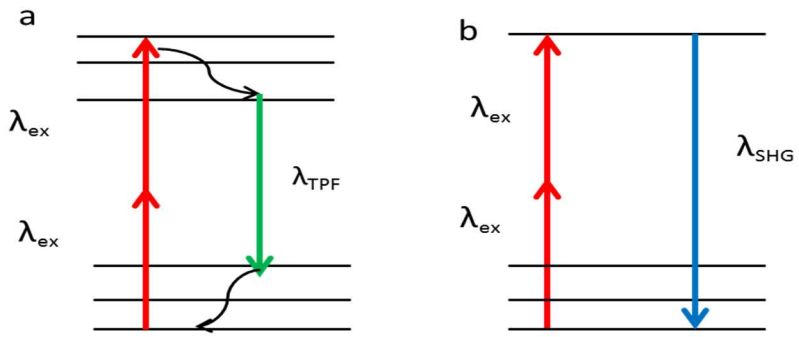

Figure 3.6: Schematic diagram showing difference between (a) two-photon fluorescence and (b) second harmonic generation.

Second harmonic generation is a non- linear optical process in which multiple photons with same frequency, interacting with non-linear material, are combine to form a new photon of twice the frequency. The near infra-

red light from the Ti: Sapphire laser incident in the brain tissue or cells (non-linear medium) has been found to have higher probability of producing second harmonic wavelength (with 25% efficiency) [109]. Furthermore, when the all-trans retinal molecule (chromophore) is closely linked with the channelrhodopsin-2, there is the possibility of energy transfer from the neighboring molecule by the process called resonance energy transfer.

As NIR light is used for two-photon optogenetic stimulation, we cannot disregard the possibility of photothermal effect since water has non-negligible absorption in NIR region. Thus, the mechanism underlying neuronal stimulation by NIR light is thought to be mediated by photothermal transients, which can also potentially be induced using extrinsic absorbers (Photo-Absorber Induced Neural-Thermal Stimulation or PAINTS) [110]. Recent research shows the mechanism of IR neuronal stimulation is due to change in capacitance of cell membrane caused by increase in temperature [62].

3.6 Materials and Methods

3.6.1 Cell culture

HEK 293 cells were transfected with the ChR2-EYFP construct, cloned into pcDNA3.1 neo (Invitrogen, USA). Transgene-expressing cells were identified by visualizing the EYFP fluorescence under suitable illumination (514 nm). Stable clones were selected with 200 mg/l G418 and

colonies were picked after 2 weeks, and then expanded. Clones that showed the highest level of EYFP fluorescence were chosen for the optogenetics experiments. Cells were maintained at 37°C, 5% CO_2 in DMEM containing 10% fetal bovine serum. For generating light activation, cells were loaded with all-trans retinal (1 μM) for at least 6 hours and activated with fiber-optic laser beam.

3.6.2 Patch-clamp recording from optical stimulated cells

The opto-electrophysiology setup was developed on the Olympus-upright laser-microscope platform using a computer-controlled amplifier system (Axon Multiclamp 700B, Molecular Devices Inc., USA) as shown in Figure 3.7. Parameters of the pipette puller were optimized to obtain the desired borosilicate micropipettes of resistance from 3 to 7 MΩ for a whole-cell patch-clamp. The micropipette was filled with an intra-cellular solution containing (in mM) 130 K-Gluoconate, 7 KCl, 2 NaCl, 1 $MgCl_2$, 0.4 EGTA, 10 HEPES, 2 ATP-Mg and 0.3 GTP-Tris (pH 7.4). The electrode head stage was mounted on a XYZ micromanipulator (Newport Inc.). The standard extracellular solution containing (in mM): 150 NaCl, 10 Glucose, 5 KCl, 2 $CaCl_2$, 1 $MgCl_2$ was buffered with 10mM HEPES (pH 7.3). The output from the amplifier was digitized using a National Instruments DAQ card (PCI 6221). For electrophysiological recording, the hardware was interfaced with patch-clamp software from the University of Strathclyde (Glasgow, UK;

noncommercial use). Electrical recordings were performed at a holding-potential of -60 mV at room temperature (20-24ºC). The whole system was built on a vibration isolation table (Newport Inc.) and electrical isolation was done by means of a Faraday cage that was placed around the setup. Aluminum foil was used wherever necessary to reduce noise level. Temperature of the sample stage was adjusted during the patch-clamp experiments.

The Ti: Sapphire laser wavelength was tuned from 800 nm to 920 nm using computer-controlled software (Mai Tai), to compare the wavelength-dependent efficacy in stimulating the targeted ChR2-sensitized and control cells. The number of pulses at each point of irradiation was controlled by a computer-controlled mechanical shutter (S). The pulse energy of the fs (femto second) laser beam was varied by controlling the orientation of a circular variable neutral density filter (NDF). The laser beam power at the focal plane was measured using a power meter (PM100D, Thorlabs Inc.). Using motorized stage movement, the region of interest was aligned with the center of the laser spot.

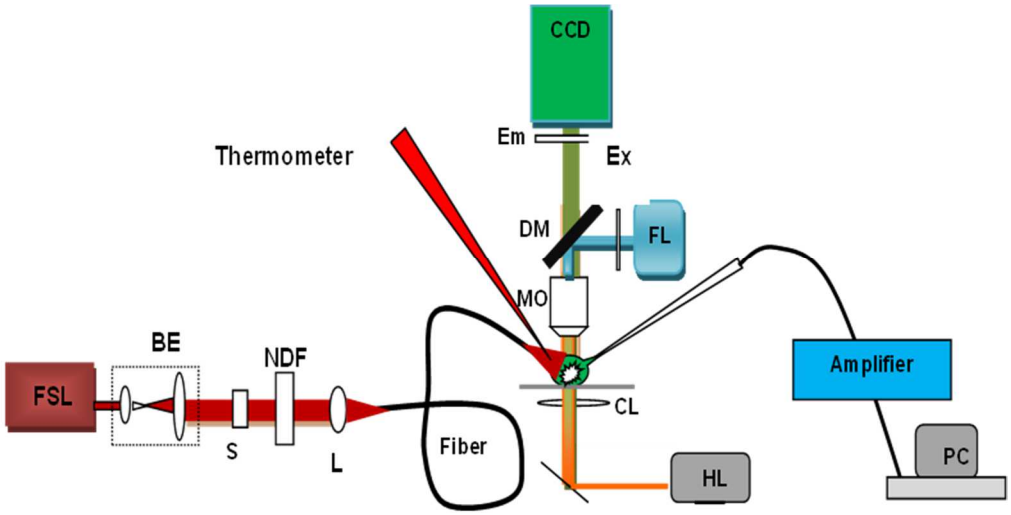

Figure 3.7: Patch-clamp set up for fiber-optic two-photon optogenetic stimulation. FSL: Tunable Ti: Sapphire Laser; BE: Beam Expander; S: Shutter; NDF: Neutral density filter; L: Lens for fiber coupling; FL: Fluorescence excitation source; Ex: Excitation Filter; Em: Emission Filter; MO: Microscope Objective; CL: Condenser lens; DM: Dichroic Mirror; M: Mirror; HL: Halogen Lamp.

For activation of ChR2-expressing cells (identified by YFP fluorescence), the optogenetic stimulation beam (473 nm, or NIR) was delivered via a 50 µm core optical fiber, mounted on a mechanical micromanipulator so as to position the tip of the fiber near the desired cell being patch-clamped. For generating and controlling pulses of light, the electromechanical shutter in the laser beam path was interfaced with a PC. TTL pulses of desired frequency were generated using National Instruments (PCI 6221) card in order to generate required laser pulses for activation. For electrophysiological measurements subsequent to optical

activation, the shutter was synchronized with the patch-clamp recording electrode. The whole system was built on a vibration isolation table (Newport Inc.) and pClamp software was used to analyze the data.

3.7 Results

3.7.1 Multimode fiber beam leads to non-linear two-photon excitation

Since first demonstration [111] of *in vitro* two-photon optogenetic stimulation (TPOS) of excitable cells and brain slices by using point or scanning laser beam, there has been growing [106, 112-114] applications of this method for better probing of neural circuitry. TPOS using near infrared (NIR) laser beams provides deeper penetration as compared to conventional single-photon [115] due to low absorption and scattering coefficients of tissue in the NIR spectral region [116-118] . Further, high spatial precision (important for activating sub-cellular structures) is achieved by virtue of the non-linear nature of ultrafast light interaction with the opsins. It is important to note that the two-photon cross-section of opsins such as channelrhodopsin-2 (ChR2) has been estimated to be larger than that of most fluorophores [106], and therefore two-photon beam has potential for efficient stimulation of genetically-targeted opsin-expressing cells in a dense tissue. It is important to note here that different scanning modes (spiral, raster) have been applied for the excitation of ChR2-expressing cells to optimize the efficiency of excitation [106]. While there

have been recent advancements in TPOS-technology by spatial-sculpting [112] and/or temporal-focusing [113] of the laser beam, the two-photon activation has only been demonstrated using bulky microscopic objectives. In contrast to the use of a microscope objective and scanning two-photon laser beam, here, we have used a multimode beam for non-scanning fiber-optic two-photon optogenetic activation (FO-TPOS) of ChR2-transfected excitable cells.

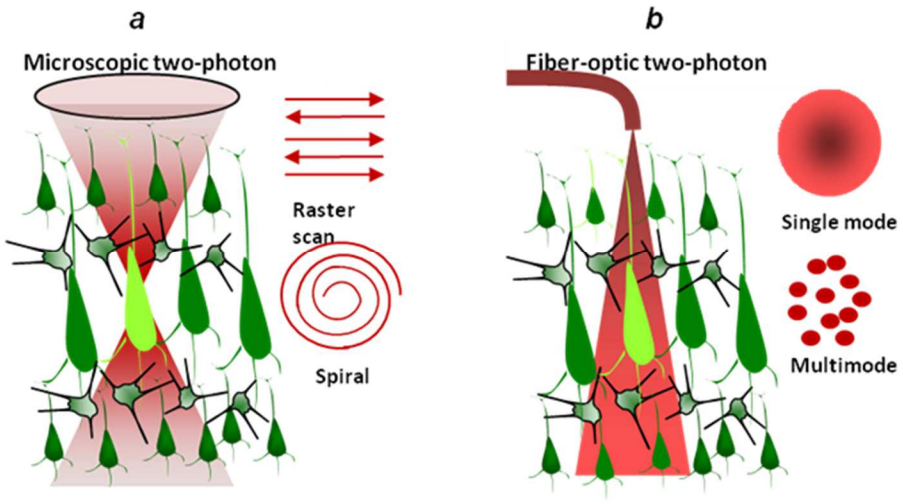

Figure 3.8: (a) Schematic of conventional two-photon stimulation of targeted cells by scanning pattern with femtosecond laser beam delivered by objective. (b) Schematic of fiber-optic two-photon activation of targeted cells.

This two-photon optogenetic stimulation technology paves the way for precise *in vivo* probing of neural circuitry in a minimally-invasive manner. Figure 3.8 shows the schematic comparison of conventional objective

based scanning (raster and spiral, Figure 3.8a) and fiber optic non-scanning patterns (defocused single mode and multimode, Figure 3.8b). In the case of single mode fiber-optic beam or laser beam focused by microscope objective, the intensity and, therefore, the two-photon stimulation is maximum at the center and slowly decays towards periphery (Gaussian nature). However, in case of the multimode fiber-optic beam, as used here, the maximum intensity is distributed in multiple spots over the irradiated cell(s), and two-photon stimulation is expected to occur in these spots leading to non-scanning activation of the cell(s).

Before evaluating two-photon activation of cells by multimode fiber-optic beam, we examined if the ultrafast fiber-optic near-infrared beam has sufficient photon densities to result in two-photon excitation. Therefore, two-photon excitation of fluorescent polystyrene particles was first carried out before applying it on cells. In order to confirm multimode fiber-optic two-photon excitation of fluorescent polystyrene microspheres (dia: 45 μm, Bangs Lab) an ultrafast laser beam (FSL, Maitai HP, Newport-Spectra Physics Inc.) was expanded using a beam expander (BE) and coupled to a multimode optical fiber (core dia: 50 μm) using a fiber coupler (Newport Inc.). Polystyrene particles were illuminated by placing the cleaved multi-mode fiber tip near the particles.

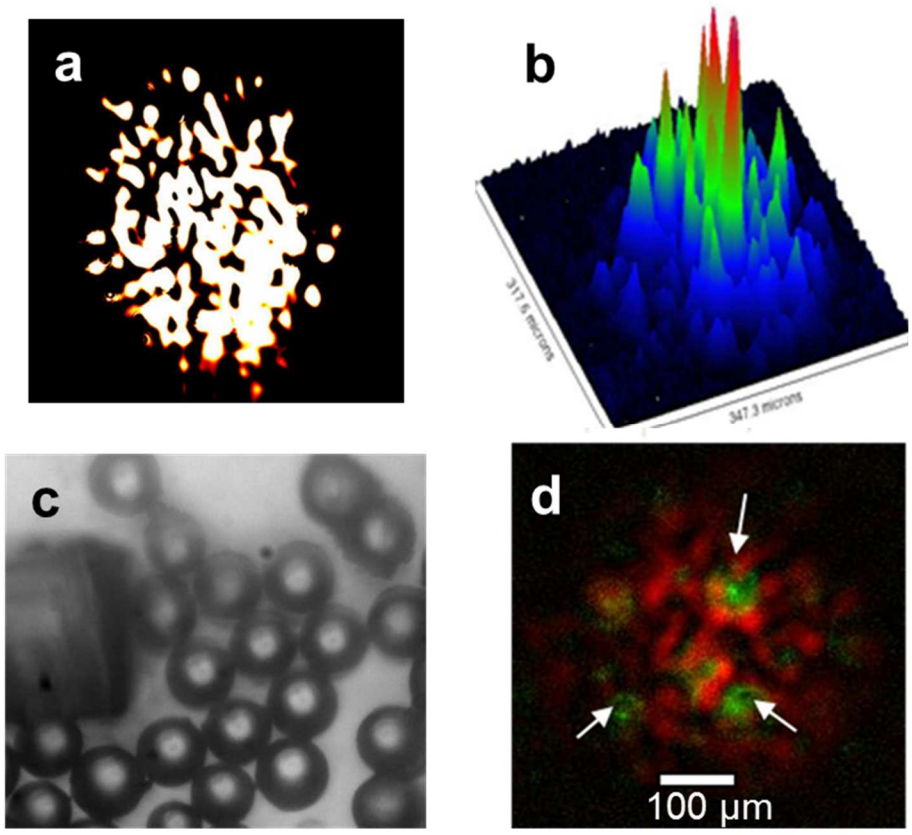

Figure 3.9: Two-photon excitation by multimode fiber optic beam. (a) Typical transverse beam profile emanating from the multimode fiber. (b) Surface plot show the some point of beam patterns has maximum intensity. (c) Position of multimode fiber near the polystyrene particles from multimode fiber. (d) Overlay image of two-photon fluorescence (green) and beam pattern (in red).

Circular neutral density filter (NDF) to control the intensity and a shutter (S) for controlling the exposure (macro-pulse) duration was used in the path of the tunable Ti: Sapphire laser beam (FSL) as shown in Figure 3.7. The cleaved multimode fiber was mounted on a mechanical

micromanipulator and positioned near the fluorescent particles. Figure 3.9a shows transverse the beam profile of NIR laser emanating from the multimode fiber and Figure 3.9b shows the surface plot of the intensity distribution over the field of view of a multimode fiber imaged using 10X microscope objective. Figure 3.9c shows the image of experimental set up of multimode fiber in the vicinity of polystyrene particles. In mode lock-off condition, no fluorescence was observed by camera (EMCCD, Photometrics Inc.). However, in mode lock-on (pulsing) condition, localized fluorescence was observed. Figure 3.9d shows a composite image of the bright field and two-photon fluorescence, excited by the multimode fiber-optic beam in mode lock-on (pulsing) condition.

For intensity-dependent characterization of multimode fiber-optically induced two-photon fluorescence excitation, the integrated fluorescence intensity was plotted as function of incident laser beam power (Figure 3.10). The non-linear rise in fluorescence intensity confirmed the ability of multimode fiber-optic ultrafast laser beam in two-photon stimulation of opsin sensitized cells.

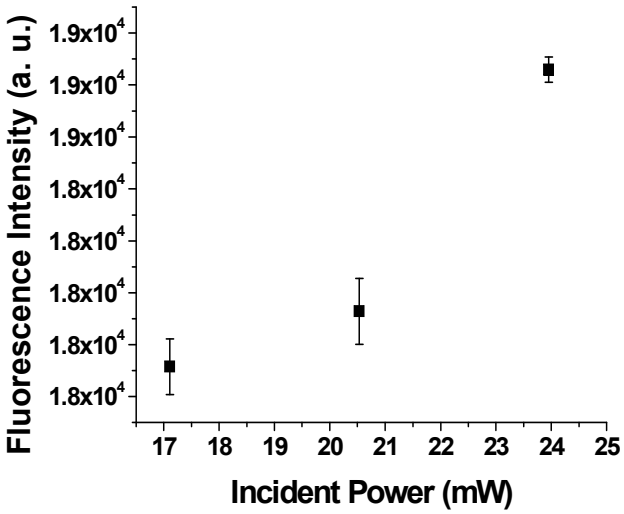

Figure 3.10: Nonlinear increase in florescence intensity with laser power.

3.7.2 In vitro fiber-optic near-infrared ultrafast laser irradiation led to optogenetic stimulation

In contrast to the use of a microscope objective for focusing the two-photon laser beam, a tunable (800 nm-900 nm), ultrafast laser (200 fs) beam coupled with multimode fiber (fiber-optic beam) was employed for two-photon optogenetic activation. In this case, similar to out-of-focus excitation [106, 119], diverging ultrafast fiber-optic near-infrared beam is believed to have sufficient photon densities to result in two-photon activation of the ChR2-transfected cells. For testing the efficiency of fiber-based two-photon activation *in vitro*, HEK-293 cells expressing ChR2 were used and photo-induced current in whole cell was recorded with patch-clamp. The

patch-clamp set up for electrophysiology measurement subsequent to FO-TPOS is shown in Figure 3.7.

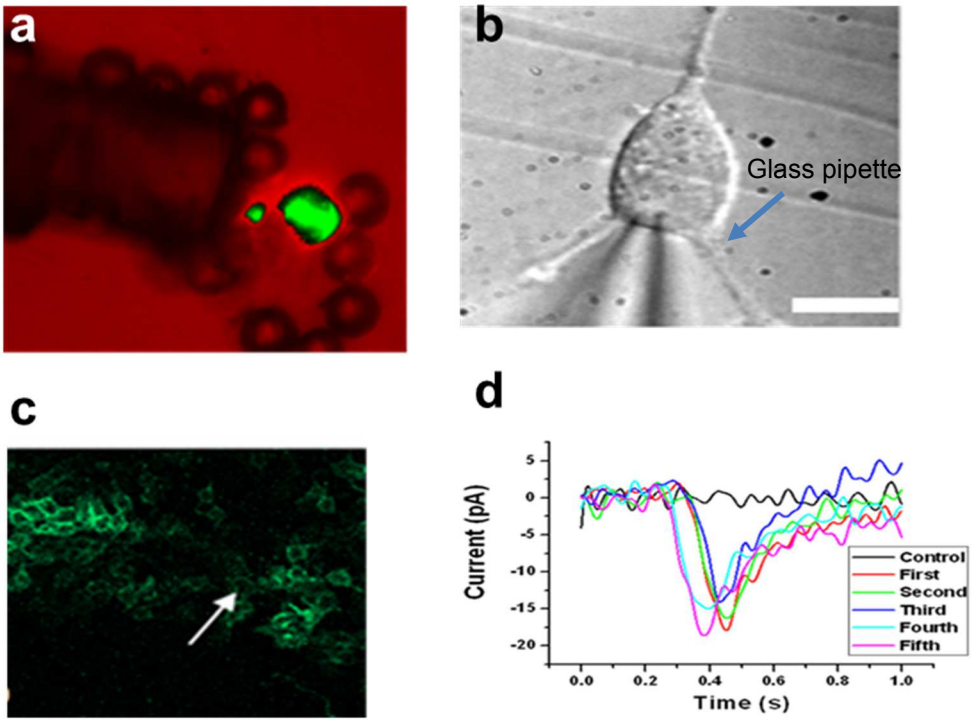

Figure 3.11: *In vitro* two-photon activation of ChR2-expressing cells with ultrafast NIR laser beam: (a) Two-photon fluorescence (green) from polystyrene particle excited by fiber- multimode beam profile (b) Bright field zoomed image of a patch-clamped HEK cell transfected with ChR2, (c) YFP fluorescence (marked by arrow) of HEK cells transfected with ChR2-YFP genes, (d) Inward current in response to macro-pulses (100 ms) comprising of ultrafast (200 fs) laser pulses (Scale bar: 10 μm).

The tunable Ti:Sapphire laser (FSL, 76 MHz) was expanded using a beam expander (BE) and coupled to a fiber using a lens (L). A shutter (S)

controlled the exposure (macro-pulse) duration and a circular neutral density filter (NDF) was used to control the average beam power.

After conforming the two-photon excitation of multimode fiber beam in polystyrene particles as described earlier, which has been shown in Figure 3.11a (green florescence at the center of fiber beam), experiments were performed on cultured cells using this method as potential tool for efficient way of light delivery for localized stimulation. Cells were sub-cultured in Petri dish and ChR2 channel kinetics were measured using patch-clamp. Figure 3.11b shows the bright field image of a patch-clamped HEK cell transfected with ChR2. Before patching the cell, YFP fluorescent images were taken and expression of ChR2 in HEK 293 cells was confirmed by fluorescence imaging of reporter fluorescent protein (YFP). Figure 3.11c shows the YFP fluorescent images of HEK cells. Figure 3.11c shows raw recordings of inward current in response to five different randomly-selected macro-pulses (100 ms) of ultrafast (200 fs) laser pulses emanating from the fiber tip positioned 100 μm away from the clamped-cell resulting in a power density of 0.012 mW/μm^2. The current amplitude was similar to the current reported by previous microscope objective-based defocus laser spot study [106]. The fact that continuous wave (control) laser beam (operated in mode lock-off condition), having same average power density (and exposure) did not evoke any inward current (Figure 3.11 c) confirms contribution of non-

linear interaction of femto-second laser beam with the ChR2-expressing cells. The importance of this randomly selected macro-pulse in mode lock - off (continuous) and mode lock-on (pulsing) is to determine whether optogenetic stimulation was dominant or photothermal stimulation was also giving contribution to the inward current. Though we did not see the inward current for continuous (mode-lock off) laser beam, we cannot completely rule out the contribution of photothermal effect or contribution of heat sensing channels such as TRPV channels during the two-photon optogenetic stimulation due to the fact that the high power density in NIR can generate sufficient heat due to laser absorption by the media. Other researchers have shown that cells could be activated during continuous wave NIR laser irradiation (without any light sensitive opsins) [120].

3.7.3 Fiber-optic two-photon optogenetic activation spectrum is blue shifted.

In order to map the two-photon activation spectrum of ChR2, the wavelength of the near-infrared fiber-optic stimulation laser beam was tuned from 800 nm to 900 nm.

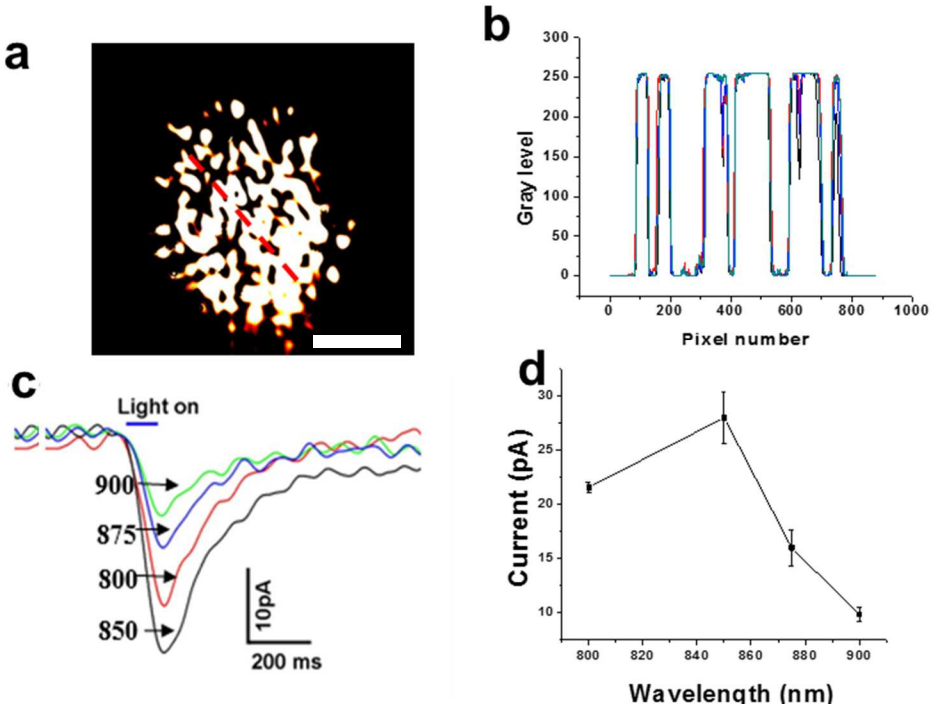

Figure 3.12: (a) Typical transverse beam profile emanating from the multimode fiber, (b) Time-lapse (1sec) intensity profiles (in different colors) along a line drawn across the beam profile shown in a. (c) Representative current responses to ultrafast NIR laser beam at different wavelengths (in nm), (d) Fiber-optic two-photon activation spectrum at 0.02 mW/ μm^2 (100 ms pulses).

Before determining the optimal activation spectrum of two-photon optogenetic stimulation of ChR2, stability of the fiber-optic beam was measured by using the correlation coefficient between the two frames (1 sec) and found to be highly correlated (correlation coefficient was 0.98). Figure 3.12a shows the intensity profile of the NIR (875 nm) beam emanating from the multimode fiber at a distance of ~1.3 mm from the

cleaved end. Figure 3.12b shows the time-lapse (1sec) intensity profiles (in different colors) along a line drawn across the beam profile (Figure 3.12a). Figure 3.12c shows representative current responses recorded from a single cell, irradiated with ultrafast NIR laser beam (100 ms pulses, with average power density of 0.02 mW/μm^2, at cell membrane) at different wavelengths. The fiber-optic two-photon activation spectrum of ChR2 (Figure 3.12c) *in vitro* shows that the peak of activation wavelength is at 850 nm. Theoretically, two-photon optogenetic stimulation of cells is expected to be maximal near 900-920 nm (double the single photon activation peak wavelength). However in practice, the two-photon activation spectrum is always shifted from the theoretical spectrum. The current amplitude at 900 nm was 9.9 ± 0.6 pA (n = 18), which was lower than the current amplitude at 850 nm (28.0 ± 2.4 pA, n = 19). Optimal activation FO-TPOS spectrum is around 850 nm *in vitro*. So the activation spectrum is shifted by 70 nm towards the visible spectrum. The shifting of spectrum towards the visible range is termed as “blue-shift”. The shift in excitation spectrum with respect to single-photon excitation is similar to the previously studied phenomena in two-photon absorption of many florescence dyes [121, 122]. The observed blue-shift of the two-photon activation spectrum can be attributed to the parity selection rules, favoring the two-photon activation of ChR2 (in

closed form) to higher energy (open) state than the respective single-photon-induced activation.

3.7.4 Fiber-optic two-photon optogenetic induced photocurrent is intensity dependent

Since the peak of the two-photon activation spectrum was observed to be at 850 nm, this wavelength was selected for studying fiber-optic two-photon intensity-dependent current-response of cells. Before studying the inward current as a function of power density, spectrum of ultra-fast laser pulse was measured by using spectrometer (USB 4000,Ocean Optics) at different wavelengths and has been shown in Figure 3.13a. It was observed that there was spectral broadening due to dispersion introduced by the fiber and optics introduced in the path of laser beam. At a fixed wavelength, variation of intensity (by changing the pump laser intensity) led to change in pulse width at lower pump power as shown in Figure 3.13b. Since no significant change in pulse width at high oscillator power (1.3 to 1.7 W) was observed, this range was used for intensity-dependent studies.

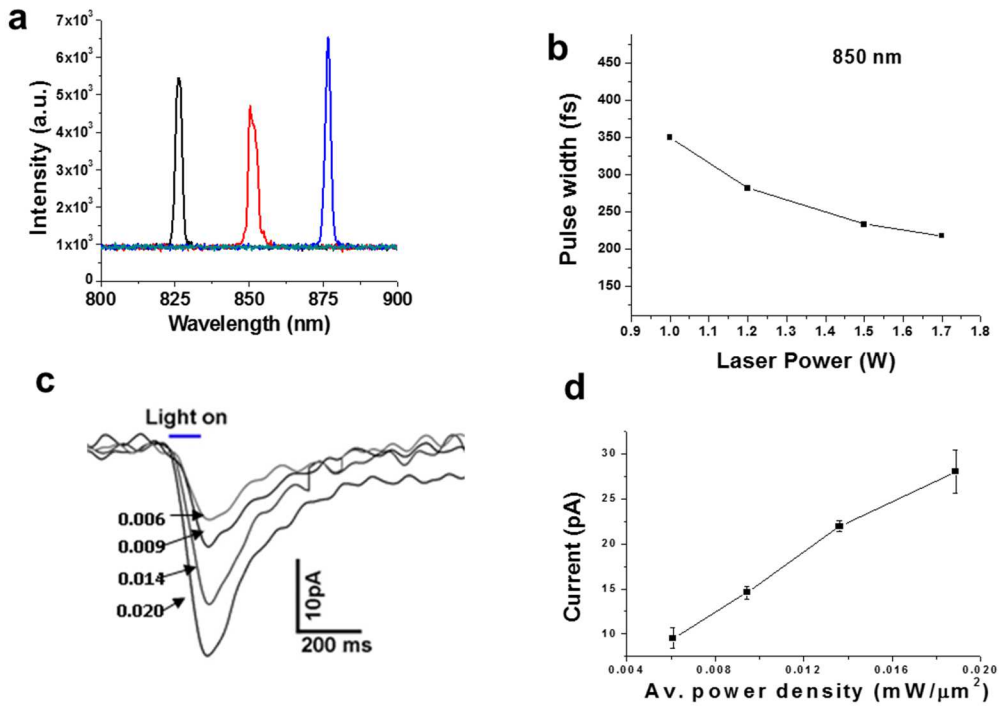

Figure 3.13: (a) Spectrum of ultrafast tunable near-infrared fiber-optic beam. (b) Variation of the width of the ultrafast laser pulses from the multimode fiber as a function of laser power. (c) Inward current responses due to FO-TPOS (at 850 nm) using different average power densities (in mW/μm^2), and (d) dependence of inward-current as a function of power densities (100 ms pulses) (N = 4).

This range of oscillator IR laser power corresponds to ~150 to 260 mW at the coupling end of the multimode fiber. With a coupling efficiency of nearly 50%, the average power at tip of the fiber was measured to be 75 to 130 mW. Figure 3.13c shows representative inward current responses due to fiber-optic ultrafast near-IR (850 nm) stimulation of a single cell at

different average power densities (0.006 mW/μm^2 to 0.02 mW/μm^2, at cell membrane). While highly non-linear response of inward current in low current regime (during focused irradiation) has been reported earlier [123], the fiber-optic two-photon stimulation at higher laser intensities led to more linear dependence [108]. The dependence of two-photon (at 850 nm, 100 ms pulses) induced inward-current as a function of incident average power densities (near cell membrane) is shown in Figure 3.13d. In contrast to the expected non-linear response of inward current, the FO-TPOS induced current in cells was found to be linearly dependent on the incident laser power density. Unlike two-photon fluorescence emission, inward current is associated with conformational change of the molecule rather than a simple two-level transition, and there is also a possibility other phenomena were also involved. Therefore, along with intensity, other parameters such as the kinetics of the opening of the ChR2-channel and two-photon absorption of all-trans-retinal [124, 125] will significantly modulate the nature of intensity and wavelength-dependent current variations. We hypothesize that there might be several possibilities that can lead to linear rise in inward current as function of intensity. First, the ChR2 may have small but significant absorption in NIR spectrum which might be contributing in photothermal stimulation. Secondly, other molecules such as the cofactor (ATR) can

absorb NIR light and transfer energy to the opsin by the process of resonance energy transfer (RET) and second harmonic generation.

3.7.5 Estimation of two-photon activation cross section

For estimation of fiber-optic two-photon cross-section of ChR2-activation we have considered the dispersion-induced measured pulse-width. We have also estimated the two-photon absorption cross section by fitting the equation to the inward current obtained from patch-clamp as shown in Figure 3.14. The inward increasing current was fitted with following equation,

$$I^*(T) = I_{\max}\{\frac{\tau_2}{\tau_g - \tau_2}(e^{-\frac{T}{\tau_g}} - e^{-\frac{T}{\tau_2}}) - \frac{\tau_1}{\tau_g - \tau_1}(e^{-\frac{T}{\tau_g}} - e^{-\frac{T}{\tau_1}})\} \quad 3\text{-}6$$

Where τ_g is the ground state life time, defined $(2/\sigma_2 I^2)$ for two-photon excitation and $(1/\sigma_1 I)$ for single photon excitation, I_{max} = maximum current, σ_2 = two-photon absorption cross-section, τ_1 = activation time-constant, and τ_2 = current decay time-constant. From the fitted parameters the two-photon absorption cross-section at λ=870 nm and 900 nm was calculated and found to be 226.48 ± 5.034 GM and 186.32 ± 33.03 GM. This estimated two-photon absorption cross-section is higher than any other fluorophores and is comparable to earlier report [106]. This is one of the reasons why fiber optics could produce two-photon activation of ChR2 at low intensities.

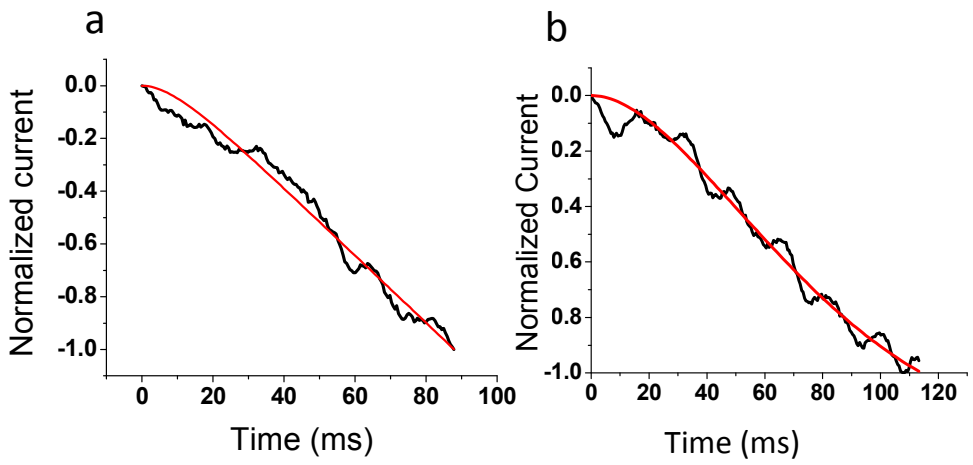

Figure 3.14: Different traces of photocurrent in ChR2-sensitized HEK cells induced by FO-TPOS pulsed laser (250 fs) beam (a) at 870 nm and (b) at 900 nm at average intensity of 0.02 mW/μm^2. The fitted data (using Eq. 3.6) is overlaid (red traces) over the measured photocurrent. The fitted parameters τ_1 and τ_2 are used to calculate the two-photon activation cross section.

3.8 Contribution from photothermal stimulation

Biological samples consists high percent of water in it (70-80 % in human). Water has very low absorbance in the visible spectrum and very high absorbance coefficient in the far NIR region (>1 μm). But in the mid NIR region (700 nm-1000 nm) water has moderate absorption. Therefore, this region often referred to the “Optical Window” or “therapeutic window” since light in this region safely propagates into the biological medium and has been used for various biomedical applications. Though mid NIR region has relatively low absorption coefficient (non-zero value) compared to far

infrared region, high intensity light in this region is still capable of inducing small temperature rise. Figure 3.15 shows the absorption of water in three different spectral regions. The original data is taken from [126, 127] and graphs are reproduced using MATLAB. We have shown that a defocused fiber optic beam of diameter 50 μm placed 100 μm from the cell is capable of inducing small temperature rise of approximately 1-2°C. Other researchers have calculated up to 5-10°C increases in temperature due to focused laser beam by microscopic objective [120, 128].

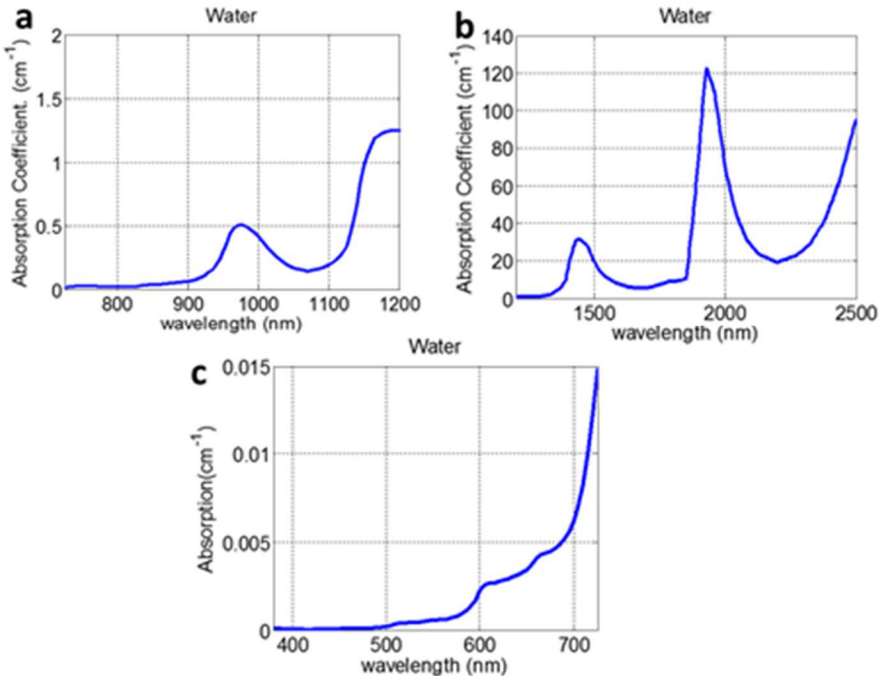

Figure 3.15: Absorption coefficient of water in (a) visible region (b) near infrared region (c) far infrared region.

This small change in temperature might also cause TRPV (heat sensing channel) [129] in the cells to open which could contribute to the overall rise in inward current in optogenetic stimulation. On the other hand, the NIR irradiance in cells could cause change in capacitance of cell membrane [130], which also stimulates the cells. Due to these reasons, we cannot completely rule out the contributions from other sources like photothermal, resonance energy transfer and second harmonic generation in two-photon optogenetic stimulation.

3.8.1 Simulation of laser-induced temperature

It is known that the absorption of NIR light in tissues and cells leads to rise in temperature. Whether this is from heat sensing channels or from direct stimulation due to change in capacitance of the cell membrane [129],[130], rise in temperature in cell or tissue due to its absorbance of light contributes to the overall inward current along with optogenetic stimulation. We have carried out the finite element simulations to determine the magnitude and distribution of the temperature due to a defocused fiber beam (dia=50 μm, NA=0.15) placed 100 μm away from the cell surface. The temporal- and spatial- dependent temperature rise will be given by the standard heat diffusion equation:

$$\rho c\left(\frac{\partial T}{\partial t}\right)=\frac{k}{r^2}\frac{\partial}{\partial r}\left(r^2\frac{\partial T}{\partial r}\right)+q(r,t) \qquad 3\text{-}7$$

where the source term, q(r,t) is proportional to the z-dependent intensity (I_o(r,t)) of a focused, Gaussian laser beam. Due to the exponentially decay of laser intensity, the dissipated power density is equivalent the loss of intensity due to absorption of the medium multiplied by the linear absorption of the cell culture medium (water), α. We have assumed roughly 10 % of the laser light is lost due to absorption in cell medium. This is based on the absorption of light by the 20 μm thickness of tissue.

$$\delta_z(r,t) = -\alpha I_0(r,t) \qquad 3\text{-}8$$

I_o(r,t) is related to the measured laser power at the sample site (P) and the radial distance from the laser spot center:

$$I_0(r,t) = \frac{2P}{\pi w^2(z)} \exp\left[-\frac{2a^2(r,t)}{w^2(z)}\right] \qquad 3\text{-}9$$

where w(z) is typically the z-dependent beam waist diameter, with z measured from the laser focal plane. In this study, we have reduced the problem to two-dimensions, assuming the fiber tip (dia=50 μm, NA=0.15) was placed 100 μm away from the cell surface, the beam waist can be calculated by using following relation.

$$w(z) = 50 + 2*100*\sin^{-1}(0.15) \qquad 3\text{-}10$$

The second order differential equation (3.7) can be solved in MATLAB using the PDE toolbox. Dirichlet boundary conditions were

imposed at the geometrical limits of the cell culture medium. We have neglected any conventional heat transfer at air liquid boundary as temperature difference is very small. In order to simplify the problem, we have assumed the laser intensity is uniformly distributed across circular area formed by the diameter *w*(z). The triangular mesh was initialized and refined by the PDE toolbox to have mesh growth of 1.3 from the center of the source term.

We have assumed that 10% of the laser energy is absorbed by the medium and all that goes towards temperature rise. We have neglected the higher order absorption of culture medium proteins, pH indicators (phenol red), and the direct absorption of scattered light by cells or cellular components.

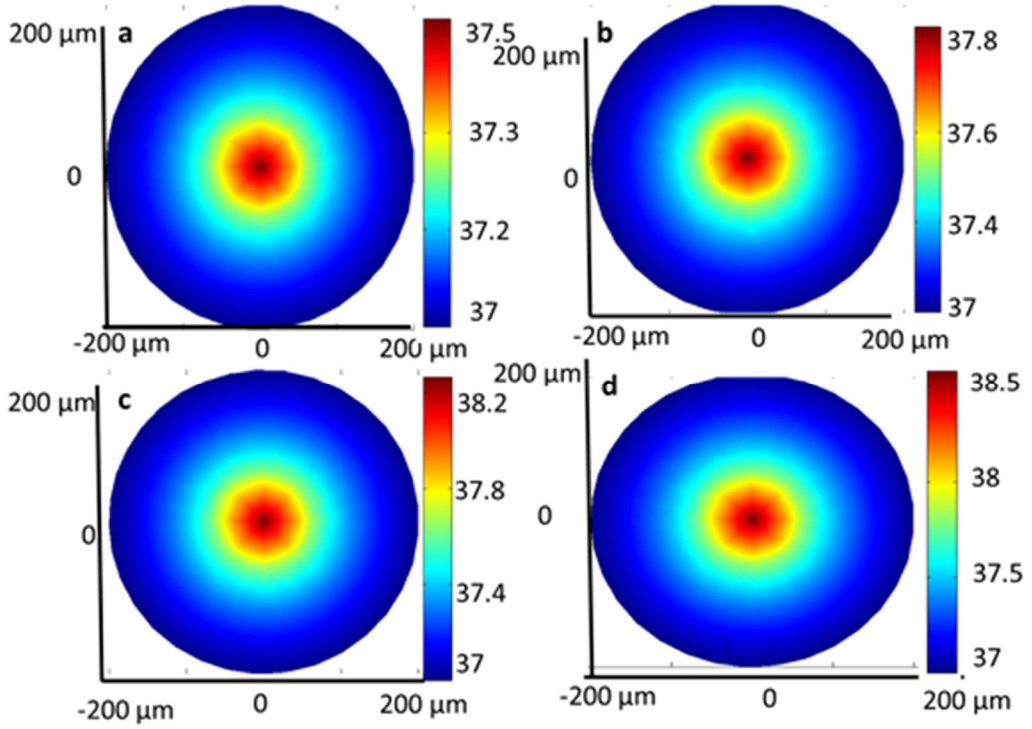

Figure 3.16: Theoretical simulation of laser induced temperature rise in medium due to pulsing laser irradiation from fiber (NA=0.15, core diameter 60 µm) and dissipation of heat at different power (a) 0.006 mW/µm^2 (b) 0.01 mW/µm^2 (c) 0.014 mW/µm^2 (d) 0.018 mW/µm^2.

The intensity was assumed uniformly distributed in the beam spot and temporal coherence factor 10^5 for pulsing (Ti:Saphire) [131] laser was considered while using average power density. The absorption of 850 nm light by the glass coverslip is assumed to be negligible compared to that of the cell culture medium as absorbance of glass at 850 nm is 0.01m^{-1}. We have created at least 10,000 nodal point while solving the Equation 3.7 to ensure grid independence results. Boundary condition was fixed to (37°C)

(no flow of heat from the boundary of the sample). Figure 3.16 shows steady state temperature contour plot in medium due to laser beam irradiation emanating from fiber (NA=0.15, core diameter 60 μm) at different average power densities. The power level chosen in this simulation is similar to the power level used in two-photon optogenetic excitation (Figure 3.13). As shown from the Figure 3.16, there is 0.3°C rise in temperature in every 0.004 mW/μm^2 increase in power level.

3.8.2 Simulating opening probability of transient receptor potential channels

Many biological phenomena and their dynamics are linked with thermodynamics.The opening probability of a protein ion-channel due to changes its conformational state is thermodynamically linked to the Gibb's free energy difference between the two states (open and closed). As Gibb's free energy is function of temperature and therefore opening probability of ion-channel is also necessarily a function of temperature.

$$P_o(T) = \frac{1}{1+\exp\left(\frac{\Delta G}{RT}\right)} \qquad 3\text{-}11$$

The temperature dependence of the Gibb's free energy difference is related by following equality.

$$\Delta G(T) = \Delta H(T) - T\Delta S(T) - zFV \qquad 3\text{-}12$$

where ΔH is the temperature dependent enthalpy change, ΔS is the temperature dependent entropy change, z is the gating charge, F is Faraday's constant, and V is the transmembrane potential. The expressions for enthalpy and entropy are also temperature dependent functions, which are related to the specific heat capacity at constant pressure (ΔC_p) as well as with temperature.

$$\Delta H(T) = (\Delta H_0 - \Delta C_p T_R) + \Delta C_p T \qquad 3\text{-}13$$

$$\Delta S(T) = (\Delta S_0 - \Delta C_p \ln(T_R)) + \Delta C_p \ln(T) \qquad 3\text{-}14$$

where ΔH_o and ΔS_o are the enthalpy and entropy values at the reference temperature (T_R). These values, along with ΔC_p are experimentally determined values, and have been taken, from previous experimental findings [132]. Since there is some discrepancy in experimental determinations of ΔC_p in the physiological range of temperatures, we have plotted the temperature dependent opening probability for minimum and maximum ΔC_p (8 and 20 kJ mol^{-1} K^{-1}) to see how it will vary the opening probability. Simulations for opening probability were carried out by solving the above interlinked equations in MATLAB and has been shown in Figure 3.17c.

Here, we have considered TRPV family of transient receptor potential channels which are temperature sensitive. Even though, there is a relatively small temperature rise in the study (maximum 2°C), this rise in

temperature would be sufficient to activate the temperature sensitive channel (TRPV1). Recently, a rigorous study done by *Black. et.al* (our lab member) [133] has shown this small increment rise in temperature would be helpful in axon-guidance. It has been shown in earlier section that there is small temperature rise (up to 2°C) while irradiating the cells with multimode fiber beam at 850 nm (at or above the intensity 0.006 mW/μm^2). We have shown that this small rise in temperature is instrumental in opening the heat sensing ion-channel (TRPV1) in the cell membrane.

From the calculation of laser induced temperature rise and temperature induced activation of heat sensing channels, there is up to 8%-10% (Figure 3.17c) probability of opening the heat sensing channels even during two-photon optogenetic stimulation based on our experimental parameters. Figure 3.17a shows exponential decay of the steady state laser induced temperature rise as a function of distance. The center was chosen at the center of the fiber-optic beam and line plot of temperature was plotted from the center to the periphery of the circular area of the picture (as function of distance) as shown in Figure 3.16. As we can see from Figure 3.17a, temperature decays with distance from center.

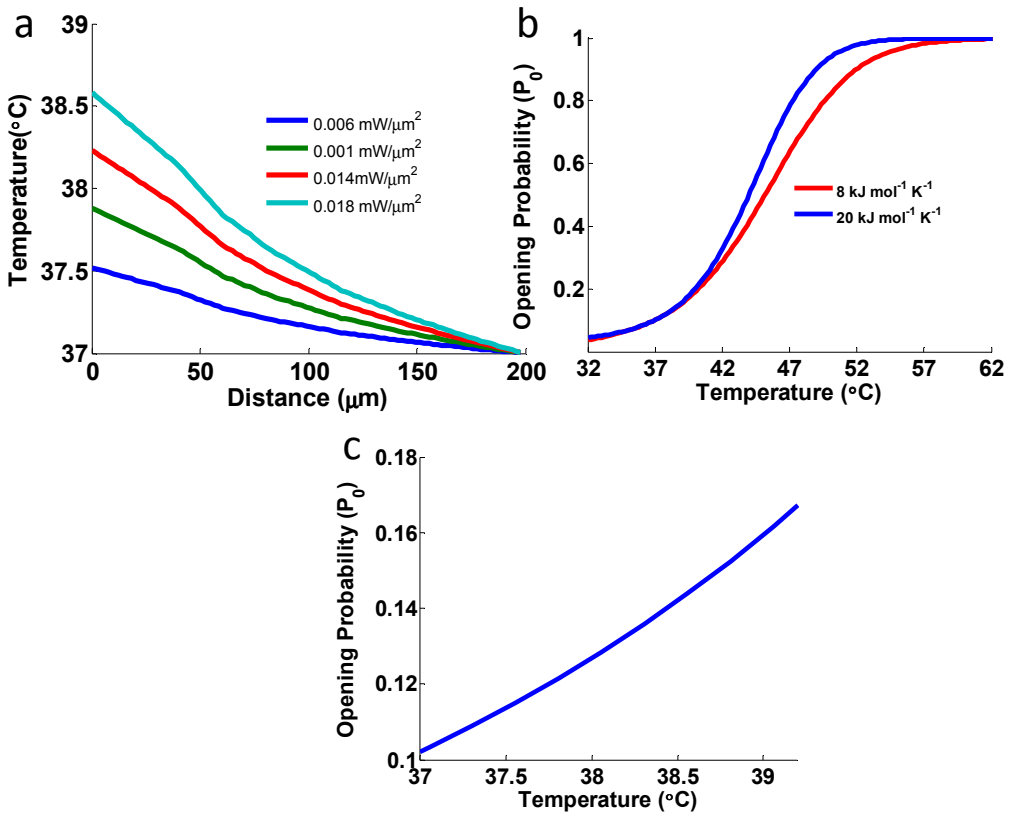

Figure 3.17: (a) Line plot of temperature profile from the center of the beam and its exponential decay as a function of the distance from the center (Figure 3.16) at different power.(b) Opening probability of heat sensing channels in the cells due to temperature rise. (c) Experimentally relevant zoomed view of temperature-dependent opening probability.

As HEK 293 cell dimension is roughly 10 μm, this rise in temperature causes up to 8% increase in opening probability of the heat sensing channels as shown in Figure 3.17(b-c). This value is well matched within the range of reported theoretical [128] and experimentally determined [134] values.

3.9 Effect of temperature in ionic flow

The role of temperature during NIR activation of cells has been discussed in earlier section. It has been shown that the rise in temperature during NIR stimulation of cells could lead to opening of heat sensing channel in various ways. In this section we discuss the how the rise in temperature also effects the dynamics of ionic currents (mainly sodium) which eventually alters the kinetics and current profile of optogenetically evoked inward currents. Photothermal effect will cause transient rise in temperature in targeted cells which changes the membrane excitability using mode lock-off (continuous) [120] as well as low intensity pulsing laser beam [135]. Here, we have simulated ionic currents (mostly sodium as they are responsible for inward currents) originating from the rise in temperature. In the earlier section, it has been shown that the infrared laser beam irradiation increases the temperature rise of 2°C (maximum) in our experimental condition, whereas other researcher have shown there could be up to 14°C rise in temperature without causing the damage in the biological cells [120].

The modified Hodgkin-Huxley model for temperature dependents rates is given by,

$$I_{Na} = Io * (1 - exp(-t/\tau_m))^3 * exp(-t/\tau_h) + y_0 \qquad 3\text{-}15$$

Where $\tau_{m,}$ τ_h and y_0 are activation rate, inactivation rate and initial offset. The temperature dependent rates were interpolated linearly from the experimental value done by *Wells* et.al [136].

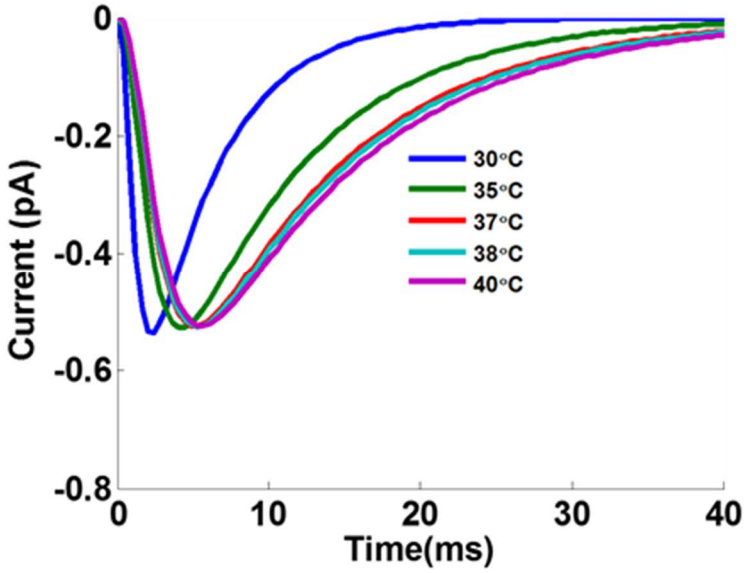

Figure 3.18: Simulation of effects of temperature in inward (sodium) currents as function of temperature.

Figure 3.18 shows theoretical simulation of effects of temperature in sodium current profile. Higher the temperature, the inward current profile broadens more. In other words, activation and inactivation time constants are significantly changed with varying the temperature.

3.10 Discussion

Optical stimulation of neurons has a long history in the field of neuroscience and has number of advantages over the electrical stimulation.

Nowadays, with advancement of optical technologies and genetic engineering, optogenetics is emerging as a powerful approach to control and manipulate the cells. The light energy interacts with the biological sample in various ways such as photomechanical, photochemical, photoelectrical and photothermal. Photomechanical effect is limited to small size particle or biomolecules. Photochemical alteration is mainly utilizes UV range and required high energy (high frequency). Photothermal effect is another phenomenon that might contribute with optogenetic stimulation. During, NIR optogenetic stimulation such as two-photon activation of ChR2, photothermal effects may play a role due to non-negligible absorbance of light by water.

Though we characterized multimode two-photon activation efficacy of ChR2 transfected cells at different near-infrared laser intensities, further studies are required to optimize the multimode FO-TPOS strategy. The large two-photon cross-section of ChR2 [106] should allow use of nanosecond or even microsecond compact near-infrared (NIR) sources for FO-TPOS. Further, by tuning the wavelength of the two-photon light source for other opsins such as NpHR, the FO-TPOS method can be useful for combinatorial modulation (both excitation as well as inhibition) of the neural activity. Use of microlens or axicon [137] on fiber tip should allow the use of focused fiber beam instead of diverging which could be more localized and

efficient. The FO-TPOS technology will allow in-depth probing of neural circuitry *in vivo* as well permit minimally-invasive and more precise anatomical delivery of light. Similarly, due to compactness and flexibility of the fiber, it would allow the study of neuro-modulation in freely-behaving animals. Using the technology already developed for non-linear endoscopy [138], both two-photon stimulation and optical imaging of neural activity can be achieved *in vivo.* Though single photon ChR2 activation spectrum has been characterized in visible region, further studies are required to measure single-photon NIR activation of ChR2. This would certainly require intense CW (continuous) light source (average power higher than used in studies reported here) owing to the low activation efficiency in the NIR.

Chapter 4

Optical detection of cellular activity

4.1 Introduction

The scope of optogenetics has been rapidly expanding and significant progress has been made in its application as this technology can be applied to manipulate the cellular activities in more precise and localized way than with other existing methods. In order to better understand how the optogenetics works , it can be subcategorized in three parts; (1) expressing of genetically encoding opsins into targeted cells or tissues, (2) delivery of light in minimal invasive and effective way to stimulate the cells (opsin-sensitized cells) and, (3) recording the photo-induced electrical changes by the optogenetic stimulation from the cells or tissues. Recording the optogenetically evoked signal from the cells or different layers of tissues still relies mostly on conventional electrodes (glass electrode or metallic micro-electrode) that are poked or patched into the cells. The conventional methods of electrophysiology recording (patch-clamp, single electrode recording, and multi-electrode recording) requires physically touching the cell which is very invasive, intrusive and often leads to the cell death and artifacts. In addition, big and bulky electrical recording system with delicate electronics creates more electrical noise and makes whole recording system very tedious. Further, *in vivo* neuroscience research, studies require

simultaneous mapping or measurement of large populations (or networks) of interconnected cells. This becomes increasingly invasive, and often logistically impossible with traditional electrode-based recording methods. Despite the sensitivity, reproducibility, and temporal resolution of patch-clamp recordings, there have been significant efforts to find alternative methods for measuring activities in cells (neurons). Further, electrical detection of cellular activities from every single opsin-expressing cell would require electrodes implanted (poked) into every single cell. Also, detection of neural activation using patch-clamp from significant depths of a tissue is not feasible. In contrast, optical methods are being developed that allow the detection of large number of cells simultaneously. With the advent of voltage sensitive dyes, it was demonstrated that membrane potential information could be detected optically with increased spatial information. In this study, we have used a noninvasive fluorescence-based optical probing method to detect the activities of cells.

4.2 Calcium imaging

Voltage-sensitive dyes (VSDs) are an ever-expanding collection of organic molecules and proteins whose optical properties change dynamically in the presence of changing electric potential (voltage) or ion transport across the cell membrane [139]. These dyes indicate the change in electrical potential based on the variation of their absorbance,

fluorescence intensity, fluorescence spectrum, or birefringence from ‘resting’ values. These molecules usually have a hydrophobic portion that sticks to the membrane and a charged chromophore that prevents crossing to the cell interior. Further, they have a high absorption coefficient and high quantum efficiency. Classical voltage sensitive dyes(VSDs) are typically split into two groups (although the distinction is often vague) based on their response time, and are unimaginatively referred to as slow and fast dyes. Slow dyes give rise to relatively large variations in fluorescence intensity (0.1 to 1 percent per millivolt of depolarization) which can typically be monitored with conventional spectrometers/detectors. VSD imaging can be readily combined with other imaging techniques, such as confocal microscopy, ion concentration imaging, or selective optical stimulation.

These problems are currently being addressed with the development of genetically encoded voltage indicators (GEVI) [140]. Genetically encoded voltage indicators are protein sensors which are selectively expressed by cell-specific promoters. In this way, subpopulations of neurons within a larger network can be specifically monitored. Furthermore, these protein sensors may even be expressed in known, specific portions or components of cell subpopulations (i.e. dendrites) so that electrical potentials can be monitored within structures which cannot be optically resolved in a conventional manner, leading to new possibilities in the realm of neural

activity imaging. To characterize neural activities *in vitro* or *in vivo* during optogenetic stimulation, there is a need for deployment of functional optical imaging method having high spatial and temporal resolution. Since GEVIs or genetically-encoded calcium indicator (GECI) can be genetically-targeted [141], it provides the cell specificity and changes in GEVI or GECI. Using this method, fluorescence intensity can be monitored in mammalian cells and organisms [142]. GCaMP is a GECI that provide less cytotoxicity and stable (less photobleaching) fluorescence over the observation period and has undergone progressive modifications (e.g. GCaMP3) [143] for enhanced fluorescence signal. Use of GECI-based optical recording method has overcome the disadvantages associated with mechanical perturbations during electrical recordings and cytotoxicity related to chemical agents such as dyes. Such functional (calcium, voltage sensitive probe) imaging can be achieved using conventional/plane illumination microscopy depending on the sample size of interest. With optical detection of neural activities, the whole process of identification, activation and detection can be made non-invasive added with the advantages of high throughput and least requirement of mechanical stability and contamination.

4.3 Experimental set up

The wide-band white light from the microscope illumination source (halogen lamp) was used for optogenetic stimulation. Activation spectrum

for opsin sensitized cells was selected by inserting the proper filter in the path of wide band illumination source. Figure 4.1 shows the schematic setup for calcium imaging of ReaChR transfected cells expressing GCaMP3. The spot size at the sample plane was controlled by the aperture and the condenser (CL). The current-controller was used to control the white light intensity. A set of filters was used in the light path to illuminate the sample with narrow-band (blue, green and red) light. In order to measure the spectrum of narrow-band light, a spectrometer (USB 4000, Ocean Optics) was used. Light power at the sample plane was measured using a power meter (PM 100D, Thorlabs). An electro-mechanical shutter was used to control the exposure (pulse) duration. A high pressure mercury lamp (Osram) served as the excitation source, which passed through manually controlled filter (in/out) placed over the electro-mechanical shutter before falling on the focal plane of Nikon microscope objective (100X or 20X), as seen in Figure 4.1. Images were collected by an EMCCD (Cascade, Photometrics) and processed/analyzed in ImageJ (NIH) software.

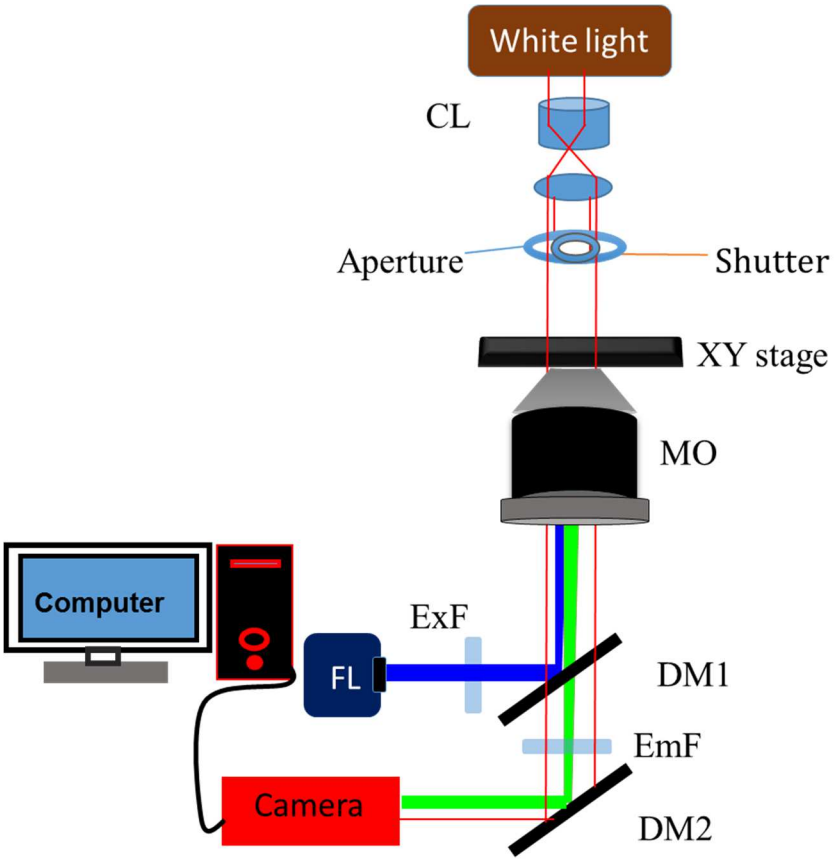

Figure 4.1: Schematic setup for calcium imaging of opsin expressing cells: CL: Condenser Lens; MO: 20X Microscope Nikon objective; DM1: Dichroic mirror; EmF: Emission filter; M: Mirror; ExF: Excitation filter; FL: Fluorescence excitation source.

Stacked time-lapse image sequences were analyzed by the Image J (ROI manager), which measured integrated intensity of selected regions. All regions of interest used in the analysis of a single experimental image sequences were of equal size.

4.4 Results

4.4.1 Optogenetic Stimulation

The distinctly different excitation spectrum of GCaMP3 (470 nm) and ReaChR (610 nm) has permitted the simultaneous identification of opsin-reporter expression and monitoring of the increase in calcium level during optogenetic activation process in same cell.

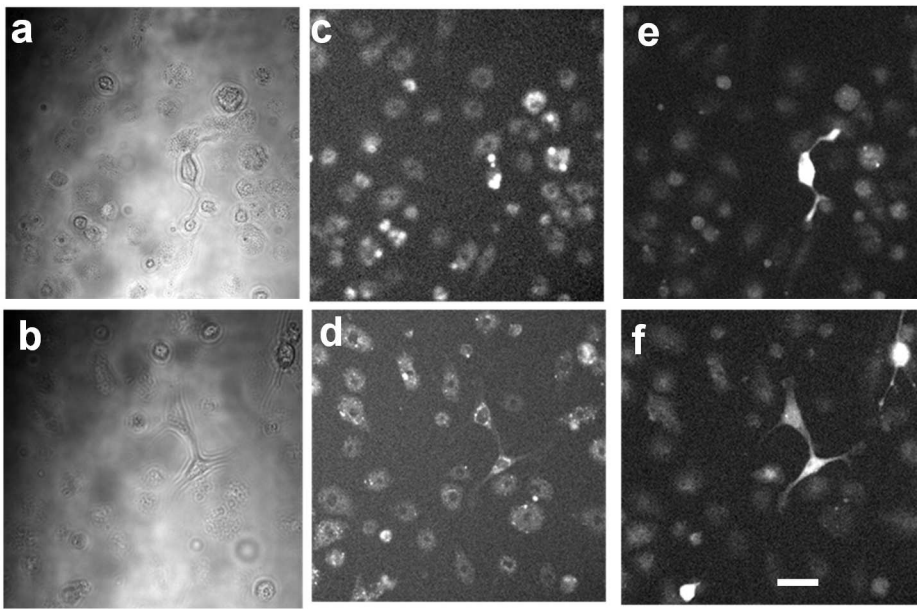

Figure 4.2: (a-b) Bright field images, (c-d) GCaMP3 expression, and (e-f) ReaChR expression of astrocytes (Scale bar: 10 μm).

Subsequent to optogenetic activation of ReaChR -expressing cells, change in intracellular Ca^{2+} levels were monitored in GCaMP3-expressed astrocytes cells simultaneously. ReaChR has very broad activation spectrum ranging from blue to red light, although the activation is maximum

at 610 nm [144]. Therefore, ReaChR transfected astrocytes were stimulated by inserting orange filter in the path of bright field illumination to achieve optimal activation using low light intensity. Ca^{2+} levels were monitored by using the blue light that was coupled from the back aperture of microscope's objective as shown in Figure 4.1. We did not used ChR2 for this study as activation spectrum of ChR2 (470 nm) overlaps GCaMP3 excitation spectrum. Figure 4.2(a-b) shows the bright field images of astrocytes cells. Figure 4.2 (c-d) shows the fluorescence image of GCaMP3 expressing astrocytes and Figure 4.2(e-f) shows the YFP fluorescence of same GCaMP3 expressing cells at two different trials. As seen in the pictures, GCaMP3 is well expressed in cells everywhere, but ReaChR is only expressed well in some of the cells. Only those cells in which GCaMP3 and ReaChR expressed well were taken into consideration in analysis.

Cells were stimulated using 1HZ frequency for one minute and with 50 ms and 100 ms exposure. Time lapse images were taken by EMCCD camera one minute before stimulation and two minute after the stimulation to estimate if there were spontaneous activity.

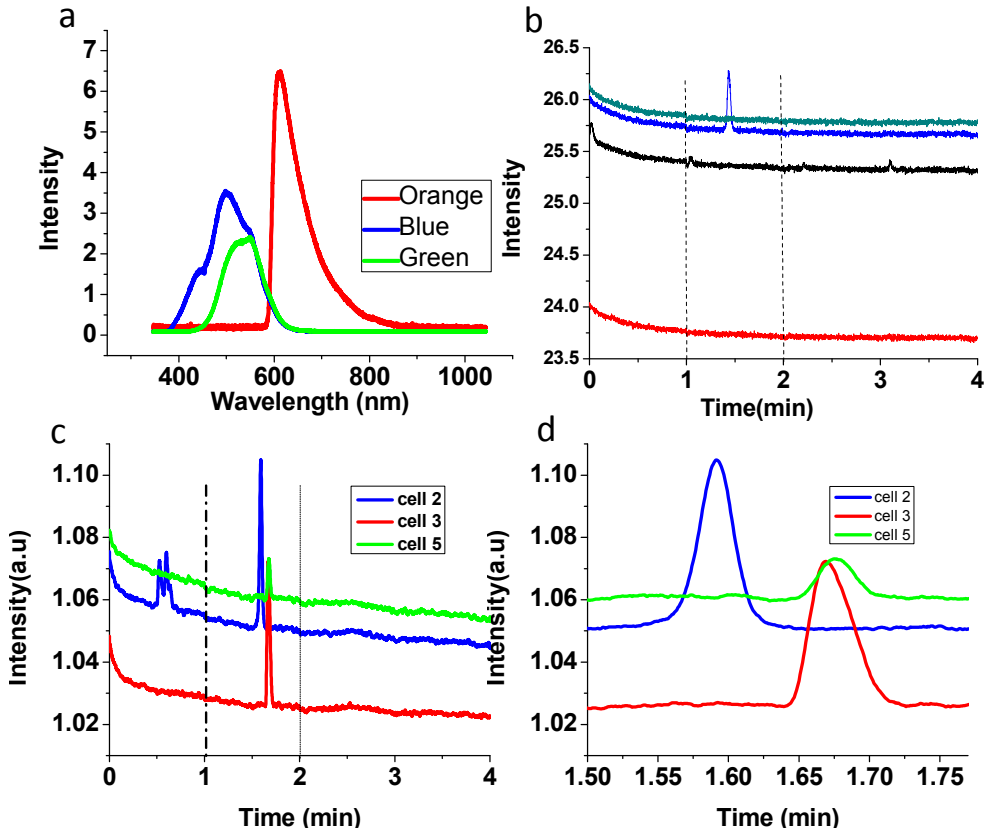

Figure 4.3: (a) Spectra of lights passing through blue, green, and red filter. (b) Average change in fluorescence intensity as a function of time in below threshold level (<0.004mW/mm2), (c) Increase in calcium intensity in the GCaMP3 astrocytes cell during the red light stimulation of ReaChR transfected cells, and (d) zoomed picture of (c). Dotted line defines the stimulation interval.

The integrated intensity profile of the different cells expressing GCaMP3 and ReaChR has been plotted as a function of time to detect activities of the cells during optogenetic stimulation. Figure 4.3(a) shows the spectra of light passing from different (blue, green and orange) filters that

were placed in the path of wide field illumination, measured by the spectrometer (USB 4000, Ocean Optics). We have used only orange light for the activation of ReaChR transfected astrocyte also expressing GCaMP3. Intensity of light was gradually increased by increasing the current driving the bright field lamp. Below 0.04 mW/mm^2 and lower exposure duration (below 50 ms) we did not observe any increase in fluorescence during the optogenetic stimulation (marked in dotted lines) as shown in Figure 4.3. But for higher pulse width of the (100 ms on, 900 ms off), there is a clear and distinct increase in calcium level during stimulation period (shown by dotted lines), in Figure 4.3(c). The zoomed picture Figure 4.3(d) shows calcium spiking activity of ReaChR transfected cells in response of light stimulation.

4.5 Discussion

By monitoring the intracellular calcium florescence intensity of genetically expressed calcium indicator (GCaMP3), we detected cellular activities in response to the optogenetic stimulation of ReaChR transfected astrocytes cells. Coupling optogenetics with other method such as calcium imaging will help us to study function of cells including neurons in a noninvasive way. The information obtained from optical method is free from artifacts as generally present in electrical recording.

Though we have detect the cellular activities my monitoring the calcium influx, this method does not allow to detect the fast cellular activities in ms-scale due to slow temporal response of GCaMP3. Use of GEVI is better than conventional calcium imaging (dye) in terms of kinetics We proposed initially to use label free detection of optogenetic stimulation by monitoring volumetric change of cell. To that end, we have used quantitative phase microcopy (digital holography) to detect optogenetic stimulation. Due to low signal to noise ratio (SNR), meaningful information form the sub-nanometer phase change happening during optogenetic stimulation could not be extracted. Though we have been able to see some changes only in few trials, we did not include the study in this dissertation.

In a nut shell, this noninvasive optical method for detection of neuronal activity in combination with optogenetics brings us a valuable approach to study and better understand cellular functions.

Chapter 5

Conclusions and Future Work

5.1 Conclusions

The laser-assisted delivery/expression of genes in spatially-targeted regions will help in controlled functionalization and manipulation of cells. In addition, the electrical activity (activation/silencing) of specific neurons can be controlled by optical stimulation, thus encoding activities in specific neurons and modulating overall behavior of an organism. The two-photon optogenetics method is paving the way for precise *in vivo* probing of neural circuitry in a minimally-invasive manner. Besides obtaining structural information, optical imaging methods hold promise to non-invasively record neural activity. All-optical manipulation of cellular activities reported in this study using near-infrared laser beam is extremely useful in functionalization of the targeted cells by optoporation, modulation of the activity by optogenetic stimulation; and detecting the information from the cells in and noninvasive manner. The all-optical approach for control and monitoring of cellular activity will allow better understanding of signal processing by single neuron and its contribution to the functioning of the complex neuronal network.and dissecting the proper pathways and neuronal circuitry.

Defocused fiber optic two-photon beam will cause minimal photo damage while stimulating cells, the threshold average power required in

generating action potential in the ChR2-transfected cells is lower than that used for microscopic-objective two-photon stimulation. The two-photon stimulation mediated sub-threshold stimuli can induce action potentials in the presence of noise and also can be used to selectively stimulate larger (100 μm-motor neuron) cells which have lower thresholds than smaller (4 μm- granule cell) cells. The fiber-optic method employed in this study causes less contamination in the vicinity of cells if this method is used in *in vivo* unlike single photon where optical fiber has to be inserted in the proximity of stimulated region . Fiber-optic two-photon stimulation depends upon the pulse width of laser, power density and excitation wavelength. We also need to characterized the properties of variety of opsins and determine its complete structure during on-off cycles.

5.2 Future work

Optical delivery of light sensitive gene-encoding plasmids and localized optogenetic stimulation will be very useful tool in clinical application such as retinitis pigmentosa and age-related macular degeneration. In order to succeed in such clinical trials, precise targeted delivery of gene-encoding plasmids and localized stimulation is required. One of future steps will be to develop gene-encoding multiple opsin plasmids and their delivery in the retina of behaving animal (*in vivo*). Also, the delivery of different cell impermeable dyes and antibodies into neurons

will allow study of the intracellular dynamics High resolution imaging technique can be combined with the optical manipulation and modulation to obtain more detailed information from cellular activities.

The non-linear optogenetics approach, combined with electrophysiology and behavioral readout(s), will provide a unique opportunity to dissect the functional neuronal circuitry of deep brain regions. Two-photon optogenetics could be a potential tool to stimulate the cells lying in deep brain as it could reach deeper than single photon light as shown in Figure 5.1. The graph in Figure 5.1 was simulated using the absorption and scattering properties presented in Table 1 (μ_a: absorption coefficient; μ_s: scattering coefficient) of the tissue at that wavelength using following relation.

$$I(x) = I_0 \exp(-\mu_{eff} * x), \qquad 5\text{-}1$$

Where I_0 is initial intensity and I(x) is the attenuated intensity as the function depth(x). Effective attenuation coefficient μ_{eff} is given by sqrt $[3\mu_a(\mu_a+\mu_s')]$; and 'μ_s' is the reduced scattering coefficient, given by μ_s (1-g), g being the anisotropy factor of the forward scattering tissue.

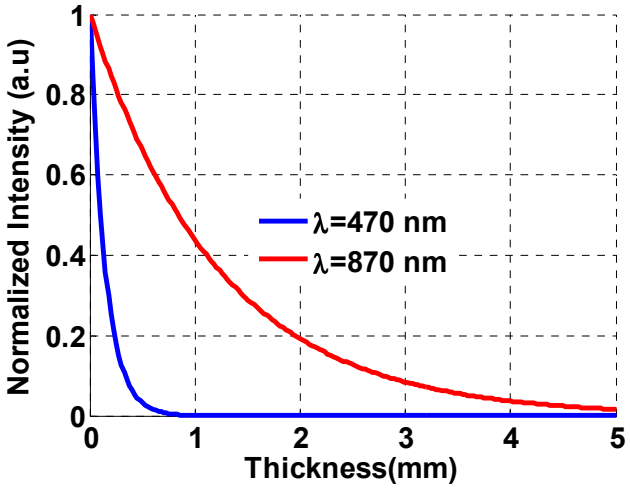

Figure 5.1: Variation of light intensity as a function of depth in brain (grey matter).

The efficacy of the two-photon beam can be further improved by controlling the divergence of the beam emanating from the fiber. Since the two-photon process is non-linear in nature, focused near infrared activation can lead to highly localized activation of the specific region of interest, which may be located deep in the ventral portion of the midbrain.

Previous studies (both experimental and Monte Carlo simulation [145-147]) show that a non-diffracting optogenetics Bessel beam is more effective for depth stimulation than a classical (Gaussian) beam [148]. Figure 5.2 shows the comparison of microscopic two-photon setup with defocused and focused fiber-optic two-photon optogenetic stimulation.

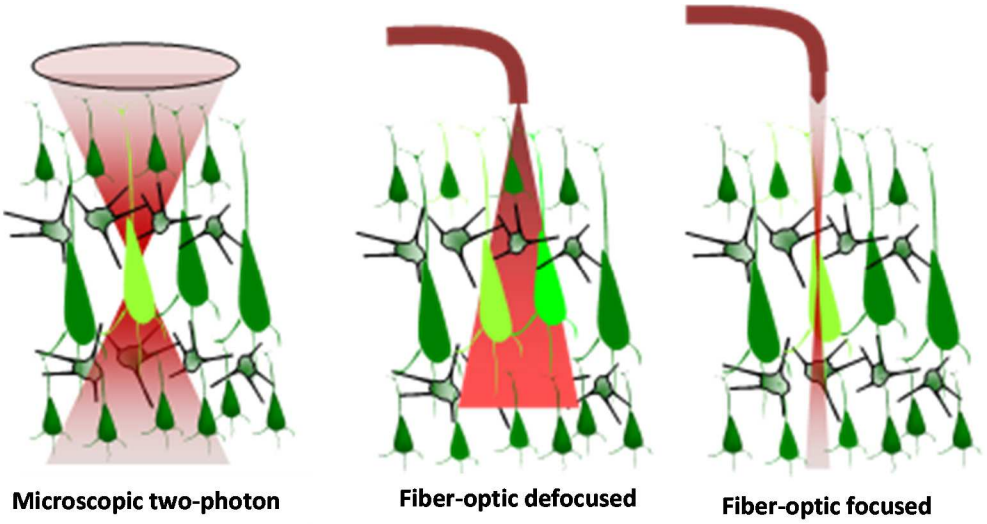

Figure 5.2: Comparison of microscopic two-photon setup with defocused and focused fiber-optic two-photon optogenetic stimulation.

The challenges in the development of optogenetic stimulation and inhibition is that these techniques still require improvements such as increasing the ion selectivity, enhancing light sensitivity and kinetics of opsins and better control on delivery/expression of opsin-constructs in the targeted cells. Further, development of opsin with a narrow activation spectrum allows the application of multiple opsins in multiple cell types simultaneously. Furthermore, the use of compact near-infrared light source and/or red-shifted activation spectrum for deeper and/or localized stimulation and inhibition would make the optogenetics an even stronger neuroscience tool. In order to have high temporal resolution and deeper penetration, we could use wide-field label-free optical imaging of neural

activities and adaptive optics for the generation of spatially and phase-modulated beams.

Appendix A

List of Tables

Table 1: Fragment size of ChR2 and restriction enzymes

Restriction enzymes	Fragment size (bp)
NotI (double digestion)	3333
	1480
BamHI (single digestion)	5605

Table 2: Parameters used in simulation of laser induced plasma and intensity profile

symbol	Definition	Units	Value
λ	Laser wavelength	nm	800
ε_0	Dielectric permittivity	F/m	8.854×10^{-12}
T	Temperature	K	310
k_B	Boltzmann constant	J/K	1.38×10^{-23}
R	Radius of dye molecule	nm	0.6997
η	Intracellular viscosity coefficient	cp	2
NA	Numerical aperture of microscope objective	-	1.3
m_c	Mass of electron	kg	9.11×10^{-31}
ω	Plasma frequency	s^{-1}	2.36×10^{15}

Appendix B

License and copyright of material

Permissions for Figure 1.1

Subject: Reuse Figure in Dissertation
Dhakal, Kamal R
Mon 10/13/2014 9:58 AM
Thank you very much. Kamal
REPLYREPLY ALLFORWARD
Mark as unread
Lucy Evans <Lucy.Evans@iop.org> on behalf of Permissions <permissions@iop.org>
Mon 10/13/2014 3:28 AM
To:
Dhakal, Kamal R;
You replied on 10/13/2014 9:58 AM.
Dear Kamal Dhakal,
Thank you for your request to reproduce IOP Publishing material.
Figure 7 - J. Neural Eng. 4 (2007) S143–S156 to be reused in your thesis.
We are happy to grant permission for the use you request on the terms set out below.

If you have any questions, please feel free to contact our Permissions team at permissions@iop.org.

I should be grateful if you would acknowledge receipt of this email.

Kind regards,
Lucy Evans
Publishing Assistant
IOP Publishing

From: "Dhakal, Kamal R" <kamal.dhakal@mavs.uta.edu>
To: "permissions@iop.org" <permissions@iop.org>,
Date: 09/10/2014 20:51
Subject: Reuse Figure in Dissertation

Dear Publisher
Would you please give me permission to use Figure 7 of "An optical neural interface: in vivo control of rodent motor cortex with integrated fiberoptic and optogenetics technology " Alexander M Aravanis et al 2007 J. Neural Eng. 4 S143 in my dissertation entitled "LASER-ASSISTED TRANSFECTION, STIMULATION AND DETECTION OF ACTIVITY IN CELLS" .

Sincerely,
Kamal Dhakal

Permission to for the picture that has been used in Figure 1.2 and Figure 1.3
Dear Mr. Kamal Dhakal,
Thank you for placing your order through Copyright Clearance Center's RightsLink service. Elsevier has partnered with RightsLink to license its content. This notice is a confirmation that your order was successful.

Your order details and publisher terms and conditions are available by clicking the link below:

Order Details
Licensee: Kamal R Dhakal
License Date: Sep 7, 2014
License Number: 3463810631516
Publication: Neuron
Title: Looking within for Vision
Type Of Use: reuse in a thesis/dissertation
Total: 0.00 USD

Permission to Figure 3.2
About the permission to use the picture of two-photon excitation picture

Dhakal, Kamal R
Mon 9/8/2014 10:10 AM
Thank you very much. Appreciate quick your response. Kamal Dhakal
REPLYREPLY ALLFORWARD
From: Dhakal, Kamal R [kamal.dhakal@mavs.uta.edu]
Sent: Monday, September 08, 2014 11:09 AM
To: Kevin Belfield
Subject: About the permission to use the picture of two-photon excitation picture
Hi Dr. Belfield
I am Kamal Dhakal from University of Texas at Arlington. I am working with Dr. Mohanty in biophotonics. I am writing my dissertation on "LASER –ASSISTED TRANSFECTION, STIMULATION AND DETECTION OF ACTIVITY IN CELLS". Chapter 2 of my dissertation is related with two-photon optogenetic stimulation. May I use the first picture from your websitehttp://chemistry.cos.ucf.edu/belfield/photophysics
just to show that two-photon is localized than single photon excitation .

Thanks
Kamal Dhakal,
Mark as unread
Kevin Belfield <belfield@ucf.edu>
Mon 9/8/2014 10:09 AM
Inbox
To:
Dhakal, Kamal R;
You replied on 9/8/2014 10:10 AM.
Dear Kamal:
Yes, no problem.

Regards,
Kevin D. Belfield, Pegasus Professor of Chemistry and Optics
Chair Department of Chemistry
AAAS Fellow 2013
University of Central Florida
4111 Libra Drive
PO Box 162366

Orlando, FL 32816-2366

Phone: 407.823.1028
Fax: 407.823.2252
E-mail: belfield@ucf.edu
http://chemistry.cos.ucf.edu/faculty_belfield.php
http://chemistry.cos.ucf.edu/belfield/

Copyright Permission for reuse
Black, Bryan J
Thu 3/26/2015 11:28 PM
To:
Dhakal, Mr Kamal R;
Cc:
Mohanty, Samarendra K;
Kamal,
You have my explicit permission to use Figures 2-1, 2-2, and 2-3 from my dissertation in your dissertation.
Bryan Black
Mark as unread
Dhakal, Mr Kamal R
Thu 3/26/2015 9:47 AM
Sent Items
Dear Dr. Black,

As we have worked together in some of our projects, I would like to ask permission to reuse the pictures (full or partial) in page 47 and 51 (Figure 2-1, Figure 2-2 and Figure 2-3) of your dissertation to include in my dissertation (academic purpose only) also.
Thanks for your response.
Sincerely,
Kamal Raj Dhakal

Hi Kamal -

Thanks much for reaching out to us. Feel free to use this picture and best wishes on your dissertation!

Sincerely,

Julie Pryor

Julie Pryor
Communications Manager
McGovern Institute for Brain Research at MIT

77 Massachusetts Avenue
Cambridge MA 02139
p: 617.715.5397
e: jpryor@mit.edu
w: mcgovern.mit.edu
Mark as unread

Dhakal, Mr Kamal R
Fri 3/27/2015 9:33 AM
Sent Items
Hi,
I am Kamal Raj Dhakal from university of Texas at Arlington at Physics department. I am defending my dissertation in this semester and my work is related to optogenetics . I am interested to reuse one of the pictures created from your group which is found in this link :http://newsoffice.mit.edu/2013/compulsive-behavior-causes-treatments-0606
May I use this picture in my dissertation for academic purpose only .
Thanks,
Kamal Dhakal

References

[1] F. H. C. Crick, "Thinking About the Brain," *Scientific American,* **241**, 219-32, (1979).

[2] K. Deisseroth, "Optogenetics," *Nat Methods,* **8**, 26-9, (2011).

[3] H. S. Seung, "Reading the Book of Memory: Sparse Sampling versus Dense Mapping of Connectomes (vol 62, pg 17, 2009)," *Neuron,* **63**, 139-139, (2009).

[4] H. Hama, H. Kurokawa, H. Kawano, R. Ando, T. Shimogori, H. Noda*, et al.*, "Scale: a chemical approach for fluorescence imaging and reconstruction of transparent mouse brain," *Nat Neurosci,* **14**, 1481-8, (2011).

[5] L. Fenno, O. Yizhar, and K. Deisseroth, "The Development and Application of Optogenetics," *Annual Review of Neuroscience, Vol 34,* **34**, 389-412, (2011).

[6] D. Schmucker, A. L. Su, A. Beermann, H. Jackle, and D. G. Jay, "Chromophore-assisted laser inactivation of patched protein switches cell fate in the larval visual system of Drosophila," *Proc Natl Acad Sci U S A,* **91**, 2664-8, (1994).

[7] L. Fenno, O. Yizhar, and K. Deisseroth, "The development and application of optogenetics," *Annu Rev Neurosci,* **34**, 389-412, (2011).

[8] D. S. Peterka, H. Takahashi, and R. Yuste, "Imaging voltage in neurons," *Neuron,* **69**, 9-21, (2011).

[9] W. Stein, C. Stadele, and P. Andras, "Optical imaging of neurons in the crab stomatogastric ganglion with voltage-sensitive dyes," *J Vis Exp,*1-5*,* (2011).

[10] M. Segal, "Fast imaging of [Ca]i reveals presence of voltage-gated calcium channels in dendritic spines of cultured hippocampal neurons," *J Neurophysiol,* **74**, 484-8, (1995).

[11] W. Stein, C. Stadele, and P. Andras, "Single-sweep voltage-sensitive dye imaging of interacting identified neurons," *J Neurosci Methods,* **194**, 224-34, (2011).

[12] A. L. Hodgkin and A. F. Huxley, "A Quantitative Description of Membrane Current and Its Application to Conduction and Excitation in Nerve," *Journal of Physiology-London,* **117**, 500-544, (1952).

[13] E. S. Boyden, "A history of optogenetics: the development of tools for controlling brain circuits with light," *F1000 Biol Rep,* **3**, 11, (2011).

[14] G. Nagel, T. Szellas, W. Huhn, S. Kateriya, N. Adeishvili, P. Berthold*, et al.*, "Channelrhodopsin-2, a directly light-gated cation-selective membrane channel," *Proc. Nat. Acad. Sci.,* **100**, 13940-13945, (2003).

[15] E. S. Boyden, F. Zhang, E. Bamberg, G. Nagel, and K. Deisseroth, "Millisecond-timescale, genetically targeted optical control of neural activity," *Nat Neurosci,* **8**, 1263-1268, (2005).

[16] G. Nagel, M. Brauner, J. F. Liewald, N. Adeishvili, E. Bamberg, and A. Gottschalk, "Light Activation of Channelrhodopsin-2 in Excitable Cells of Caenorhabditis elegans Triggers Rapid Behavioral Responses," *Curr. Biol.,* **15**, 2279-2284, (2005).

[17] R. B. Christopher and C. M. Cameron, "Role of electrode design on the volume of tissue activated during deep brain stimulation," *Journal of Neural Engineering,* **3**, 1, (2006).

[18] C. R. Butson and C. C. McIntyre, "Tissue and electrode capacitance reduce neural activation volumes during deep brain stimulation," *Clinical Neurophysiology,* **116**, 2490-2500, (2005).

[19] V. Voon, C. Kubu, P. Krack, J.-L. Houeto, and A. I. Tröster, "Deep brain stimulation: Neuropsychological and neuropsychiatric issues," *Movement Disorders,* **21**, S305-S327, (2006).

[20] M. Antkowiak, M. L. Torres-Mapa, E. C. Witts, G. B. Miles, K. Dholakia, and F. J. Gunn-Moore, "Fast targeted gene transfection and optogenetic modification of single neurons using femtosecond laser irradiation," *Scientific Reports,* **3**, 2-6, (2013).

[21] W. F. Cheong, S. A. Prahl, and A. J. Welch, "A review of the optical properties of biological tissues," *Quantum Electronics, IEEE Journal of,* **26**, 2166-2185, (1990).

[22] B. R. Arenkiel, J. Peca, I. G. Davison, C. Feliciano, K. Deisseroth, George J. Augustine*, et al.*, "In Vivo Light-Induced Activation of Neural Circuitry in Transgenic Mice Expressing Channelrhodopsin-2," *Neuron,* **54**, 205-218, (2007).

[23] M. A. Alexander, L.-P. Wang, F. Zhang, L. A. Meltzer, M. Z. Mogri, M. B. Schneider*, et al.*, "An optical neural interface: in vivo control of rodent motor cortex with integrated fiberoptic and optogenetic technology," *J. Neural Eng.,* **4**, 2-12, (2007).

[24] X. Han, X. Qian, J. G. Bernstein, H.-h. Zhou, G. T. Franzesi, P. Stern*, et al.*, "Millisecond-Timescale Optical Control of Neural Dynamics in the Nonhuman Primate Brain," *Neuron,* **62**, 191-198, (2009).

[25] H. Cao, L. Gu, S. Mohanty, and J. Chiao, "An Integrated microLED Optrode for Optogenetic Stimulation and Electrical Recording," *IEEE Trans Biomed Eng,* 1-4, (2012).

[26] F. Zhang, M. Prigge, F. Beyriere, S. P. Tsunoda, J. Mattis, O. Yizhar*, et al.*, "Red-shifted optogenetic excitation: a tool for fast neural control derived from Volvox carteri," *Nat Neurosci,* **11**, 631-633, (2008).

[27] L. A. Gunaydin, O. Yizhar, A. Berndt, V. S. Sohal, K. Deisseroth, and P. Hegemann, "Ultrafast optogenetic control," *Nat Neurosci,* **13**, 387-392, (2010).

[28] J. Y. Lin, M. Z. Lin, P. Steinbach, and R. Y. Tsien, "Characterization of Engineered Channelrhodopsin Variants with Improved Properties and Kinetics," *Biophys. J.,* **96**, 1803-1814, (2009).

[29] C. Schroll, T. Riemensperger, D. Bucher, J. Ehmer, T. Voller, K. Erbguth*, et al.*, "Light-induced activation of distinct modulatory neurons triggers appetitive or aversive learning in Drosophila larvae," *Curr Biol,* **16**, 1741-7, (2006).

[30] A. R. Adamantidis, F. Zhang, A. M. Aravanis, K. Deisseroth, and L. de Lecea, "Neural substrates of awakening probed with optogenetic control of hypocretin neurons," *Nature,* **450**, 420-4, (2007).

[31] W. Zhang, W. P. Ge, and Z. R. Wang, "A toolbox for light control of Drosophila behaviors through Channelrhodopsin 2-mediated photoactivation of targeted neurons," *European Journal of Neuroscience,* **26**, 2405-2416, (2007).

[32] P. S. Lagali, D. Balya, G. B. Awatramani, T. A. Munch, D. S. Kim, V. Busskamp*, et al.*, "Light-activated channels targeted to ON bipolar cells restore visual function in retinal degeneration," *Nat Neurosci,* **11**, 667-75, (2008).

[33] W. J. Alilain, X. Li, K. P. Horn, R. Dhingra, T. E. Dick, S. Herlitze*, et al.*, "Light-induced rescue of breathing after spinal cord injury," *J Neurosci,* **28**, 11862-70, (2008).

[34] T. R. Mahoney, S. Luo, E. K. Round, M. Brauner, A. Gottschalk, J. H. Thomas*, et al.*, "Intestinal signaling to GABAergic neurons regulates a rhythmic behavior in Caenorhabditis elegans," *Proc Natl Acad Sci U S A,* **105**, 16350-5, (2008).

[35] X. Han, X. F. Qian, J. G. Bernstein, H. H. Zhou, G. T. Franzesi, P. Stern*, et al.*, "Millisecond-Timescale Optical Control of Neural Dynamics in the Nonhuman Primate Brain," *Neuron,* **62**, 191-198, (2009).

[36] J. Noack and A. Vogel, "Laser-induced plasma formation in water at nanosecond to femtosecond time scales: Calculation of thresholds, absorption coefficients, and energy density," *Ieee Journal of Quantum Electronics,* **35**, 1156-1167, (1999).

[37] A. Vogel, J. Noack, G. Huttman, and G. Paltauf, "Mechanisms of femtosecond laser nanosurgery of cells and tissues," *Applied Physics B-Lasers and Optics,* **81**, 1015-1047, (2005).

[38] K. Zhao, Q. Zhang, M. Chini, Y. Wu, X. W. Wang, and Z. H. Chang, "Tailoring a 67 attosecond pulse through advantageous phase-mismatch," *Optics Letters,* **37**, 3891-3893, (2012).

[39] V. Kohli and A. Y. Elezzabi, "Laser surgery of zebrafish (Danio rerio) embryos using femtosecond laser pulses: Optimal parameters for exogenous material delivery, and the laser's effect on short- and long-term development," *Bmc Biotechnology,* **8**, 1-20, (2008).

[40] W. Supatto, D. Debarre, B. Moulia, E. Brouzes, J. L. Martin, E. Farge*, et al.*, "In vivo modulation of morphogenetic movements in Drosophila embryos with femtosecond laser pulses," *Proceedings of the National Academy of Sciences of the United States of America,* **102**, 1047-1052, (2005).

[41] C. B. Schaffer, A. Brodeur, and E. Mazur, "Laser-induced breakdown and damage in bulk transparent materials induced by tightly focused femtosecond laser pulses," *Measurement Science & Technology,* **12**, 1784-1794, (2001).

[42] J. S. Soughayer, T. Krasieva, S. C. Jacobson, J. M. Ramsey, B. J. Tromberg, and N. L. Allbritton, "Characterization of cellular optoporation with distance," *Analytical Chemistry,* **72**, 1342-1347, (2000).

[43] S. Mohanty, "Optically-actuated translational and rotational motion at the microscale for microfluidic manipulation and characterization," *Lab Chip,* **12**, 3624-36, (2012).

[44] H. A. Rendall, R. F. Marchington, B. B. Praveen, G. Bergmann, Y. Arita, A. Heisterkamp*, et al.*, "High-throughput optical injection of mammalian cells using a Bessel light beam," *Lab on a Chip,* **12**, 4816-4820, (2012).

[45] R. F. Marchington, Y. Arita, X. Tsampoula, F. J. Gunn-Moore, and K. Dholakia, "Optical injection of mammalian cells using a microfluidic platform," *Biomedical Optics Express,* **1**, 527-536, (2010).

[46] T. Kodama, A. G. Doukas, and M. R. Hamblin, "Shock wave-mediated molecular delivery into cells," *Biochimica Et Biophysica Acta-Molecular Cell Research,* **1542**, 186-194, (2002).

[47] T. Kodama, M. R. Hamblin, and A. G. Doukas, "Cytoplasmic molecular delivery with shock waves," *Faseb Journal,* **14**, A1473-A1473, (2000).

[48] A. Vogel, N. Linz, S. Freidank, and G. Paltauf, "Femtosecond-laser-induced nanocavitation in water: implications for optical breakdown threshold and cell surgery," *Phys Rev Lett,* **100**, 1-4, (2008).

[49] C. Schaffer, N. Nishimura, E. Glezer, A. Kim, and E. Mazur, "Dynamics of femtosecond laser-induced breakdown in water from femtoseconds to microseconds," *Opt Express,* **10**, 196-203, (2002).

[50] H. Schneckenburger, A. Hendinger, R. Sailer, W. S. L. Strauss, and M. Schmitt, "Laser-assisted optoporation of single cells," *Journal of Biomedical Optics,* **7**, 410-416, (2002).

[51] G. Palumbo, M. Caruso, E. Crescenzi, M. F. Tecce, G. Roberti, and A. Colasanti, "Targeted gene transfer in eucaryotic cells by dye-assisted laser optoporation," *Journal of Photochemistry and Photobiology B-Biology,* **36**, 41-46, (1996).

[52] S. K. Mohanty, M. Sharma, and P. K. Gupta, "Laser-assisted microinjection into targeted animal cells," *Biotechnology Letters,* **25**, 895-899, (2003).

[53] J. C. Stockert, A. Juarranz, A. Villanueva, and M. Canete, "Photodynamic damage to HeLa cell microtubules induced by thiazine dyes," *Cancer Chemotherapy and Pharmacology,* **39**, 167-169, (1996).

[54] S. L. Jackson and I. B. Heath, "The Dynamic Behavior of Cytoplasmic F-Actin in Growing Hyphae," *Protoplasma,* **173**, 23-34, (1993).

[55] M. C. Sanders and Y. L. Wang, "Exogenous Nucleation Sites Fail to Induce Detectable Polymerization of Actin in Living Cells," *Journal of Cell Biology,* **110**, 359-365, (1990).

[56] I. Hapala, "Breaking the barrier: methods for reversible permeabilization of cellular membranes," *Crit Rev Biotechnol,* **17**, 105-22, (1997).

[57] O. Gresch, F. B. Engel, D. Nesic, T. T. Tran, H. M. England, E. S. Hickman*, et al.*, "New non-viral method for gene transfer into primary cells," *Methods,* **33**, 151-163, (2004).

[58] W. C. Heiser, *Gene delivery to mammalian cells*. Totowa, N.J.: Humana Press, 2004.

[59] C. E. Thomas, A. Ehrhardt, and M. A. Kay, "Progress and problems with the use of viral vectors for gene therapy," *Nature Reviews Genetics,* **4**, 346-358, (2003).

[60] M. W. Berns, J. Aist, J. Edwards, K. Strahs, J. Girton, P. McNeill*, et al.*, "Laser microsurgery in cell and developmental biology," *Science,* **213**, 505-13, (1981).

[61] Y. Tan, D. Sun, and W. Huang, "Mechanical modeling of red blood cells during optical stretching," *J Biomech Eng,* **132**, 044504, (2010).

[62] N. Cardenas, L. F. Yu, and S. K. Mohanty, "Stretching of red blood cells by Optical Tweezers quantified by Digital Holographic Microscopy," *Optical Interactions with Tissue and Cells Xxii,* **7897**,1-8, (2011).

[63] L. Gu, A. R. Koymen, and S. K. Mohanty, "Crystalline magnetic carbon nanoparticle assisted photothermal delivery into cells using CW near-infrared laser beam," *Sci Rep,* **4**, 1-4, (2014).

[64] U. K. Tirlapur and K. Konig, "Targeted transfection by femtosecond laser," *Nature,* **418**, 290-1, (2002).

[65] L. Gu and S. K. Mohanty, "Targeted microinjection into cells and retina using optoporation," *J Biomed Opt,* **16**, 128003-6, (2011).

[66] P. Soman, W. D. Zhang, A. Umeda, Z. J. Zhang, and S. C. Chen, "Femtosecond Laser-Assisted Optoporation for Drug and Gene Delivery into Single Mammalian Cells," *Journal of Biomedical Nanotechnology,* **7**, 334-341, (2011).

[67] F. Stracke, I. Rieman, and K. Konig, "Optical nanoinjection of macromolecules into vital cells," *Journal of Photochemistry and Photobiology B-Biology,* **81**, 136-142, (2005).

[68] L. E. Barrett, J. Y. Sul, H. Takano, E. J. Van Bockstaele, P. G. Haydon, and J. H. Eberwine, "Region-directed phototransfection

reveals the functional significance of a dendritically synthesized transcription factor," *Nature Methods,* **3**, 455-60, (2006).

[69] C. Peng, R. E. Palazzo, and I. Wilke, "Laser intensity dependence of femtosecond near-infrared optoinjection," *Physical Review E,* **75**, (2007).

[70] M. Lei, H. P. Xu, H. Yang, and B. L. Yao, "Femtosecond laser-assisted microinjection into living neurons," *Journal of Neuroscience Methods,* **174**, 215-218, (2008).

[71] A. Uchugonova, K. Konig, R. Bueckle, A. Isemann, and G. Tempea, "Targeted transfection of stem cells with sub-20 femtosecond laser pulses," *Optics Express,* **16**, 9357-9364, (2008).

[72] K. Dhakal, B. Black, and S. Mohanty, "Introduction of impermeable actin-staining molecules to mammalian cells by optoporation," *Sci Rep,* **4**, 6553, (2014).

[73] V. Kohli and A. Y. Elezzabi, "Laser surgery of zebrafish (Danio rerio) embryos using femtosecond laser pulses: optimal parameters for exogenous material delivery, and the laser's effect on short- and long-term development," *BMC Biotechnol,* **8**, 7, (2008).

[74] E. Zeira, A. Manevitch, A. Khatchatouriants, O. Pappo, E. Hyam, M. Darash-Yahana*, et al.*, "Femtosecond infrared laser - An efficient and safe in vivo gene delivery system for prolonged expression," *Molecular Therapy,* **8**, 342-350, (2003).

[75] L. Gu and S. K. Mohanty, "Targeted microinjection into cells and retina using optoporation," *Journal of Biomedical Optics,* **16**, (2011).

[76] C. Bamann, T. Kirsch, G. Nagel, and E. Bamberg, "Spectral Characteristics of the Photocycle of Channelrhodopsin-2 and Its Implication for Channel Function," *Journal of Molecular Biology,* **375**, 686-694, (2008).

[77] J. Y. Lin, P. M. Knutsen, A. Muller, D. Kleinfeld, and R. Y. Tsien, "ReaChR: a red-shifted variant of channelrhodopsin enables deep transcranial optogenetic excitation," *Nat Neurosci,* **16**, 1499-1508, (2013).

[78] O. Yizhar, L. E. Fenno, M. Prigge, F. Schneider, T. J. Davidson, D. J. O/'Shea*, et al.*, "Neocortical excitation/inhibition balance in information processing and social dysfunction," *Nature,* **477**, 171-178, (2011).

[79] J. Baumgart, W. Bintig, A. Ngezahayo, S. Willenbrock, H. Murua Escobar, W. Ertmer*, et al.*, "Quantified femtosecond laser based opto-perforation of living GFSHR-17 and MTH53 a cells," *Opt Express,* **16**, 3021-31, (2008).

[80] A. A. Davis, M. J. Farrar, N. Nishimura, M. M. Jin, and C. B. Schaffer, "Optoporation and genetic manipulation of cells using femtosecond laser pulses," *Biophys J,* **105**, 862-71, (2013).

[81] X. Kong, S. K. Mohanty, J. Stephens, J. T. Heale, V. Gomez-Godinez, L. Z. Shi*, et al.*, "Comparative analysis of different laser systems to study cellular responses to DNA damage in mammalian cells," *Nucleic Acids Res,* **37**, e68, (2009).

[82] J. A. Cooper, "Effects of cytochalasin and phalloidin on actin," *J Cell Biol,* **105**, 1473-8, (1987).

[83] L. Gu and S. K. Mohanty, "Targeted microinjection into cells and retina using optoporation," *Journal of Biomedical Optics,* **16**, 128003, (2011).

[84] L. Luo, E. M. Callaway, and K. Svoboda, "Genetic dissection of neural circuits," *Neuron,* **57**, 634-60, (2008).

[85] A. Waggoner, "Fluorescent labels for proteomics and genomics," *Current Opinion in Chemical Biology,* **10**, 62-66, (2006).

[86] A. C. Tien, S. Backus, H. Kapteyn, M. Murnane, and G. Mourou, "Short-pulse laser damage in transparent materials as a function of pulse duration," *Physical Review Letters,* **82**, 3883-3886, (1999).

[87] V. M. Gordienko, P. M. Mikheev, and V. S. Syrtsov, "Nonmonotonic behavior of the absorption of the tightly focused femtosecond radiation of a Cr : Forsterite laser in a dielectric due to an increase in the number of photons involved in the process," *Jetp Letters,* **82**, 228-231, (2005).

[88] M. Born and E. Wolf, *Principles of optics : electromagnetic theory of propagation, interference and diffraction of light*, 7th expanded ed. Cambridge ; New York: Cambridge University Press, 1999.

[89] S. Grill and E. H. K. Stelzer, "Method to calculate lateral and axial gain factors of optical setups with a large solid angle," *Journal of the Optical Society of America a-Optics Image Science and Vision,* **16**, 2658-2665, (1999).

[90] W. C. Parker, N. Chakraborty, R. Vrikkis, G. Elliott, S. Smith, and P. J. Moyer, "High-resolution intracellular viscosity measurement using time-dependent fluorescence anisotropy," *Optics Express,* **18**, 16607-16617, (2010).

[91] A. P. Alivisatos, M. Y. Chun, G. M. Church, K. Deisseroth, J. P. Donoghue, R. J. Greenspan*, et al.*, "The Brain Activity Map," *Science,* **339**, 1284-1285, (2013).

[92] D. B. Murphy and M. W. Davidson, *Fundamentals of light microscopy and electronic imaging*, 2nd ed. Hoboken, N.J.: Wiley-Blackwell, 2013.

[93] A. Dragomir, J. G. McInerney, and D. N. Nikogosyan, "Femtosecond measurements of two-photon absorption coefficients at lambda =

264 nm in glasses, crystals, and liquids (vol 41, pg 4365, 2002)," *Applied Optics,* **41**, 5655-5655, (2002).

[94] P. T. C. So, C. Y. Dong, B. R. Masters, and K. M. Berland, "Two-photon excitation fluorescence microscopy," *Annual Review of Biomedical Engineering,* **2**, 399-429, (2000).

[95] W. Kaiser and C. G. B. Garrett, "Two-Photon Excitation in CaF2: Eu2+," *Physical Review Letters,* **7**, 229-231, (1961).

[96] G. V. Goddard, D. C. McIntyre, and C. K. Leech, "A permanent change in brain function resulting from daily electrical stimulation," *Exp Neurol,* **25**, 295-330, (1969).

[97] A. M. Lozano, J. Dostrovsky, R. Chen, and P. Ashby, "Deep brain stimulation for Parkinson's disease: disrupting the disruption," *Lancet Neurology,* **1**, 225-231, (2002).

[98] J. S. Han, "Acupuncture: neuropeptide release produced by electrical stimulation of different frequencies," *Trends in Neurosciences,* **26**, 17-22, (2003).

[99] A. Berndt, P. Schoenenberger, J. Mattis, K. M. Tye, K. Deisseroth, P. Hegemann*, et al.*, "High-efficiency channelrhodopsins for fast neuronal stimulation at low light levels," *Proc Natl Acad Sci U S A,* **108**, 7595-600, (2011).

[100] C. Schmitt, C. Schultheis, S. J. Husson, J. F. Liewald, and A. Gottschalk, "Specific expression of channelrhodopsin-2 in single neurons of Caenorhabditis elegans," *PLoS One,* **7**, e43164, (2012).

[101] A. Kiselev and S. Subramaniam, "Activation and regeneration of rhodopsin in the insect visual cycle," *Science,* **266**, 1369-73, (1994).

[102] F. J. Braun and P. Hegemann, "Two light-activated conductances in the eye of the green alga Volvox carteri," *Biophysical Journal,* **76**, 1668-1678, (1999).

[103] K. Nikolic, N. Grossman, M. S. Grubb, J. Burrone, C. Toumazou, and P. Degenaar, "Photocycles of channelrhodopsin-2," *Photochem Photobiol,* **85**, 400-11, (2009).

[104] P. Hegemann, W. Gartner, and R. Uhl, "All-trans retinal constitutes the functional chromophore in Chlamydomonas rhodopsin," *Biophys J,* **60**, 1477-89, (1991).

[105] B. A. Nemet, V. Nikolenko, and R. Yuste, "Second harmonic imaging of membrane potential of neurons with retinal," *J Biomed Opt,* **9**, 873-81, (2004).

[106] J. P. Rickgauer and D. W. Tank, "Two-photon excitation of channelrhodopsin-2 at saturation," *Proc Nat Acad Sci,* **106**, 15025-15030, (2009).

[107] D. A. McCormick and H. C. Pape, "Properties of a hyperpolarization-activated cation current and its role in rhythmic oscillation in thalamic relay neurones," *J Physiol,* **431**, 291-318, (1990).

[108] P. e. a. Rhohit "Two-photon optogenetic toolbox for fast inhibition, excitation and bistable modulation," *Nat. Method,* (2012).

[109] B. A. Nemet, V. Nikolenko, and R. Yuste, "Second harmonic imaging of membrane potential of neurons with retinal," *Journal of Biomedical Optics,* **9**, 873-881, (2004).

[110] N. Farah, Matar, S., Marom, A., Golan, L. & Shoham, S., "Photo-absorber based neural stimulation for an optical retinal prosthesis,"*. Res. Vis. Opth. (ARVO)* (2010).

[111] S. K. Mohanty, R. K. Reinscheid, X. B. Liu, N. Okamura, T. B. Krasieva, and M. W. Berns, "In-depth activation of channelrhodopsin 2-sensitized excitable cells with high spatial resolution using two-photon excitation with a near-infrared laser microbeam," *Biophysical Journal,* **95**, 3916-3926, (2008).

[112] B. K. Andrasfalvy, B. V. Zemelman, J. Y. Tang, and A. Vaziri, "Two-photon single-cell optogenetic control of neuronal activity by sculpted light," *Proceedings of the National Academy of Sciences of the United States of America,* **107**, 11981-11986, (2010).

[113] E. Papagiakoumou, F. Anselmi, A. Begue, V. de Sars, J. Gluckstad, E. Y. Isacoff*, et al.*, "Scanless two-photon excitation of channelrhodopsin-2," *Nature Methods,* **7**, 848-U117, (2010).

[114] R. Prakash, O. Yizhar, B. Grewe, C. Ramakrishnan, N. Wang, I. Goshen*, et al.*, "Two-photon optogenetic toolbox for fast inhibition, excitation and bistable modulation," *Nature Methods,* **9**, 1171-U132, (2012).

[115] E. S. Boyden, F. Zhang, E. Bamberg, G. Nagel, and K. Deisseroth, "Millisecond-timescale, genetically targeted optical control of neural activity," *Nature Neuroscience,* **8**, 1263-1268, (2005).

[116] J. D. Johansson, "Spectroscopic method for determination of the absorption coefficient in brain tissue," *Journal of Biomedical Optics,* **15**, 057005, (2010).

[117] A. N. Yaroslavsky, P. C. Schulze, I. V. Yaroslavsky, R. Schober, F. Ulrich, and H. J. Schwarzmaier, "Optical properties of selected native and coagulated human brain tissues in vitro in the visible and near infrared spectral range," *Phys Med Biol,* **47**, 2059-73, (2002).

[118] W. F. Cheong, S. A. Prahl, and A. J. Welch, "A Review of the Optical-Properties of Biological Tissues," *Ieee Journal of Quantum Electronics,* **26**, 2166-2185, (1990).

[119] S. Shivalingaiah, L. Gu, and S. K. Mohanty, "Non-linear stimulation of excitable cells with and without optogenetic sensitization," *Proc. SPIE* **7883**, 788355, (2011).

[120] S. Liang, F. Yang, C. Zhou, Y. Wang, S. Li, C. K. Sun*, et al.*, "Temperature-dependent activation of neurons by continuous near-infrared laser," *Cell Biochem Biophys,* **53**, 33-42, (2009).

[121] M. A. Albota, C. Xu, and W. W. Webb, "Two-Photon Fluorescence Excitation Cross Sections of Biomolecular Probes from 690 to 960 nm," *Appl Opt,* **37**, 7352-6, (1998).

[122] F. Bestvater, E. Spiess, G. Stobrawa, M. Hacker, T. Feurer, T. Porwol*, et al.*, "Two-photon fluorescence absorption and emission spectra of dyes relevant for cell imaging," *J Microsc,* **208**, 108-15, (2002).

[123] S. Shivalingaiah, L. Gu, and S. K. Mohanty, "Non-linear stimulation of excitable cells with and without optogenetic sensitization," *Photonic Therapeutics and Diagnostics Vii,* **7883**, (2011).

[124] S. Yamaguchi and T. Tahara, "Two-photon absorption spectrum of all-trans retinal," *Chemical Physics Letters,* **376**, 237-243, (2003).

[125] M. G. Vivas, D. L. Silva, L. Misoguti, R. Zalesny, W. Bartkowiak, and C. R. Mendonca, "Degenerate two-photon absorption in all-trans retinal: nonlinear spectrum and theoretical calculations," *J Phys Chem A,* **114**, 3466-70, (2010).

[126] K. F. Palmer and D. Williams, "Optical properties of water in the near infrared," *Journal of the Optical Society of America,* **64**, 1107-1110, (1974).

[127] R. M. Pope and E. S. Fry, "Absorption spectrum (380-700 nm) of pure water. II. Integrating cavity measurements," *Appl Opt,* **36**, 8710-23, (1997).

[128] C. L. Ebbesen and H. Bruus, "Analysis of laser-induced heating in optical neuronal guidance," *J Neurosci Methods,* **209**, 168-77, (2012).

[129] D. E. Clapham, "TRP channels as cellular sensors," *Nature,* **426**, 517-524, (2003).

[130] M. G. Shapiro, K. Homma, S. Villarreal, C. P. Richter, and F. Bezanilla, "Infrared light excites cells by changing their electrical capacitance," *Nature Communications,* **3**, (2012).

[131] C. Xu and W. W. Webb, "Measurement of two-photon excitation cross sections of molecular fluorophores with data from 690 to 1050 nm," *Journal of the Optical Society of America B-Optical Physics,* **13**, 481-491, (1996).

[132] T. Voets, "Quantifying and modeling the temperature-dependent gating of TRP channels," *Rev Physiol Biochem Pharmacol,* **162**, 91-119, (2012).

[133] B. Black, A. Mondal, Y. Kim, and S. K. Mohanty, "Neuronal beacon," *Optics Letters,* **38**, 2174-2176, (2013).

[134] D. J. Stevenson, T. K. Lake, B. Agate, V. Garces-Chavez, K. Dholakia, and F. Gunn-Moore, "Optically guided neuronal growth at near infrared wavelengths," *Opt Express,* **14**, 9786-93, (2006).

[135] J. Wells, C. Kao, P. Konrad, T. Milner, J. Kim, A. Mahadevan-Jansen*, et al.*, "Biophysical mechanisms of transient optical stimulation of peripheral nerve," *Biophys J,* **93**, 2567-80, (2007).

[136] A. D. Rosen, "Nonlinear temperature modulation of sodium channel kinetics in GH(3) cells," *Biochim Biophys Acta,* **1511**, 391-6, (2001).

[137] S. K. Mohanty, K. S. Mohanty, and M. W. Berns, "Manipulation of mammalian cells using a single-fiber optical microbeam," *Journal of Biomedical Optics,* **13**, (2008).

[138] L. Fu, A. Jain, H. K. Xie, C. Cranfield, and M. Gu, "Nonlinear optical endoscopy based on a double-clad photonic crystal fiber and a MEMS mirror," *Optics Express,* **14**, 1027-1032, (2006).

[139] L. B. Cohen and B. M. Salzberg, "Optical measurement of membrane potential," *Rev Physiol Biochem Pharmacol,* **83**, 35-88, (1978).

[140] G. Cao, J. Platisa, V. A. Pieribone, D. Raccuglia, M. Kunst, and M. N. Nitabach, "Genetically Targeted Optical Electrophysiology in Intact Neural Circuits," *Cell,* **154**, 904-913, (2013).

[141] G. Ji, M. E. Feldman, K. Y. Deng, K. S. Greene, J. Wilson, J. C. Lee*, et al.*, "Ca2+-sensing transgenic mice: postsynaptic signaling in smooth muscle," *J Biol Chem,* **279**, 21461-8, (2004).

[142] Y. N. Tallini, M. Ohkura, B. R. Choi, G. Ji, K. Imoto, R. Doran*, et al.*, "Imaging cellular signals in the heart in vivo: Cardiac expression of the high-signal Ca2+ indicator GCaMP2," *Proc Natl Acad Sci U S A,* **103**, 4753-8, (2006).

[143] L. Tian, S. A. Hires, T. Mao, D. Huber, M. E. Chiappe, S. H. Chalasani*, et al.*, "Imaging neural activity in worms, flies and mice with improved GCaMP calcium indicators," *Nature Methods,* **6**, 875-81, (2009).

[144] J. Y. Lin, P. M. Knutsen, A. Muller, D. Kleinfeld, and R. Y. Tsien, "ReaChR: a red-shifted variant of channelrhodopsin enables deep transcranial optogenetic excitation," *Nat Neurosci,* **16**, 1499-508, (2013).

[145] B. C. Wilson and S. L. Jacques, "Optical reflectance and transmittance of tissues: principles and applications," *Quantum Electronics, IEEE Journal of,* **26**, 2186-2199, (1990).

[146] S. L. Jacques, "Time resolved propagation of ultrashort laser pulses within turbid tissues," *Appl. Opt.,* **28**, 2223-2229, (1989).

[147] A. Kienle, L. Lilge, M. S. Patterson, R. Hibst, R. Steiner, and B. C. Wilson, "Spatially resolved absolute diffuse reflectance measurements for noninvasive determination of the optical

scattering and absorption coefficients of biological tissue," *Appl. Opt.,* **35**, 2304-2314, (1996).

[148] A. Kanneganti, S. Shivalingaiah, L. Gu, G. Alexandrakis, and S. Mohanty, "Deep Brain Optogenetic Stimulation Using Bessel Beam " *Biophys. J,,* **100**, 95a, (2011).

Biographical Information

Kamal Raj Dhakal was born in India but raised in Phaparthum-7, Syangja, Nepal. He received his Bachelor's degree in Physics from Tribhuvan University, Nepal in 2004. He graduated (M.Sc-Physics) from Tribhuvan University in 2007.His research during the master degree was on equilibrium configuration of BeH and its dimer using first-principle study. After Competing his Masters, He started working as a lecturer at Central Department of Environment Science in Tribhuvan University, Kirtipur and St. Xavier's College, Maitighar Kathmandu Nepal from 2007-2010.

In 2010, he came to the University of Rhode Island, RI, USA for his PhD. Being interested in Biophotonics, he transferred to University of Texas at Arlington in 2011 and began working in Dr. Mohanty's lab. Kamal earned his Master of Science degree in Physics in the fall of 2012 from UT-Arlington and his master thesis was on two-photon optogenetics. He continued his study to pursue Ph.D. after MS. He received his Ph. D. degree in May, 2015. Following graduation, Kamal plans to work as a postdoctoral researcher in Biophtonics and Imaging field.